Check for updates

ADVANCED FUNCTIONAL MATERIALS
www.afm-journal.de

Transient Implantable Electronics for Postsurgery Preventive Medicine

Hadi Mirzajani, Parviz Zolfaghari, Sattar Akbari Nakhjavani, Beril Yagmur Koca, Mehrdad Khodapanahandeh, and Hakan Urey**

The field of postoperative care has seen a remarkable shift toward the utilization of electronic implantable devices, including sensors, biosensors, stimulators, and drug delivery systems, all designed with a biodegradable form factor and wireless data/power transmission capability. These technologies hold immense potential for postsurgery out-of-hospital monitoring during the postdischarged period, where continuous monitoring of physiological signals is lacking. Furthermore, these devices eliminate the need for secondary surgeries required for device retrieval as they can safely degraded in the body, thus enhancing patient recovery. This review delves into the latest advancements in biodegradable implantable devices, examining their application in monitoring vital signs, the innovative wireless communication and powering technologies they employ, and the biodegradable materials that enable their function. The analysis extends to evaluating the efficacy and limitations of these devices across various medical applications. Moreover, it explores future research directions, emphasizing material advancements, device miniaturization, customization, and the integration of artificial intelligence to create closed-loop therapeutic systems. This comprehensive review underscores the transformative potential of these technologies in enhancing postoperative care and outlines the pathway for future innovations in this dynamic field.

1. Introduction

1.1. Addressing the Problems

Effective postoperative care requires diligently monitoring various chemical and physical factors to prevent complications and infections. Real-time tracking of physiological parameters, such as blood pressure, hemodynamics, temperature regulation, acid-base balance, and electrophysiological activity, is crucial.[1–3] However, current medical practice in hospitals and emergency departments (employing X-rays, computed tomography (CT) scans, magnetic resonance imaging (MRI), and blood sampling for biomarker monitoring) are often insufficient for timely diagnosis of postoperative issues, which typically manifest as acute symptoms like a sudden increase in cardiac biomarkers concentration as the result of postoperative atrial fibrillation (POAF),[4,5] rapidly raised respiratory rate as the result of postoperative hemorrhage,[6] opioid overdose, or withdrawal as the result of postoperative pain management,[7] rapid elevation in serum creatinine as the result of acute kidney injury (AKI) after a urological surgery,[8] rapid change in serum electrolytes or blood pressure as the result of hypovolemia after gastrointestinal surgery.[9]

In modern healthcare, implantable medical devices are indispensable, providing essential functions in diagnosis, treatment, and rehabilitation, thereby significantly enhancing patients' quality of life.[10–12] However, these durable, nonresorbable devices pose long-term risks of infection and inflammatory responses, leading to increased treatment costs and patient discomfort.[12–14] To address these limitations, recent advances in bioresorbable counterparts aim to develop devices for short-term monitoring or treatment that naturally dissolve, eliminating the need for extraction surgeries.[15–17] These bioresorbable devices, initially conceptualized as alternatives to metal and nonresorbable plastic materials in orthopedic treatments, have benefitted from advancements in material science and microfabrication. This progress has enabled the miniaturization of bioresorbable implantable electronics capable of advanced functions, such as sensing, stimulation, and real-time wireless data transmission. These devices provide targeted treatment or monitoring for specific periods before de-

H. Mirzajani, P. Zolfaghari, S. Akbari Nakhjavani, B. Y. Koca, M. Khodapanahandeh, H. Urey
Department of Electrical and Electronics Engineering
Koç University
Istanbul 34450, Türkiye
E-mail: hmirzajani@ku.edu.tr; hurey@ku.edu.tr
S. Akbari Nakhjavani, H. Urey
Koç University Research Center for Translational Medicine (KUTTAM)
Istanbul 34450, Türkiye

The ORCID identification number(s) for the author(s) of this article can be found under https://doi.org/10.1002/adfm.202413324

© 2024 The Author(s). Advanced Functional Materials published by Wiley-VCH GmbH. This is an open access article under the terms of the Creative Commons Attribution-NonCommercial-NoDerivs License, which permits use and distribution in any medium, provided the original work is properly cited, the use is non-commercial and no modifications or adaptations are made.

DOI: 10.1002/adfm.202413324

16163028, 2025, 3, Downloaded from https://advanced.onlinelibrary.wiley.com/doi/10.1002/adfm.202413324 by Koc University, Wiley Online Library on [22/05/2025]. See the Terms and Conditions (https://onlinelibrary.wiley.com/terms-and-conditions) on Wiley Online Library for rules of use; OA articles are governed by the applicable Creative Commons License

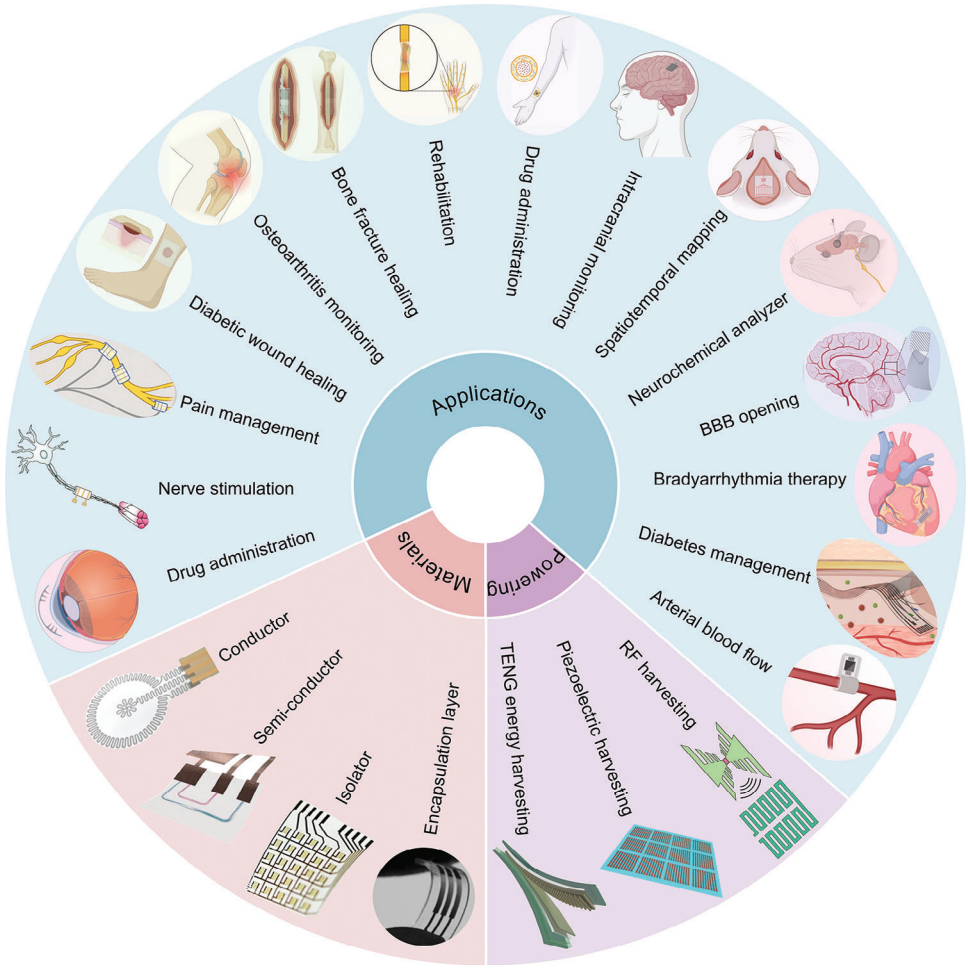


Figure 1. Schematic illustration of transient implantable electronics, required materials, and powering techniques.

grading into harmless byproducts, thus addressing the drawbacks of permanent implants.

The development of transient and bioresorbable implantable electronics represents a significant technological advancement, offering various innovative applications. Unlike conventional electronics, transient electronics are engineered to disintegrate, resorb, or dissolve through chemical or physical processes at predetermined rates or upon specific triggers. This revolutionary approach is particularly beneficial for applications requiring temporary functionality, similar to postoperational monitoring that eliminates the need for surgical removal.

Bioresorbable electronics involve materials that interact with biological environments through controlled metabolic, hydrolytic, or physical disintegration processes.[17–19] These materials can break down naturally within the body (bioresorbable), making them especially promising for medical applications. Bioresorbable mechanical devices, including sutures, stents, scaffolds, and drug delivery systems, have long demonstrated their clinical value by negating the need for removal. Although the operation efficiency of these devices can be significantly enhanced by optimization techniques available in the literature,[20–26] integrating electronic functionalities into these devices further broadens their potential applications. Thus far, prototypes including transistors, biosensors, and wireless communication systems have been implemented, thanks to a broad array of bioresorbable materials for conductors, semiconductors, and insulators. These advancements have enabled the creation of sophisticated diagnostic and therapeutic systems, often enhanced by wearable sensors and wireless controllers for comprehensive, multimodal operations.

The development of bioresorbable electronics involves careful material selection, compatible fabrication processes, and structural optimization. As research in this field progresses, the potential for bioresorbable electronics to transform medical treatments and improve patient care continues to grow, promising a future where medical technology is both advanced and patient-friendly. In the context outlined, this review aims to comprehensively understand body-integrated bioresorbable electronic platforms equipped with wireless capabilities. This includes the critical physiological indicators targeted for monitoring, biodegradable materials integrated into device construction, wireless power and data transmission techniques, and diverse applications (**Figure 1**). Furthermore, the advantages of this review paper concerning previously published works are summarized in **Table 1**.

 © 2024 The Author(s). Advanced Functional Materials published by Wiley-VCH GmbH

Table 1. Comparison among previously published review papers (from 2022 to 2024) in the area of biodegradable electronic implants and this review paper.

Refs.	Year	Objective of the paper	Differences with this review paper
[27]	2021	A review of materials and device structures dedicated to diagnosis and treatment of brain diseases	Lack of comprehensive discussion on various materials and device structures for application in various body systems.
[28]	2022	A comprehensive overview of various biodegradable polymeric materials for biomedical applications	Lack of discussion on the application of polymeric materials, especially in the development of transient electronics.
[29]	2022	A comprehensive discussion on encapsulation of various wearable and implantable sensors/biosensors.	Lack of discussion on the encapsulation of transient electronics for postsurgery monitoring.
[30]	2022	A comprehensive discussion on permanent flexible and stretchable implantable devices.	Lack of discussion on biodegradable materials and devices for postsurgery monitoring.
[31]	2022	A review of biodegradable materials and their degradation process.	There is limited discussion on their application in different organs of the body and body systems.
[32]	2023	A review of biocompatible materials for implementing implantable/wearable biosensors and their application.	Lack of discussion on biodegradable materials and their diverse applications.
[17]	2023	A comprehensive review of biodegradable materials and devices, their fabrication methods and application.	Lacking an overview of the application of transient electronics in different body systems.
[33]	2024	A comprehensive discussion on permanently implantable electronics for continuous physiological signal monitoring.	Lack of discussion on transient electronics for stimulation and sensing at various body systems.
[34]	2024	A comprehensive review of biodegradable materials, fabrication process flow, and device development for biosensing applications.	Lack of discussion on biodegradable electronics for stimulation and sensing and their application on various body systems.
[35]	2024	A comprehensive discussion on permanently implantable electronics for continuous physiological signal monitoring.	Limited discussion on biodegradable devices and their materials.
[36]	2024	A comprehensive discussion on permanently implantable electronics and their materials for continuous heart stimulation and sensing.	Lack of discussion on biodegradable electronics for stimulation and their application on various body systems.

1.2. Requirements

The implanted device is situated within a notably aggressive environment known by a dynamic pH spectrum. This results from various ions and enzymes in the system's biological fluids. In such a circumstance, organic and inorganic substances may be degraded or harmed. Hence, when designing biodegradable electronics for implantable purposes, one must consider many influencing factors. In this area, biocompatibility stands as a paramount concern. This critical facet is subject to rigorous inspection, with its assessment encompassing a hierarchical structure of tests, which can be classified into in vitro cytocompatibility and in vivo biocompatibility evaluations. Variations in cellular responses to target materials underscore the importance of cytocompatibility assessments, elucidating the intricate relation between cells and materials within controlled, in vitro settings. Although such tests offer valuable insights, they may not consistently align with clinical appraisals. Furthermore, during in vivo biocompatibility assessments, a comprehensive view of metabolic processes is revealed. This holistic perspective allows researchers to understand the complex interactions between the biomaterial and the living system. Detailed analysis of these interactions is crucial for determining the suitability of the material for medical applications. Through such assessments, potential adverse effects can be identified and mitigated, ensuring the safety and efficacy of the biomaterial in clinical use.[17,37–39]

Evaluating the biodegradation rate constitutes a crucial facet in the area of biodegradable electronics. Numerous factors, including but not limited to crystallinity, hydrophilicity, and morphology, significantly influence the pace of biodegradation.[40,41] Depending on their specific applications, the biodegradation rate spans a spectrum from mere hours to extended years. Reactive materials, such as corrosive metals, display instability in physiological conditions, leading to a rapid degradation tempo. In such instances, a reasonable solution is applying a passivating layer, which effectively slows down the biodegradation process.[42] In the fabrication of intricate and advanced biodegradable bioelectronics, the ability to regulate the biodegradation rate is imperative, with the requirement for either on-demand or flexible control contingent upon the specific application.[17] Numerous design approaches have emerged for the fabrication of electroactive materials, considering both biocompatibility and the rate of biodegradation. These strategies encompass a range of options: 1) the utilization of natural materials, 2) the integration of biodegradable synthetic polymers, 3) the incorporation of dissolvable inorganic materials, and 4) harnessing unique living systems with the capacity to break down these materials. Notably, the combination of biodegradable synthetic polymers and

© 2024 The Author(s). Advanced Functional Materials published by Wiley-VCH GmbH

16163028, 2025, 3, Downloaded from https://advanced.onlinelibrary.wiley.com/doi/10.1002/adfm.202413324 by Koc University, Wiley Online Library on [22/05/2025]. See the Terms and Conditions (https://onlinelibrary.wiley.com/terms-and-conditions) on Wiley Online Library for rules of use; OA articles are governed by the applicable Creative Commons License

16163028, 2025, 3, Downloaded from https://advanced.onlinelibrary.wiley.com/doi/10.1002/adfm.202413324 by Koc University, Wiley Online Library on [22/05/2025]. See the Terms and Conditions (https://onlinelibrary.wiley.com/terms-and-conditions) on Wiley Online Library for rules of use; OA articles are governed by the applicable Creative Commons License

natural substances has gained significant traction in biomedical applications.

2. Material Engineering

The inception of bioresorbable electronic systems hinges on a comprehensive grasp of the chemical properties inherent to the materials involved. Practical deployments are governed by timeframes specific to clinical scenarios, imposing varied demands on these materials. Critical to these applications are two temporal benchmarks: operational stability duration and total bioresorption window. Generally, the operational phase is considerably briefer (spanning days to weeks), in stark contrast to the protracted period required for full bioresorption, which usually extends over several months or more. The typical design of bioresorbable systems seeks to narrow the gap between operational stability and the onset of rapid bioresorption, which a specific triggering event may precipitate. Regardless of the mechanism, employing biocompatible materials is imperative to prevent any negative bodily responses throughout the device's operational tenure. Bioresorbable systems typically comprise operational (conductors, semiconductors, or isolators), supportive (such as substrates), and encapsulating elements. The infiltration of biological fluids, either through the dissolution of the outer encapsulation or its permeability, triggers the degradation of the internal functional components, consequently leading to a decline in device performance. Therefore, the disintegration kinetics of the encapsulating layer, along with its permeability—and often that of the supporting substrate—play a pivotal role in defining the functional lifespan of the device, as these factors frequently constitute the rate-limiting steps. Subsequent sections will review the progress in bioresorbable electronic materials, encompassing a review of the most efficacious and prospective candidates. Such materials span both inorganic and organic categories and include conductors, semiconductors, and insulators applied in devices and electronic systems that are entirely bioresorbable.

2.1. Conductors

The bioresorbable conductors can be categorized as inorganic and organic conductors. In the field of inorganic conductors, key material choices encompass alkali-earth metals, such as magnesium (Mg) and calcium (Ca), transition metals including molybdenum (Mo), tungsten (W), zinc (Zn), iron (Fe), and their alloys. These materials are employed in the forms of thin films, foils, micrometer-scale particles, wires, or as part of composites with bioresorbable polymers. The corrosion of such metals is a result of a sequence of electrochemical processes that yield a multifaceted assortment of byproducts. The primary chemical dissolution process for these materials involves electrochemical oxidation, resulting in the production of metal cations (Mn^+) and electrons (e^-), which together constitute the anodic reaction ($M \rightarrow Mn^+ + ne^-$). Concurrently, the cathodic reaction produces additional compounds, including hydroxide ions, dihydrogen, metal hydroxides, and possibly phosphates.[43,44] Thin metallic films of Mg, Zn, Mo, W, and Fe are appealing for their use as electrodes in both active and passive electronic elements, as well as interconnects due to their superior electrical conductivities (with respective values at 20 °C of Mg at 2.3×10^7 S m^{-1}; Zn at 1.7×10^7 S m^{-1}; Mo at 2.0×10^7 S m^{-1}; W at 2.0×10^7 S m^{-1}; Fe at 1.0×10^7 S m^{-1}). Specifically, Mg sheets are increasingly used to implement inductive coils for wireless powering of implantable electronics due to their thicknesses in the 50–200 µm range, resulting in significantly low resistance and power loss.[17] Their conductive properties are complemented by the relative ease of deposition and manufacturing processes.[45] The dissolution rates for thin metallic films of Mg, Zn, W, Mo, and Fe, which are deposited via electron evaporation to thicknesses ranging from several tens to hundreds of nanometers, have been recorded at 480, 300, 20, 0.7, and 7 nm per day, respectively. Similarly, the degradation of 50 µm thick metal foils used as substrates for Mg, Zn, W, Mo, and Fe occurs at rates of 4000, 3500, 150, 20, and 5–80 nm per day, respectively. These rates were measured in Hank's Balanced Salt Solution with a pH of 7.4 at 37 °C.[46–48]

Furthermore, conductive polymers (CPs) present a compelling alternative to conventional metals in organic conductors due to their advantageous processing capabilities and mechanical attributes. Notable examples encompass polypyrrole (PPy), which, when doped with iron(III) chloride [$FeCl_3$], exhibits a conductivity of ≈1.0×10^2 S cm^{-1}; polyaniline (PANI), with a conductivity of 2.8×10^{-2} S cm^{-1} when doped with sulfuric acid; and poly(3,4-ethylene dioxythiophene) (PEDOT), achieving a conductivity of 4.6×10^3 S cm^{-1} when doped with polystyrene sulfonate. Introducing dopants boosts the charge carrier density, leading to enhanced electrical conductivity. While most CPs exhibit chemical stability in physiological environments and are inherently nondegradable, contemporary design, and manufacturing innovations have paved the way for varying degrees of degradability.[49–53]

2.2. Semiconductors

Traditional silicon wafers are deemed nonbiodegradable due to their substantial thickness (on the order of millimeters) and their inherent surface oxides. However, its various configurations in the form of nanomembranes, nanowires, and nanoribbons have been found to fully disintegrate in biological fluids and have been extensively used in the development of bioresorbable implantable biomedical devices. Interestingly, their dissolution timeframes are suitable for real-world use, namely several days to weeks.[17] In general, the dissolution rate is contingent on the size, shape, and surface chemistry of the structure.[54] Research indicates that the bioresorption of silicon is a chemical process where interaction with ambient water molecules produces orthosilicic acid and hydrogen gas by the following reaction $Si + 4H_2O \rightarrow Si(OH)_4 + 2H_2$.[2] Ex vivo experiments reveal that monocrystalline silicon with a thickness of 100 nm dissolves at a rate of ≈2–5 nm per day in phosphate-buffered saline (PBS) (0.1 M, pH 7.4 at 37 °C),[55] in cell culture conditions at body temperature, without negatively affecting cellular metabolic functions.[56]

The specific doping type and concentration within the silicon matrix influence the dissolution kinetics of silicon nanostructures. For instance, doping silicon nanomembranes (NMs) that are 70 nm thick with phosphorus or boron to induce n-type or p-type properties, respectively, markedly decelerates the hydrolysis-induced degradation rates. These rates drop from 3.1 and 2.9 nm per day at lower doping levels (1017–1019 cm^{-3}) to just 0.4 and

© 2024 The Author(s). Advanced Functional Materials published by Wiley-VCH GmbH

16163028, 2025, 3, Downloaded from https://advanced.onlinelibrary.wiley.com/doi/10.1002/adfm.202413324 by Koc University, Wiley Online Library on [22/05/2025]. See the Terms and Conditions (https://onlinelibrary.wiley.com/terms-and-conditions) on Wiley Online Library for rules of use; OA articles are governed by the applicable Creative Commons License

0.2 nm per day when dopant concentrations surpass a critical threshold (≈10^{20} cm^{-3}), as determined by immersing the materials in PBS (0.1 M, pH 7.4 at 37 °C).[57]

Silicon-based nanostructures, such as nanorods, nanowires, and nanoneedles are also viable for integration into bioresorbable frameworks, particularly favored for their potential in minimally invasive and prolonged drug delivery applications.[58] Their appeal lies in the nanoscale dimensions, minimal toxicity, and a measured degradation pace of less than 20 nm per day. The degradation process for these silicon forms is consistent with that of silicon NMs, involving hydrolytic reactions where surface Si bonds are attacked by hydroxide ions (OH^-) present in water.[59] For instance, porous silicon NMs, measuring 900 nm in diameter and 60 µm in length, have been observed to gradually disintegrate over two months within a 1.4% agarose gel bathed in 1 mL of simulated tear fluid at body temperature.[58]

Beyond monocrystalline silicon (mono-Si), alternative manifestations of silicon, including amorphous silicon (a-Si) and polycrystalline silicon (poly-Si), as well as materials like germanium (Ge), silicon-germanium (Si-Ge) alloys, zinc oxide (ZnO), aluminum-doped zinc oxide (Al: ZnO), and indium-gallium-zinc oxide (IGZO, with elements indium [In] and gallium [Ga]), are identified as candidates for fully or partially bioresorbable inorganic semiconductors.[55,60] Silicon-germanium (Si-Ge) alloys, with a thickness of 100 nm, hold significance for their utilization in high-speed electronic applications. The dissolution rate of silicon-germanium (Si-Ge, which holds significance for their utilization in high-speed electronic applications) in PBS (0.1 M, pH 7.4 at 37 °C) is ≈0.1 nm per day, which is nearly 30-fold less rapid than that of monolithic silicon (Si) and germanium (Ge). However, its dissolution kinetics enhanced by ≈185-fold in the presence of bovine serum.[55] A detailed overview of the semiconductor materials and their characteristics are provided in **Table 2**.

2.3. Isolators

Dielectric materials with dissolution capability, such as metal oxides, metal nitrides, and polymers, are suitable for various isolation roles within electronic devices. They can function as gate dielectrics in transistors, isolation layers between conductive pathways or electrodes, protective passivation coatings, structural encapsulation, or foundational substrates. This section will consolidate the latest advancements in bioresorbable isolators.

In the domain of inorganic insulators, recent investigations have focused on silicon dioxide (SiO_2), silicon nitride (Si_3N_4), and magnesium oxide (MgO). These materials can be patterns over various regions of a substrate through several different deposition techniques. This signifies the suitability of these materials for biodegradable implantable microdevices. They have been successfully utilized in the literature for the realization of various electronic components, such as capacitors,[2,61] transistors,[62,63] interlayer barriers,[3,64] and passivation layers.[54,65,66] These materials dissolve in physiological environments through hydrolytic degradation.[66] Constructing multilayered structures of these materials is advantageous to mitigate the influence of pinholes and defects, which is a main challenge in the encapsulation of electronic implants.[66] The chemistry underlying resorption of polymers encompasses four principal pathways: i) Dissolution, where water molecules engage with solvated polymers; ii) Enzymatic reaction, signified by depolymerization under the enzymatic influence; iii) Hydrolysis, which entails depolymerization due to water's action; and iv) Oxidative reaction, where depolymerization is precipitated by reactive oxygen or nitrogen species. For polymers, such as polylactic acid (PLA), polyglycolic acid (PGA), polycaprolactone (PCL), polyamide (PA), and their copolymers like poly(lactic-*co*-glycolic acid) (PLGA), the predominant decomposition products resulting from hydrolysis are extremely small molecular entities comprising lactic acid, glycolic acid, and 6-hydroxyhexanoic acid.[67,68]

Table 2 presents a detailed summary of various materials extensively used in biodegradable implantable electronics, including conductors, semiconductors, and insulators. It provides comprehensive information on their degradation processes, rates, applications, and potential fabrication techniques.

2.4. Encapsulation

When implanting a bioresorbable device, its outermost layer, the encapsulation layer, first interacts with body fluids and surrounding tissues. This layer serves dual purposes: it shields the device from the potentially aggressive internal environment, ensuring its functionality for the intended duration, and it curtails foreign body reactions. The perfect encapsulation layer should lack surface flaws, be water-repellent, resist biofluid permeation, suit the device's function (e.g., not significantly thicken a sensitive pressure sensor's thin diaphragm or diminish an LED's clarity for optogenetic stimulation), and, crucially, be bioresorbable.[132] There's a spectrum of fabrication techniques ranging from simple ones feasible in typical labs (like solution casting or lamination[133]) to advanced methods necessitating cleanroom facilities and high-end equipment, such as plasma-enhanced chemical vapor deposition (PECVD).[134] Some research regarding oxide encapsulation highlighted issues like pinholes in PECVD-deposited oxide and nitride layers, leading to premature infiltration of biofluids into the device. Employing multiple oxide and nitride layers has been suggested to counteract these defects.[66,135] Advanced encapsulation techniques such as layer-by-layer (LbL) assembly,[136–138] electrospinning,[139–142] molecular layer deposition (MLD),[143,144] and microfluidic encapsulation[145–147] offer enhanced barrier properties against biofluids while maintaining biodegradability. LbL assembly provides precise control over thickness and composition,[67] electrospinning produces customizable nanofiber mats,[148] and MLD allows for ultrathin, defect-free layers with molecular precision.[149] Microfluidic encapsulation ensures uniform coverage and enhanced barrier properties. Emerging techniques like in situ polymerization, sol–gel processing, and ionic crosslinking further improve encapsulation by forming intimate, robust, and multifunctional protective layers.[150–152] Advanced biodegradable polymers like poly(lactic-*co*-glycolic acid) (PLGA), polycaprolactone (PCL), polydioxanone (PDO), and polylactic acid (PLA) are used to create encapsulation layers that degrade at controlled rates, matching the device's lifespan.[48] By integrating these advanced and emerging encapsulation techniques, the performance and longevity of biodegradable implantable bioelectronics can be significantly

© 2024 The Author(s). Advanced Functional Materials published by Wiley-VCH GmbH

Table 2. A list of biodegradable materials used in the fabrication of transient electronics along with their characteristics.

Material classification		Materials type[a)]	Degradation process	Degradation metrics	Degradation environment	Deposition methods	Mechanical Properties	Thermal Properties	Applications	Refs.
Conductors	Inorganic	Mg/Mg alloys	Hydrolysis: $Mg + 2H_2O \rightarrow Mg(OH)_2 + H_2$	0.05–0.5 µm h^{-1} [69]	pH 7.4 SBF 37 °C[69,70]	Sputtering, e-beam, thermal evaporation, ALD, DLD	Good compressive and tensile strength	Thermal stability through alloying	Implants, stents, orthodontic devices, electrodes	[71–73]
		Mo	Hydrolysis: $2Mo + 2H_2O + 3O_2 \rightarrow 2H_2MoO_4$	20 nm day^{-1}	PBS (pH 7.4) at 37 °C[74]	Sputtering, PECVD, ALD	High strength and stiffness	High thermal conductivity, low thermal expansion	Flexible & stretchable electronics, implants, supercapacitors	[75–77]
		W	Hydrolysis: $2W + 2H_2O + 3O_2 \rightarrow 2H_2WO_4$	150 nm day^{-1}	HBSS at room temperature[69]	E-beam, PVD, ALD, LCVD	High creep resistance, brittle in low temperatures	High melting point, good thermal conductivity	Flexible & stretchable electronics, implants	[76,78]
		Fe	Hydrolysis: $4Fe + 3O_2 + 10\ H_2O \rightarrow 4Fe(OH)_4 + 4H$	100 nm day^{-1}	HBSS at 37 °C[69]	Vacuum magnetron sputtering, SLM, CVD, PLD	High strength, high elastic modulus, high ductility	High thermal conductivity, high melting point	Implants, stents, batteries, inks & pastes	[79–81]
		Zn	Hydrolysis: $Zn + 2H_2O \rightarrow Zn(OH)_2 + H_2$	5×10^{-3} [69,82]	In vivo[69]	Magnetron sputtering deposition, ALD	Low toughness, generally brittle, high impact strength through alloying	Moderate thermal conductivity, relatively low melting point	Implants, stents, batteries	[83,84]
		Highly doped Si NM	Hydrolysis	0.01–398.11 nm day^{-1}	(In aqueous solutions pH 2.6–8.2)[85]	Thermal evaporation, solid state diffusion + SOI wafer	Enhanced flexibility in nanomembrane form	High thermal stability	Electronics, wearable sensors, interface for neural recordings	[59,86]
	Synthetic polymer	DCPU	Hydrolysis and enzymatic	12%–14% (in 8 weeks)	PBS (pH 7.4) at 37 °C	Polymerization	Good balance of strength and flexibility	Moderate thermal conductivity, low thermal expansion	Flexible & stretchable electronics, electrodes, scaffolds, inks & coatings	[87]
		PGAP	Hydrolysis	50% (in 70 days)	PBS (pH 7.4) at 37 °C	Polymerization	–	–	Scaffolds, drug carriers, films & coatings	[88]
		HPLAAT	Hydrolysis	40%–45% (in 3 days)	PBS (pH 7.4) at 37 °C	Polymerization	Excellent ductility	Good thermal stability	Scaffolds, ductile electroactive materials	[52]

(*Continued*)

© 2024 The Author(s). Advanced Functional Materials published by Wiley-VCH GmbH

16163028, 2025, 3, Downloaded from https://advanced.onlinelibrary.wiley.com/doi/10.1002/adfm.202413324 by Koc University, Wiley Online Library on [22/05/2025]. See the Terms and Conditions (https://onlinelibrary.wiley.com/terms-and-conditions) on Wiley Online Library for rules of use; OA articles are governed by the applicable Creative Commons License

Table 2. (Continued)

Material classification	Materials type[a)]	Degradation process	Degradation metrics	Degradation environment	Deposition methods	Mechanical Properties	Thermal Properties	Applications	Refs.
Composite	PPy/PLA	Hydrolysis	14%–24% (in 12 weeks)	PBS (pH 7.4) at 37 °C	Sputtering	Elastic & flexible	High thermal diffusivity, enhanced thermal conductivity	Flexible electronics, scaffolds, nanofibers	[50,89]
	PPy/SF	Enzymatic	82% (in 15 days)	PBS (pH 7.4) at 37 °C	Chemical deposition	Enhanced mechanical stability	Enhanced thermal stability	Biobatteries, nanofibers, coatings, flexible electronics	[90,91]
	SPT/PEI	Hydrolysis	100% (in 12–18 weeks)	PBS (pH 7.4) at 37 °C	Chemical deposition	High tensile strength	High thermal stability	Tissue engineering	[51,92]
Semiconductors Natural polymer	Melanin	Enzymatic	100% (in 8 weeks)	In vivo condition	Electrochemical deposition	Low tensile strength, soft	High thermal stability	Electrochemical sensors, batteries	[93–95]
Inorganic	Ge	Hydrolysis: $Ge + O_2 + H_2O \rightarrow H_2GeO_3$	3.1 nm day^{-1}	Buffer solutions (pH 7.4) at 37 °C[55]	PECVD	Low tensile strength	Moderate thermal conductivity, high melting point	Implants, batteries, thin films, imaging	[60]
	Si-Ge	Hydrolysis	0.1 nm day^{-1}	Buffer solutions (pH 7.4) at 37 °C[55]	LPCVD	Low residual stress, high fracture strength	High thermal stability, moderate thermal conductivity	Flexible electronics, thin films, optoelectronics	[55,96]
	Amorphous Si	Hydrolysis: $Si + 4H_2O \rightarrow Si(OH)_4 + 2H_2$	4.1 nm day^{-1}	–	LPCVD	Limited elasticity, hard	Lower thermal conductivity than crystal Si	Thin-film transistors, sensors	[97]
	Polycrystalline Si	Hydrolysis: $Si + 4H_2O \rightarrow Si(OH)_4 + 2H_2$	2.8 nm day^{-1}	–	LPCVD	Lower tensile strength than crystal Si	Lower thermal conductivity than crystal Si	Implants, thin films, biomedical electronics	[98]
	Si NM	Hydrolysis: $Si + 4H_2O \rightarrow Si(OH)_4 + 2H_2$	0.01–398.11 nm day^{-1}	Aqueous solutions pH 2.6–8.2)[85]	Silicon wafer, SOI wafer	Higher flexibility and stretchability in reduced thickness	Low thermal conductivity in reduced thickness	Flexible electronics, sensors	[59,99,100]
	ZnO	Hydrolysis: $ZnO + H_2O \rightarrow Zn(OH)_2$ $ZnO + H_2O \rightarrow Zn^{2+} + 2OH$	100 nm day^{-1}	PBS (pH 7.4) at 37 °C	Sputtering	High fracture strain, lower elastic modulus in nanowire form	Low thermal expansion, high melting temperature	Thin-film transistors, nanocarriers	[101]
Synthetic polymer	PDPP-PD	Hydrolysis	100% (in 40 days)	PBS (pH 4.6) at 37 °C	Spin coating	Moderate tensile strength	Low thermal conductivity	Flexible electronics, transient electronics	[102,103]

(*Continued*)

© 2024 The Author(s). Advanced Functional Materials published by Wiley-VCH GmbH

16163028, 2025, 3, Downloaded from https://advanced.onlinelibrary.wiley.com/doi/10.1002/adfm.202413324 by Koc University, Wiley Online Library on [22/05/2025]. See the Terms and Conditions (https://onlinelibrary.wiley.com/terms-and-conditions) on Wiley Online Library for rules of use; OA articles are governed by the applicable Creative Commons License

Table 2. (Continued)

Material classification		Materials type[a)]	Degradation process	Degradation metrics	Degradation environment	Deposition methods	Mechanical Properties	Thermal Properties	Applications	Refs.
Insulators/ Dielectrics	Inorganic	SiO_2	Hydrolysis: $SiO_2 + H_2O \rightarrow Si(OH)_4$	1.4 nm day^{-1}	PBS (pH 4.6) at room temperaturef.[66] –rate varies from 4.7×10^{-4} µm h^{-1} to 282 nm day^{-1} depending on pH, ion concentration, temperature, and deposition methods	Thermal oxidation, PECVD, e-beam, ALD, sputtering deposition	High hardness and strength	Low thermal conductivity, high thermal stability	Drug delivery systems	[104]
		Si_3N_4	Hydrolysis: $Si_3N_4 + 6H_2O \rightarrow 2SiO_2 + 4NH_3$	0.16 nm day^{-1}	Buffer solutions (pH 7.4) at 37 °C[66]	PECVD, LPCVD	High wear resistance, high strength, and ductility	High thermal stability, high melting point, thermoschock resistant	Orthopedic applications	[105,106]
	Natural polymer	Cellulose	Enzymatic	Several hours to thousands of years[107]	Conditions not available	Spin coating	High tensile strength	Low thermal conductivity	Tissue engineering, drug delivery systems	[108,109]
		Silk fibroin (SF)	Hydrolysis and enzymatic	In 4 weeks	Protease solution	Electrospinning, spin coating	Flexible, high tensile strength	High thermal stability	Textiles, sutures, tissue engineering, drug delivery, sensors	[110,111]
	Natural polyester	Shellac	Hydrolysis	1% (after 2 h for 100 µm thickness)	–	Solution casting	Moderate tensile strength	Low thermal conductivity, low melting point	Tissue engineering, drug delivery systems, dielectric layers in OFETs	[112]
	Synthetic elastomer	PGS	Enzymatic	150% (after 70 days)	PBS (pH 7) at 37 °C[107]	Solution casting	High elasticity	Low melting point	Tissue engineering, drug delivery, biomedical adhesives	[113,114]
		POMaC	Hydrolysis	77% (in 10 weeks)	PBS (pH 7.4) at 37 °C	Spin coating	Tunable initial modulus, high elongation at break	Good thermal stability	Scaffolds, heart patches, temporary implants	[115,116]
	Synthetic polyester	PBS	Hydrolysis and enzymatic	70% (after 72 h)	PBS (pH 7.4) at 37 °C[107]	Solution casting	High ductility	Good thermal stability	Textiles, wearable electronics, orthopedic applications, drug encapsulation systems	[117]

(*Continued*)

© 2024 The Author(s). Advanced Functional Materials published by Wiley-VCH GmbH

16163028, 2025, 3, Downloaded from https://advanced.onlinelibrary.wiley.com/doi/10.1002/adfm.202413324 by Koc University, Wiley Online Library on [22/05/2025]. See the Terms and Conditions (https://onlinelibrary.wiley.com/terms-and-conditions) on Wiley Online Library for rules of use; OA articles are governed by the applicable Creative Commons License

Table 2. (Continued)

Material classification	Materials type[a)]	Degradation process	Degradation metrics	Degradation environment	Deposition methods	Mechanical Properties	Thermal Properties	Applications	Refs.
	PLA	Hydrolysis	64% (in 12 months)	PBS (pH 7.4) at 37 °C	Electrospinning	High tensile modulus and yield strength	Low thermal conductivity	Implants, sutures, textiles, drug delivery systems	[118]
	PCL	Hydrolysis	3% (in 5 weeks)	PBS (pH 7.4) at 37 °C	Spin coating	High toughness, moderate tensile strength	Low melting point	Implants, sutures, drug delivery systems, adhesion barrier	[119–121]
Synthetic polymer	PA	Hydrolysis	100% (in 3–4 days)	PBS (pH 7.4) at 37 °C	Polymerization	Enhanced mechanical properties by polymer structure modification	Enhanced thermal properties by polymer structure modification	Tissue engineering, drug delivery systems,	[122]
	PVA	Hydrolysis	100% (in 30 min)	PBS (pH 7.4) at 37 °C	LbL deposition, electrospinning, electroblowing	Good balance of strength and flexibility	Low thermal conductivity, decomposes before melting	Tissue engineering, surgical threads & sponges, textiles	[123,124]
Composite	PBS/natural graphite	–	–	–	Solution casting	Flexible	–	Dielectrics	[125]
	PBS/PANI	–	–	–	Compression molding	Improved crystallinity	Enhanced thermal stability	Supercapacitors, batteries, sensors	[126,127]
Inorganic	Doped β-TCP	Hydrolysis: 3β-$Ca_3(PO_4)_2 + H_2O \rightarrow Ca_9(HPO_4)(PO_4)_5OH$	8% (in 20 days)	–	Electrospinning	Inherently brittle, low tensile properties	High thermal stability	Bone grafts, dental applications	[128–131]

[a)] Mg: Magnesium, Mo: Molybdenum, W: Tungsten, Fe: Iron, Zn: Zinc, Si: Silicon, DCPU: Dopant-free conductive polyurethane, PGAP: Poly[(glycine ethyl ester) (aniline pentamer) phosphazene, HPLAAT: Hyperbranched ductile polylactide copolymerized with aniline tetramer, PPy: Polypyrrole, PLA: Poly(lactic acid), PLLA: Poly-l-lactic Acid, SF: Silk Fibroin, SPT: poly[ammonium(3-thienyl)ethoxypropanesulfonate], PEI: poly(ethyleneimine), Ge: Germanium, ZnO: Zinc oxide, PDPP-PD: poly(diketopyrrolopyrrole-pphenylenediamine), SiO_2: Silicon dioxide, Si_3N_4: Silicon nitride, PGS: Polyglycerol sebacate, POMaC: Poly(octamethylene maleate (anhydride) citrate), PBS: Poly (Butylene Succinate), PCL: Polycaprolactone, PA: Polyanhydride, PVA: Polyvinyl alcohol, PANI: Polyaniline, β-TCP: Beta tricalcium phosphate, β-TCP: Beta tricalcium phosphate, DCPU: Dopant-free conductive polyurethane, Fe: Iron, Ge: Germanium, HPLAAT: Hyperbranched ductile polylactide copolymerized with aniline tetramer, Mg: Magnesium, Mo: Molybdenum, PANI: Polyaniline, PA: Polyanhydride, PBS: Poly (Butylene Succinate), PCL: Polycaprolactone, PDPP-PD: poly(diketopyrrolopyrrole-pphenylenediamine), PEI: poly(ethyleneimine), PGAP: Poly[(glycine ethyl ester) (aniline pentamer) phosphazene, PLA: Poly(lactic acid), POMaC: Poly(octamethylene maleate (anhydride) citrate), PPy: Polypyrrole, PGS: Polyglycerol sebacate, PVA: Polyvinyl alcohol, SF: Silk Fibroin, Si: Silicon, SiO_2: Silicon dioxide, Si_3N_4: Silicon nitride, SPT: poly[ammonium(3-thienyl)ethoxypropanesulfonate], W: Tungsten, Zn: Zinc, ZnO: Zinc oxide.

© 2024 The Author(s). Advanced Functional Materials published by Wiley-VCH GmbH

16163028, 2025, 3, Downloaded from https://advanced.onlinelibrary.wiley.com/doi/10.1002/adfm.202413324 by Koc University, Wiley Online Library on [22/05/2025]. See the Terms and Conditions (https://onlinelibrary.wiley.com/terms-and-conditions) on Wiley Online Library for rules of use; OA articles are governed by the applicable Creative Commons License

Table 3. A list of biodegradable materials used in the fabrication of encapsulation layers of the transient electronics.

Classification and material type		Materials	Degradation process	Degradation environment	Degradation metrics	Transition temperature T_g [°C]	Young's Modulus E [GPa]	Refs.
Encapsulation	Inorganic	MgO	Hydrolysis	–	–	–	249	[2]
		SiO_2	Hydrolysis: $SiO_2 + H_2O \rightarrow Si(OH)_4$	PBS (pH 4.6) at room temperature[66] —rate varies from 4.7×10^{-4} μm h^{-1} to 282 nm day^{-1} depending on pH, ion concentration, temperature, and deposition methods	1.4 nm day^{-1}	1475	75	[66,104,153]
		Si_3N_4	Hydrolysis: $Si_3N_4 + 6H_2O \rightarrow 2SiO_2 + 4NH_3$	Buffer solutions (pH 7.4) at 37 °C[66]	0.16 nm day^{-1}	1056.85	120–315.05	[66,105,106,153]
	Natural polymer	Candelilla wax organogel 5%	Hydrolysis: 300 μm thickness	–	0.1 mg cm^{-1} in 7.5 days	35.58	0.0001	[154–156]
		Collagen	Hydrolysis	–	60% weight loss in 5 weeks	35	10	[157–159]
		Silk fibroin (SF)	Hydrolysis and enzymatic	Protease solution	4 weeks	175	14-36	[110,111]
	Synthetic polymer	PCL	Hydrolysis	PBS at 37 °C[107]	48.7% (in 45 months)	−60	24.6	[160–162]
		PHB	Hydrolysis	In soil at 58 °C[107]	80% (in 35 days)	120	3–3.5	[135]
		PHB/PHV (PHB/V or PHBV)	Hydrolysis	PBS (pH 7.2) at 37 °C[107]	2.5% (in 300 days)	–	1.7	[135]
		PLA	Hydrolysis	PBS (pH 7.4) at 37 °C	64%	60	4.107	[118]
		PLGA	Hydrolysis	–	100% weight loss in 50 days	37	0.092	[163,164]
		PLLA	Hydrolysis	–	100% weight loss in 42–70 days	58	10-20	[159,165]
		PMMA	Enzymatic	PBS (pH 7.5) at 37 °C[107]	0.05 mg cm^{-1} weight loss in 70 h	116	3	[166]
		POMaC	Hydrolysis: 1000 μm thickness	–	80% weight loss in 10 weeks	−80	0.00 029	[115]
		Polyanhydeides	Enzymatic	–	100% weight loss in 14 days	92	1.28	[167,168]
		PU	Enzymatic	–	100% weight loss in 100 h	−41	0.016	[169,170]
		PVA	Hydrolysis	–	100% (in 90 days)[107]	77	0.00032	[171,172]

© 2024 The Author(s). Advanced Functional Materials published by Wiley-VCH GmbH

16163028, 2025, 3, Downloaded from https://advanced.onlinelibrary.wiley.com/doi/10.1002/adfm.202413324 by Koc University, Wiley Online Library on [22/05/2025]. See the Terms and Conditions (https://onlinelibrary.wiley.com/terms-and-conditions) on Wiley Online Library for rules of use; OA articles are governed by the applicable Creative Commons License

16163028, 2025, 3, Downloaded from https://advanced.onlinelibrary.wiley.com/doi/10.1002/adfm.202413324 by Koc University, Wiley Online Library on [22/05/2025]. See the Terms and Conditions (https://onlinelibrary.wiley.com/terms-and-conditions) on Wiley Online Library for rules of use; OA articles are governed by the applicable Creative Commons License

enhanced, ensuring their functionality and biocompatibility in the challenging internal environment of the body.[17] **Table 3** provides some of the most important materials used for the encapsulation of implantable transient electronics.

3. Application-Specific Transient Biomedical Implants

The convergence of biodegradable materials with their sensing/biosensing capabilities has captured the attention of clinical researchers.[17] These systems enable real-time assessment of vital physiological metrics, such as tissue-specific strain/pressure, temperature, pH, and oxygen levels and provide on-demand tissue/nerve stimulation, offering immense potential in personalized medical scenarios, including postoperation monitoring and wound healing.[3,173] Additionally, these biodegradable sensors present a solution to growing concerns about medical waste disposal.[174] The journey of biodegradable sensors commenced in the past decade, anchored in degradable materials.[175,176] Including advanced technological elements, encompassing electrical circuits, power sources, and wireless modules, further enriched its trajectory. Yet, active research is being done in material sciences with the aim of identifying novel materials and new fabrication techniques that seamlessly blend superior electrical and mechanical properties with biocompatibility and nontoxicity.[176] Such materials must also have inherent flexibility to mitigate immoderate stress on adjacent soft tissues. Drawing from naturally available, renewable materials with biocompatibility and biodegradability appears to be the ideal avenue for creating these sensors.[177,178] This review will spotlight the diverse applications of transient bioanalytical tools in various body systems, particularly emphasizing their significance in continuous postsurgical health monitoring. **Figure 2** illustrates the application of bioresorbable implants in the human body for postsurgery monitoring. Six major physiological systems can be addressed across the body (nervous, visual, circulatory, digestive, integumentary, and musculoskeletal). Furthermore, an overview of these devices with their application in various body systems is provided in **Table 4**, and in the rest of the paper we provide a detailed overview of their application-specific properties.

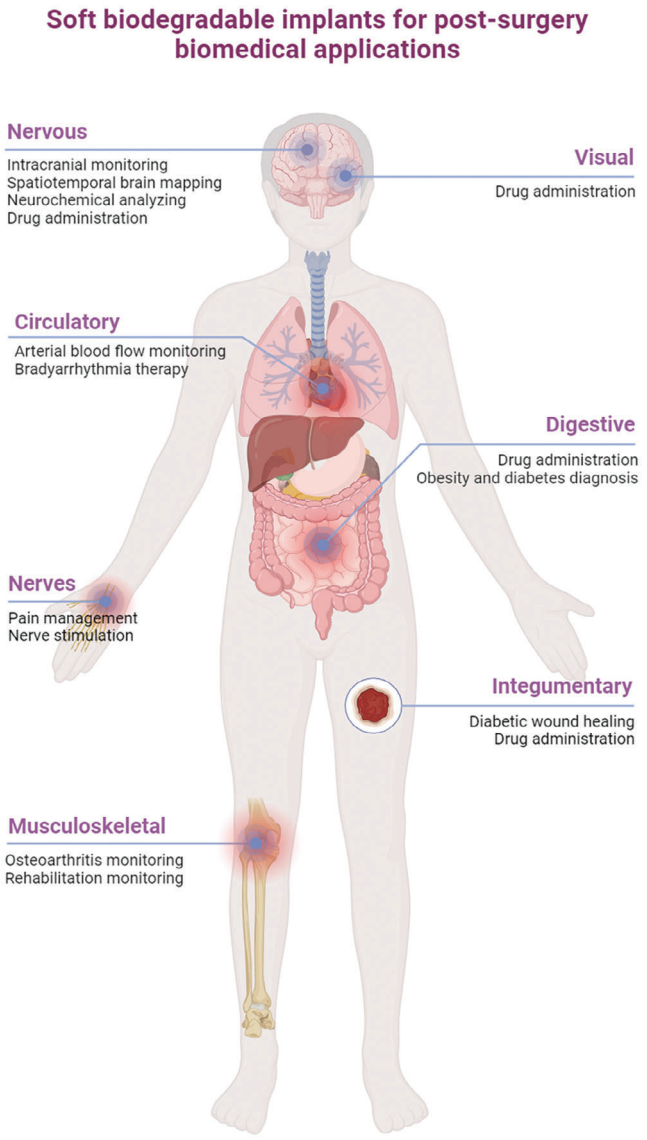


Figure 2. Application of bioresorbable implants in the human body for postsurgery monitoring. Six major physiological systems can be accessed across the body (nervous, visual, circulatory, digestive, integumentary, and musculoskeletal). (created with BioRender.com).

3.1. Sensors

3.1.1. Physical Sensors

Rehabilitation Monitoring: The capacity for continuous, real-time tracking of tendon modifications due to mechanical influences can significantly enhance the formulation of individualized rehabilitation strategies. In this context, implantable biosensors must ensure accurate and instantaneous assessments of both strain and pressure dynamics. Notably, the magnitude and pace of strain are critical biochemical parameters in gauging soft tissue health and postoperative recovery.[203] To be truly effective, these sensing technologies should encompass several key attributes: i) the ability to discern inherent strains of tendons, notably those less than 10%, without impeding their natural function,[203,204] ii) the capability to gauge pressure applied to recuperated areas, an indicator directly linked to the healing timeline,[203] and iii) a composition entirely of biodegradable components, circumventing the necessity for a secondary surgical procedure for sensor removal.

An implantable and biodegradable sensor was developed by Boutry et al. to measure pressure and strain in real time and concurrently.[199] Vertical configurations were adopted in the sensor's design, ensuring discrete detection of both pressure and strain, devoid of any signal interference. The strain transduction mechanism was based on a pair of thin film comb Mg electrodes. External strain induced a relative shift between these electrodes, leading to perceptible variations in the sensor's capacitance. Drawing from their earlier research, they harnessed poly(glycerol sebacate) to engineer a pyramid-like framework

 © 2024 The Author(s). Advanced Functional Materials published by Wiley-VCH GmbH

Table 4. Body system integrated bioresorbable implants and specifications.

Body system	Biomedical application	Device materials	Device components	Fabrication technique	Possible biomedical function	Clinical application specifications	System-level integration	Powering and data reading method
Nervous	Intracranial monitoring[48,104,179]	(Nanoporous silicon, PLGA, SiO_2, Si-NM),[48] (Si-NM, Si, t-SiO_2),[104] (PLA, Mg, PLGA, BPT)	(Pressure and temperature sensors)[48,104] Pressure[179]	Photolithographic (nanoporous Si trench)[48,104] Laser ablation[179]	intracranial pressure (ICP) monitoring in traumatic brain injury (TBI),[180] stroke management,[181] and neurosurgical Procedures[182]	Dynamic range of > 0–100 mmHg, Temperature > 37 °C, Continuous monitoring, Sensor stability for days, weeks, or months (depends on disease severity)	No[48],[104] Yes[179]	(Wire connection)[48,104] (inductive coupling)[179]
	Spatiotemporal mapping of electrical activity[3,183]	(PLGA, Si, SiO_2, Si-NM)[3] (PLLA:PCL, Tungsten)[183]	Multiplexed electrodes array[3,183]	Photolithographic[3,183]	ECoG and EEG (Parkinson's disease,[184] epilepsy,[185] guiding surgical procedures on complex, interconnected peripheral nerve structures[186]	Direct attachment to the exposed cortex, electrode contacts ranging from 4 to 256, flexible electrodes	Yes (external readout electronics)[3,183]	Wire connection[3,183]
	Neurochemical analyzer[187,188]	(PLGA, Si-NM, Mo, MoS_2, Mg)[187] (PCL, Si-NM, SiO_2, Fe^{3+}_CPPY, Mg)[188]	(Dopamine sensor, pH sensor, temperature sensor, epinephrine sensor)[187] Dopamine sensor[188]	Photolithographic[187,188]	Assessment and treatment of postoperative complications	Temperature > 37 °C, Continuous monitoring, Sensor stability for days, weeks, or months (depending on surgery severity), dopamine concentration depends on surgery type and the location on the brain	Yes (external readout electronics)[187] No[189]	Wire connection[187,188]
	Blood–brain barrier opening and drug-administration[190,191]	(PLLA, Mo)[190] (PLA, PLGA, Mg)[191]	(Ultrasonic transducer)[190] (temperature sensor, heater, drug reservoir)[191]	PLA film electrospinning,[190] Photolithographic[191]	Drug administration[190] temperature measurement and drug administration[191]	Localized delivery, sustained release with dosage adjustments, delivery in different treatment cycles[192]	No[193] Yes[191]	Wire connection[190] Inductive coupling[191]
	Pain management[189]	PLGA, Mo, Mg, conductive wax	Blocking and extension electrodes, electrical connections	Photolithographic	Peripheral nerve stimulation	Biphasic pulses with appropriate inter-phase delay, pulse frequencies around 20 Hz, pulse durations range from 1 to 300 µs, stimulation per session: 20–60 min, stimulation intensity from 3 to 30 V.	No	Wire connection[189]
	Nerve stimulation[193]	PLGA, Mo, Si NM, b-DCPU	Stimulation cuff, stretchable electrode, inductor coil	electrospinning process	Neuromuscular regeneration		Yes	Inductive coupling

(*Continued*)

© 2024 The Author(s). Advanced Functional Materials published by Wiley-VCH GmbH

16163028, 2025, 3, Downloaded from https://advanced.onlinelibrary.wiley.com/doi/10.1002/adfm.202413324 by Koc University, Wiley Online Library on [22/05/2025]. See the Terms and Conditions (https://onlinelibrary.wiley.com/terms-and-conditions) on Wiley Online Library for rules of use; OA articles are governed by the applicable Creative Commons License

Table 4. (Continued)

Body system	Biomedical application	Device materials	Device components	Fabrication technique	Possible biomedical function	Clinical application specifications	System-level integration	Powering and data reading method
Visual	Drug administration[58]	Si nanoneedles, PVA	Nanoneedles	Photolithographic	Drug release	Slowly release antibiotic, treatment period of a few weeks to a month.	Passive	Passive
Circulatory	Arterial blood flow[194]	Mg, PGS, POMaC, PLLA	Pressure sensor, inductor coil	Bench-top process	Real-time postmicrosurgical anastomoses monitoring	Small and conformal structure, high sensitivity. Material selection based on surgery severity and duration of healing process.	Yes	Inductive coupling
	Bradyarrhythmia therapy[195]	W/Mg, Si-NM, PLGA	Inductor coil, diode, contact pads	Photolithographic	Pacemaker	Pacing voltage ≈0.5 V, Pacing rate: 60–100 beats min^{-1},	Yes	Inductive coupling
Digestive	Obesity and diabetes diagnosis[196]	PLGA, Mo, Zn, Mo-W	Glucose sensor, temperature sensor, oxygen sensor, and external reader	Screen printing	Personalized continuous glucose monitoring	Capable of covering large dynamic range of hypoglycemic levels (below 70 mg dL^{-1}), euglycemic levels (70–180 mg dL^{-1}), and hyperglycemic levels (above 180 mg dL^{-1}).	Yes (external readout electronics)	Wire connection
Integumentary	Diabetic wound healing[197]	Mo	Flexible electrodes	Laser ablation	Electrotherapy	Treatment durations of 4 – 12 months, soft and flexible electrodes	Yes (external readout electronics)	Wire connection
	Drug administration[198]	Silk, Mg, MgO	Inductor loop and heater	Chemical-free processes (shadow mask deposition for the Mg, thin-film casting for the silk substrates, and low-temperature embossing)	Drug release (ampicillin solution)	Small and conformal size, constant rate drug delivery or drug delivery on demand,	Yes	Inductive coupling

(*Continued*)

© 2024 The Author(s). Advanced Functional Materials published by Wiley-VCH GmbH

16163028, 2025, 3, Downloaded from https://advanced.onlinelibrary.wiley.com/doi/10.1002/adfm.202413324 by Koc University, Wiley Online Library on [22/05/2025]. See the Terms and Conditions (https://onlinelibrary.wiley.com/terms-and-conditions) on Wiley Online Library for rules of use; OA articles are governed by the applicable Creative Commons License

Table 4. (Continued)

Body system	Biomedical application	Device materials	Device components	Fabrication technique	Possible biomedical function	Clinical application specifications	System-level integration	Powering and data reading method
Musculoskeletal	Rehabilitation[199]	PGS, PLLA, Mg, POMaC	Capacitor	Molding	Mechanical forces on tendons	Highly sensitive with wide dynamic range from kPa to less than a Pa	No	Wire connection
	Osteoarthritis monitoring[200,201]	PLLA–PTMC, Au	No sensor	Shadow mask	Nitric oxide detection and quantification	Dynamic range from the low nanomolar (e.g., 1–10 nM) to the low micromolar (e.g., 1–10 µM) range, results should be available in less than	No	Wire connection
	Bone fracture healing promotion[202]	PLGA, Mg, P-PLGA	Triboelectric nanogenerator and interdigitated electrodes	Molding and lithography	Nonpharmacological treatment in orthopedic	Stimulation voltage between 1 and 100 V, Frequency depend on application: for pain relief is 1–20 Hz and for muscle stimulation is between (30–100 Hz), duration of stimulation pulse between 50–300 ms, and treatment duration from 5 to 30 min	Yes	In vivo powering

that served as the pressure sensor's dielectric layer. Such a design meant that external pressure variabilities altered the proximity between the Mg electrodes' top and bottom layers, subsequently influencing capacitance. To enhance the lifetime of the sensor against degradation, specifically surface erosion, the sensor was encapsulated in poly(octamethylene maleate (anhydride) citrate)—which is a flexible, stretchable, and biodegradable polymer. In subsequent in vivo experiments the fabricated sensor exhibited proper operation for 3.5 weeks postimplantation. In a related research,[201] a fiber-based strain sensor was conceptualized for the real-time assessment of standard orthopedic strain pressures. The designed sensor exhibited efficiency in identifying minute tensile strains within connective tissue, attributed to its fiber-centric passive RLC circuitry and capacitive fibers susceptible to saturation. The strain sensor was composed of twin fibers in a helical formation surrounding a vacant core. The sensor's functionality could be tailored to specific needs by modifying its helical configuration. This sensor was constructed from highly conductive, stretchable fibers based on a blend of silver nanoparticles (AgNPs) and elastomeric strands. In vivo validation on a minipig's Achilles tendon demonstrated a resonant frequency shift of ≈1.45 at 25.21 MHz, which corresponds to an estimated 3.9% strain variation in the fiber sensor, aligning closely with the anticipated physiological strain observed in an Achilles tendon.

In a recent study aimed at advancing nerve injury recovery evaluation, Shan et al. developed a biodegradable piezoelectric sensor (PBPS) for real-time assessment of motor function recovery after nerve injury.[205] The sensor was designed using PLA fibers doped with barium titanate nanoparticles, enhancing the material's piezoelectric properties. The PBPS sensor converts biomechanical motion signals into electrical signals, allowing wireless monitoring of motor function recovery in vivo. The study involved implanting the PBPS sensor into a rat model with sciatic nerve injury. The sensor was placed subcutaneously near the injury site, and a wireless module was used to transmit real-time data on motor function recovery. As the rats moved, the sensor detected deformation caused by leg movements, generating electrical signals corresponding to mechanical motion. The output from the PBPS was consistent with traditional electromyographic (EMG) signals, demonstrating the effectiveness of the sensor in evaluating nerve recovery. In addition to its piezoelectric sensing capabilities, the PBPS was designed to be fully biodegradable, with poly-l-lactic Acid (PLLA) and polycaprolactone (PCL) as the main materials, both approved by the Food and Drug Administration (FDA) for biomedical use. The sensor exhibited high flexibility and biocompatibility, ensuring safe implantation without causing significant inflammation or fibrous encapsulation. Furthermore, the sensor's materials degraded within a stable operational timeframe, reducing the need for surgical removal. The PBPS demonstrated a high degree of linearity between applied force and output voltage ($R^2 = 0.9445$), and it maintained performance stability over 1500 cycles of mechanical stress.

Cardiovascular Monitoring: In a separate study aimed at propelling advancements in cardiovascular monitoring, Boutry et al. developed a wireless biodegradable sensor dedicated to blood flow monitoring that can be seamlessly implanted into the body without wires for data reading or power transmission.[194] The device incorporated a fringe-field capacitive sensor for pressure

© 2024 The Author(s). Advanced Functional Materials published by Wiley-VCH GmbH

16163028, 2025, 3, Downloaded from https://advanced.onlinelibrary.wiley.com/doi/10.1002/adfm.202413324 by Koc University, Wiley Online Library on [22/05/2025]. See the Terms and Conditions (https://onlinelibrary.wiley.com/terms-and-conditions) on Wiley Online Library for rules of use; OA articles are governed by the applicable Creative Commons License

16163028, 2025, 3, Downloaded from https://advanced.onlinelibrary.wiley.com/doi/10.1002/adfm.202413324 by Koc University, Wiley Online Library on [22/05/2025]. See the Terms and Conditions (https://onlinelibrary.wiley.com/terms-and-conditions) on Wiley Online Library for rules of use; OA articles are governed by the applicable Creative Commons License

monitoring and a bilayer Mg inductor coil facilitated wireless data transfer through inductive coupling. After device implantation, the arterial dilation modulates capacitance, affecting the resonant frequency f_0 of the inductor-capacitor–resistor (LCR) resonator. An external vector network analyzer (VNA) was employed for wireless interrogation of f_0 shifts. A major constraint of this system was its dependency on a superficial reading device, necessitating proximity (on the scale of a millimeter) to the implantation site for data collection. Overcoming such hurdles could expedite the clinical adoption of these biodegradable pressure sensors, especially pertinent in monitoring minute vessel pressures postsurgery, such as during cardiovascular procedures and organ transplants where vascular anastomosis is performed to examine blood flow.

In another study aimed at enhancing cardiovascular postoperative care, Ouyang et al. developed a bioresorbable dynamic pressure sensor that can be implanted in vivo for real-time monitoring of vascular conditions postsurgery.[206] The working mechanism of this sensor is based on the triboelectric effect, which allows it to convert ambient pressure change into electrical signals. The bioresorbable triboelectric sensor (BTS) has two layers made of PLA-chitosan films and Mg electrodes. Furthermore, the BTS was made with antibacterial and biocompatible materials, guaranteeing that it breaks down safely in vivo in about 84 days and has a 5-day service life for postoperative care. After 450 000 cycles, the sensor's output stayed constant, demonstrating its robustness for real-time monitoring applications. Device degradation was tested in PBS to simulate in vivo environment, and its biocompatibility and antibacterial properties were validated through in vitro cell viability tests and antibacterial assays using PLA/C materials. The sensor detects pressure changes within blood vessels, and the contact-separation mechanism of the triboelectric layers, influenced by diastolic and systolic phases of blood pressure, produces an electrical output proportional to the applied pressure. The BTS was able to track aberrant vascular occlusion episodes due to its high linearity (R^2 = 0.993) and sensitivity (11 mV $mmHg^{-1}$). The device showed promise for use in the prognosis of cardiovascular surgery when implanted in dogs for testing and effectively detected five simulated blood artery blockage occurrences.

Intracranial Monitoring: Intracranial monitoring devices are crucial for developing therapeutic strategies and excel in continuously and precisely monitoring temperature and pressure conditions in the brain.[207–209] One significant hurdle in advancing bioabsorbable sensors for intracranial monitoring involves ensuring uniform mechanical properties and electrophysical or optoelectronic performance during immersion in biological fluids. These properties must be maintained throughout pertinent medical observation durations, preceding their total assimilation through biosorption. Most pressure and temperature sensors that can be biologically absorbed demonstrate stability in artificial biofluid environments for mere days, a duration that falls short for numerous prospective uses. Scenarios like monitoring within the skull post-traumatic brain injury recovery phases exemplify this limitation.[48,210] Predominantly, constraints emerge due to the ineffectiveness of absorbable protective coatings, encompassing polymers like silk fibroin[2] and poly(lactic-*co*-glycolic acid) (PLGA),[46] along with inorganic layers comprising silicon dioxide[211] and several metal oxides[212] deposited through chemical or physical vapor deposition techniques. These materials struggle to obstruct water infiltration into the devices' functional domains over prolonged durations. A potential remedy for these deficiencies involves the utilization of thermally derived, ultrathin silicon dioxide layers on device-grade silicon wafers (t-SiO_2). This can serve as bioresorbable encapsulating layers, facilitating the consistent functionality of intracranial pressure (ICP) and temperature (ICT) sensors for extended days. In another development,[213] researchers have introduced two variants of bioresorbable optical pressure sensors as illustrated in **Figure 3**. The first variant incorporates a Fabry–Pérot interferometer (FPI) configuration, while the second is grounded on photonic crystal (PC) architectures. Both modalities are dependent on the pressure-triggered deflections of silicon nanomembrane (Si NM) diaphragms, inducing alterations in an air cavity's thickness or the lattice constants of a PC, subsequently leading to measurable shifts in the resonance peaks within reflection spectra. These structures are adaptable for temperature sensing, utilizing the thermal dependency of silicon's refractive index. The fabrication techniques involve a wafer-bonding process using silicon-on-insulator (SOI) wafers, succeeded by an etching method from the back of the wafers, which allows for the formation of device architectures covered by a slender t-SiO_2 coating. These structures exhibit operational stability extending beyond a week with an in vitro dynamic range of 0–100 mmHg and 35–43 °C for the pressure and temperature sensors, respectively. Preliminary ICP and ICT measurements in rat models indicated promising results for medical utilization. In another implementation,[190] Curry and coworkers developed a new class of sensors based on PLLA nanofiber. Initially, they showcased that biodegradable force sensors derived from PLLA nanofiber films exhibit enhanced sensitivity and adaptability compared to thermally stretched PLLA bulk films.[210] This technological advancement enabled wireless and accurate vital physiological signal recordings. Next, they demonstrated that the same PLLA nanofiber sensor has the capability of operating as an implantable and biodegradable ultrasonic transducer, uniquely designed for non-invasive blood–brain barrier (BBB) penetration with a safe and autonomous degradation process, posing no threat to the individual's well-being. Incorporating PLLA nanofibers, molybdenum electrodes, and a PLLA layer, a biodegradable device was crafted and tested in vivo on mouse animal models employing a near-field communication (NFC) reader for data collection. The results revealed the dual functionality of the PLLA nanofiber sensor, confirming its use as a biodegradable ultrasonic transducer. By adjusting variables, such as the encapsulating PLLA layers' thickness[210] or by employing different biodegradable encapsulating materials, achieving extended functional durations was feasible.

3.1.2. Chemical sensors

The continuous monitoring of nitric oxide (NO) concentrations within biological fluids is crucial for various physiological processes, including neurotransmitter signaling, immunological defenses, cardiovascular functions, formation of new blood vessels, and microcirculatory pathways.[214,215] Studies indicate a critical correlation between anomalous nitric oxide prevalence

 © 2024 The Author(s). Advanced Functional Materials published by Wiley-VCH GmbH

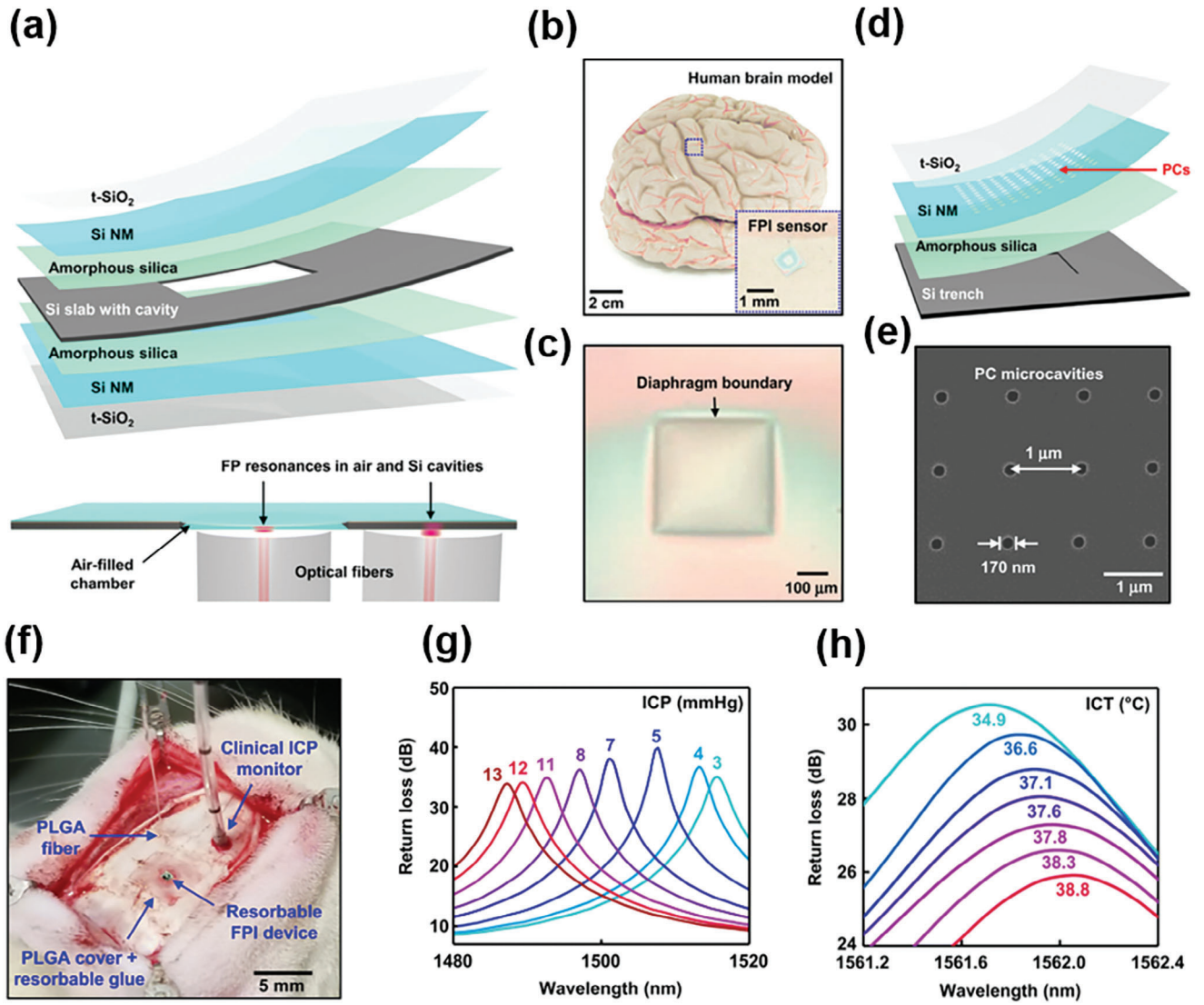


Figure 3. a) Schematic illustration indicating device layers of a bioresorbable Fabry–Pérot Interferometer pressure and temperature sensor. b) Optical image of the developed sensor placed on a brain model. c) A magnified optical image of the device. d) A schematic illustration of bioresorbable photonic crystal microcavity pressure and temperature sensor. e) SEM image of the PC structure. f) Optical image of the device implanted in the intracranial for intracranial pressure and intracranial temperature monitoring during in vivo experiments. g) Optical spectra of the sensor measured as the result of the application of different intracranial pressure and intracranial temperature ranges to the sensors. Reproduced with permission.[213] Available under a Creative Commons CC BY license. Copyright 2019, American Association for the Advancement of Science.

and various pathological conditions, such as inflammatory responses, neuronal toxicity, and the advancement of oncological ailments.[216,217] The utilization of implantable and biodegradable chemical sensors for continuous biomolecular signal monitoring inside the body after surgery is of great interest.[218] However, balancing precise detection capabilities with intended degradation remains a significant hurdle. Documented methodologies for extending the durability of dissolvable devices often involve using protective coatings or electrode constituents characterized by gradual decomposition rates, such as molybdenum or heavily doped silicon. Nevertheless, these approaches may fall short in ensuring enduring stable functionality and could necessitate intricate manufacturing procedures.[219–225] Furthermore, prevalent strategies for encapsulation typically encompass the application of coating substances to the sensing electrodes, a technique potentially unsuitable for devices requiring direct contact with targeted biological solutions.[104,214] Li and colleagues have developed an approach encompassing material selection, structure design, and fabrication methods to realize a flexible, biodegradable electrochemical sensor.[226] The sensor employed the amperometry method as the transduction technique, exhibiting a limit-of-detection (LOD) of 3.97 nM, a dynamic range of 0.01–100 μM, a turnaround time of less than 350 ms, and resistance to environmental interferences. The device exhibited the acceptable execution of real-time NO tracking, extending its applicability from cellular and organ contexts to continuous monitoring within a rabbit's joint space over 5 days, facilitated by a wireless data interrogation system. Its design ensures total physical

© 2024 The Author(s). Advanced Functional Materials published by Wiley-VCH GmbH

16163028, 2025, 3, Downloaded from https://advanced.onlinelibrary.wiley.com/doi/10.1002/adfm.202413324 by Koc University, Wiley Online Library on [22/05/2025]. See the Terms and Conditions (https://onlinelibrary.wiley.com/terms-and-conditions) on Wiley Online Library for rules of use; OA articles are governed by the applicable Creative Commons License

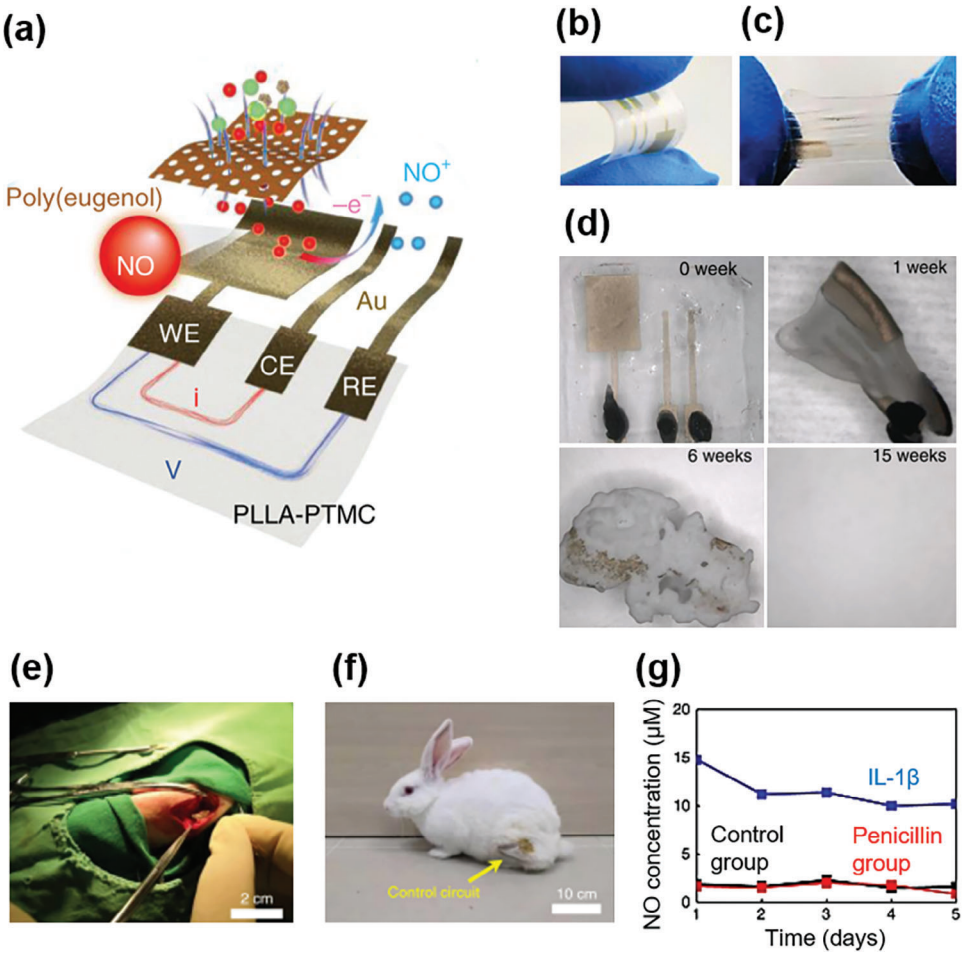


Figure 4. a) Schematic illustration of the biodegradable NO sensor presented.[227] b) Optical image of the fabricated NO sensor on PLLA–PTMC substrate. The sensor has a three-electrode configuration composed of gold electrodes and poly(eugenol) thin film. The figure also indicates the flexibility of the fabricated biosensor. c) The optical image indicating the stretchability of the developed biosensor. d) Optical images of the device at different time frames indicating the degradation of the biosensor during the accelerated degradation process with phosphate-buffered saline (PBS) with a temperature of 65 °C. the device almost disappears after 15 weeks during the accelerated degradation test. e) Optical image of showing implantation of NO biosensor into the joint cavity of a rat. f) Image of the rat after implantation of NO sensor and all required readout circuits and wireless communication on the thigh. g) Results of real-time NO concentration measurement during in vivo experiment for three group of rabbits administrated with different drugs including IL-1β (blue), penicillin treatment (red), and control group with no drug administration treatment (black). Reproduced with permission.[226] Available under a Creative Commons CC BY license. Copyright 2020, Springer Nature.

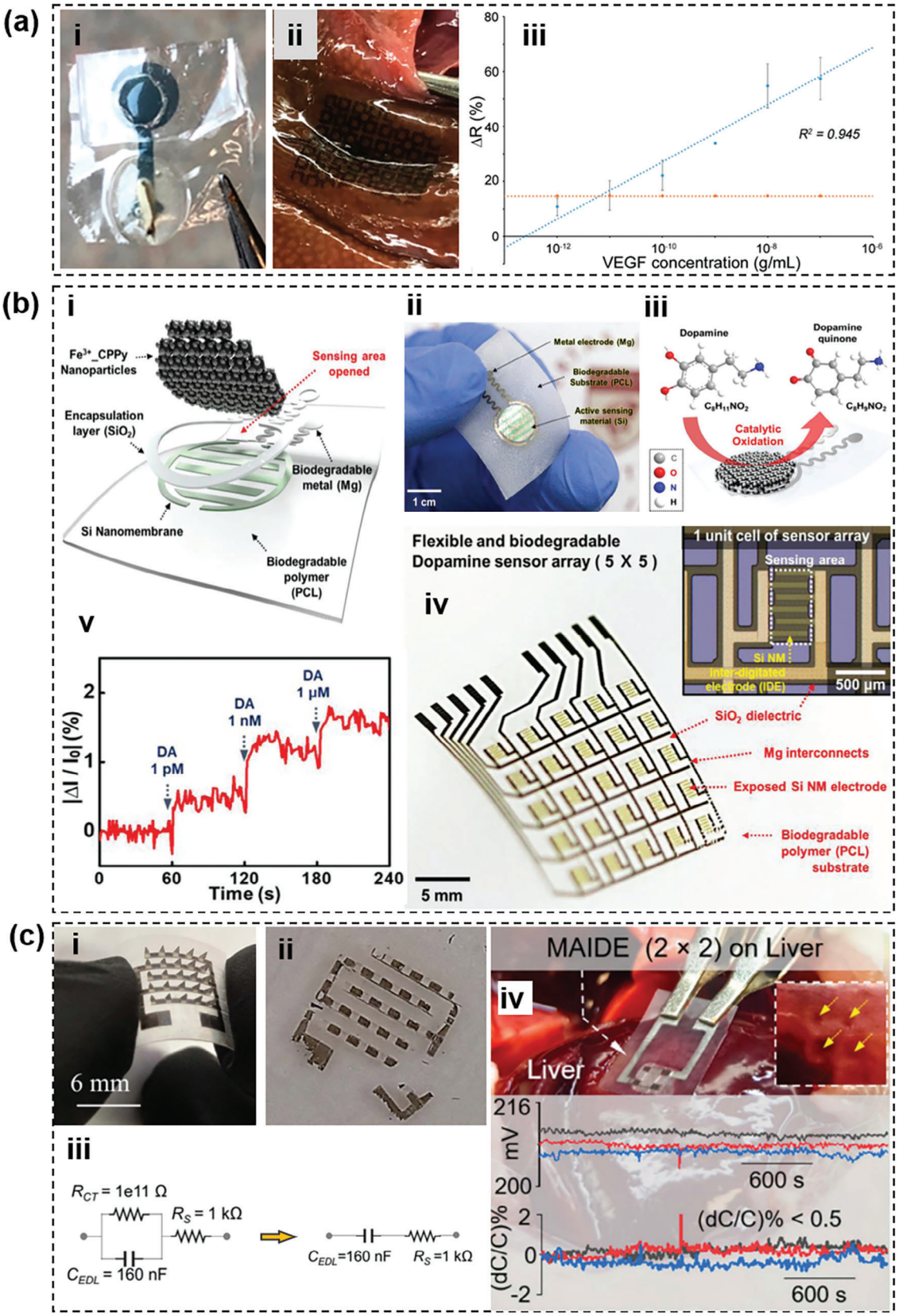
dissolvability through prospective mechanisms such as hydrolysis, fragmentation, phagocytosis, and subsequent metabolic elimination, both in laboratory conditions and within living organisms (**Figure 4**).[200,227]

Ko et al. demonstrated a flexible and bioresorbable NOx sensing system based on a single-crystal silicon nanomembrane (SC-Si NM) that functions at ambient temperature.[228] The device integrated soft and bioresorbable gas sensors that are both highly sensitive and selective. Additionally, it incorporated sensors for monitoring temperature and hydration to calibrate the gas sensor properties influenced by these variables. The electronic system was constructed from patterned SC-Si NMs with a thickness of ≈100 nm doped with phosphorus using a spin-on dopant for reactivity. Magnesium (Mg) electrodes with a thickness of around 300 nm were employed alongside a silicon dioxide interlayer dielectric of about 100 nm thickness. An elastomeric polymer (PDMS) membrane, ≈20 μm thick, was used as a semipermeable barrier to ensure stable gas sensing performance in humid and wet environments. An LOD of 20 ppb was calculated during in vitro examinations of the sensor.[229] In another research,[230] a fully organic, biodegradable, and flexible impedimetric biosensor was designed to quantify vascular endothelial growth factor (**Figure 5a**). This factor is an essential protein biomarker that orchestrates vasculogenesis, angiogenesis, and the proliferation of endothelial cells.[230] Variations in the concentration of this biomarker within human blood serum are documented as significant precursors to various illnesses, notably cancerous conditions.[231] Microstructures of conductive ink were fabricated by integrating a cross-linkable sericin with PEDOT:PSS. Electroactive interfaces were imprinted on flexible fibroin bases, having conformal structures suitable for flexible surfaces. The specificity in detecting vascular endothelial growth factor was

© 2024 The Author(s). Advanced Functional Materials published by Wiley-VCH GmbH

16163028, 2025, 3, Downloaded from https://advanced.onlinelibrary.wiley.com/doi/10.1002/adfm.202413324 by Koc University, Wiley Online Library on [22/05/2025]. See the Terms and Conditions (https://onlinelibrary.wiley.com/terms-and-conditions) on Wiley Online Library for rules of use; OA articles are governed by the applicable Creative Commons License

16163028, 2025, 3, Downloaded from https://advanced.onlinelibrary.wiley.com/doi/10.1002/adfm.202413324 by Koc University, Wiley Online Library on [22/05/2025]. See the Terms and Conditions (https://onlinelibrary.wiley.com/terms-and-conditions) on Wiley Online Library for rules of use; OA articles are governed by the applicable Creative Commons License



© 2024 The Author(s). Advanced Functional Materials published by Wiley-VCH GmbH

realized by enhancing the conductive electrode ink through antibody incorporation.[230] The electrochemical impedance spectroscopy was selected as the interrogation mechanism, and electrical current as the sensor output metric. The device was utilized for vascular endothelial growth factor (VEGF) detection and quantification within buffered mediums (with a LOD of 1.03 pg mL^{-1}), human blood serum (LOD of 81.46 pg mL^{-1}), and artificial urinary conditions (LOD of ≈20 pg mL^{-1}).

Dopamine serves as a crucial neurotransmitter governing the neural circuits involved in the motivational aspects of behavior driven by the anticipation of rewards. Tim et al.[188] proposed a bioresorbable and implantable dopamine biosensor (Figure 5b). The biosensor was designed using ultrathin monocrystalline silicon nanomembranes (Si NMs) with an approximate thickness of 300 nm, which were heavily doped with boron at a concentration of about 10^{20} cm^{-3}. These nanomembranes were structured into interdigitated electrodes (IDEs) and uniformly coated with hybrid nanoparticles (NPs) consisting of iron (Fe) with a thickness of around 5 nm and carboxylated polypyrrole (CPPy) ≈100 nm thick, serving as the active sensing components.[2,57,232–234] Electrical contacts and interconnects were formed using Mg with a thickness of about 200 nm. A silicon dioxide layer of ≈100 nm was utilized to insulate the conducting Mg traces from biofluids and nearby tissues, except at the detection area opening.[57] Furthermore, to support the electronic materials in a flexible configuration, a thin sheet of polycaprolactone (PCL) was employed.[211,235] Postimplantation, as the result of dopamine molecules absorption over the CPPy surface of the electrodes, dopamine oxidizes, leading to the formation of dopamine-o-quinone, which consequently leads to electrons generation that corresponding current can flow through the Si NMs and is considered as the main output metric of the biosensor. The sensor demonstrated a dynamic range from 1 pM to 1 μM. During the in vitro accelerated degradation process, it showed a required time of 15 h for complete degradation in PBS solution (≈pH at 37 °C).

Mirzajani and coworkers recently demonstrated a fully biodegradable microneedle platform for in situ biomarker detection and quantification from internal body organs[236] (Figure 5c). Although microneedle arrays have been extensively employed in epidermal platforms for access to the interstitial fluid or have been used for drug delivery into internal body organs,[237–242] this is the first time that a biodegradable microneedle platform has been employed for biosensing from internal body organs, including the heart, liver, and lung.[237] The device was fabricated from PLA as the base material and Mo as the electrode material (with a thickness of around 200 nm) for biosensing. The other advantage of this platform was the interdigitated pattern of the Mo electrode over the needles, which facilitated the impedimetric or capacitive interrogation of biomarker concentrations from the internal organs. The device demonstrates a complete degradation in an accelerated degradation test in PBS during a 10 h timeframe.

Diabetes Management: Although conventional real-time glucose monitoring systems were primarily based on nonbiodegradable materials, which may cause pain and infection during removal, recently demonstrated biodegradable and implantable counterparts provide proper and accurate measurement during operational periods and safely degrade in the body after a specific timeframe. In a recently published work by Li et al.,[196] researchers employed the concept of electrochemical glucose sensing and proposed a hybrid device for continuous glucose monitoring (**Figure 6**). The hybrid device was composed of a wearable control unit attached to the skin (nonbiodegradable) and an implantable and bioresorbable unit comprising a glucose sensor and electrical connections. The glucose sensor was fabricated by screen printing GOx-coated zinc as the working electrode, molybdenum as the counter electrode, and molybdenum-tungsten as the reference electrode. Furthermore, to compensate for the effects of the slow degradation of sensor electrodes while implanted in the body, an additional sacrificial electrode called a zinc electrode was included in the structure of the sensor. Real-time in vivo glucose monitoring was carried out for 5 days, and the sensor demonstrated an extensive dynamic range of 0–25 mM with a sensitivity of 0.2458 μA mM^{-1}.

3.2. Local Electrical Stimulation

In the area of bradyarrhythmia therapy, implantable cardiac pacemakers have established themselves as foundational treatment modalities.[19,243] While permanent implants remain the traditional standard, there exists a need for temporary pacing systems tailored to patients anticipated to have transient bradyarrhythmia spanning days to weeks.[244] Building upon this, Choi et al. introduced a bioresorbable, externally powered, and programmable leadless cardiac pacemaker.[195] The device was constructed from materials that, upon interaction with biofluids, undergo timely degradation through metabolic processes and hydrolysis. Such material selection, in conjunction with a strategic design, yielded a pacemaker that is not only flexible and lightweight but also boasts optimal biocompatibility and consistent functionality

Figure 5. a) A flexible and bioresorbable impedimetric sensor for VEGF monitoring within the body.[230] i) Optical image of the fabricated VEGF biosensor, ii) placement of the fabricated biosensor over a tissue interface for possible biosensing, iii) extracted calibration curve of the biosensor for various doses of VEGF in human serum. Reproduced with permission.[230] Copyright 2019, American Society of Chemistry. b) A flexible and implantable biosensor for in vivo dopamine monitoring.[188] i) Schematic illustration of the implantable dopamine biosensor in its constitute layers and materials, ii) optical image of the fabricated device on a PCL substrate, iii) illustration indicating the detection mechanism of the developed dopamine biosensor. During the detection process, dopamine molecules were converted into dopamine-*o*-quinone as the result of catalytic oxidations at the electrode surface and the resulting electrons contribute to the sensor's output current which is the biosensor's main output metric, iv) optical image of a 5 × 5 array of dopamine biosensors having a flexible structure for multiplexed and spatial/temporal mapping of dopamine. The inset is a close-up view of a single cell from the fabricated array composed of interdigitated electrodes integrated with monocrystalline silicon nanomembranes. All components are biodegradable and can be absorbed in the body without harmful byproducts, v) dose response of the developed biosensor for various concentrations of dopamine. Reproduced with permission.[188] Copyright, 2018 Wiley. c) a flexible and biodegradable impedimetric microneedle array integrated with interdigitated electrodes for implantable applications.[236] i) Optical image of the developed microneedle array showing its flexibility, ii) accelerated degradation process of the microneedle, iii) equivalent circuit model of the microneedle while it s inserted in BPS solution, iv) in vivo capacitance reading from the microneedle while it is inserted on a liver. Reproduced with permission.[236] Copyright 2024, IEEE.

© 2024 The Author(s). Advanced Functional Materials published by Wiley-VCH GmbH

16163028, 2025, 3, Downloaded from https://advanced.onlinelibrary.wiley.com/doi/10.1002/adfm.202413324 by Koc University, Wiley Online Library on [22/05/2025]. See the Terms and Conditions (https://onlinelibrary.wiley.com/terms-and-conditions) on Wiley Online Library for rules of use; OA articles are governed by the applicable Creative Commons License

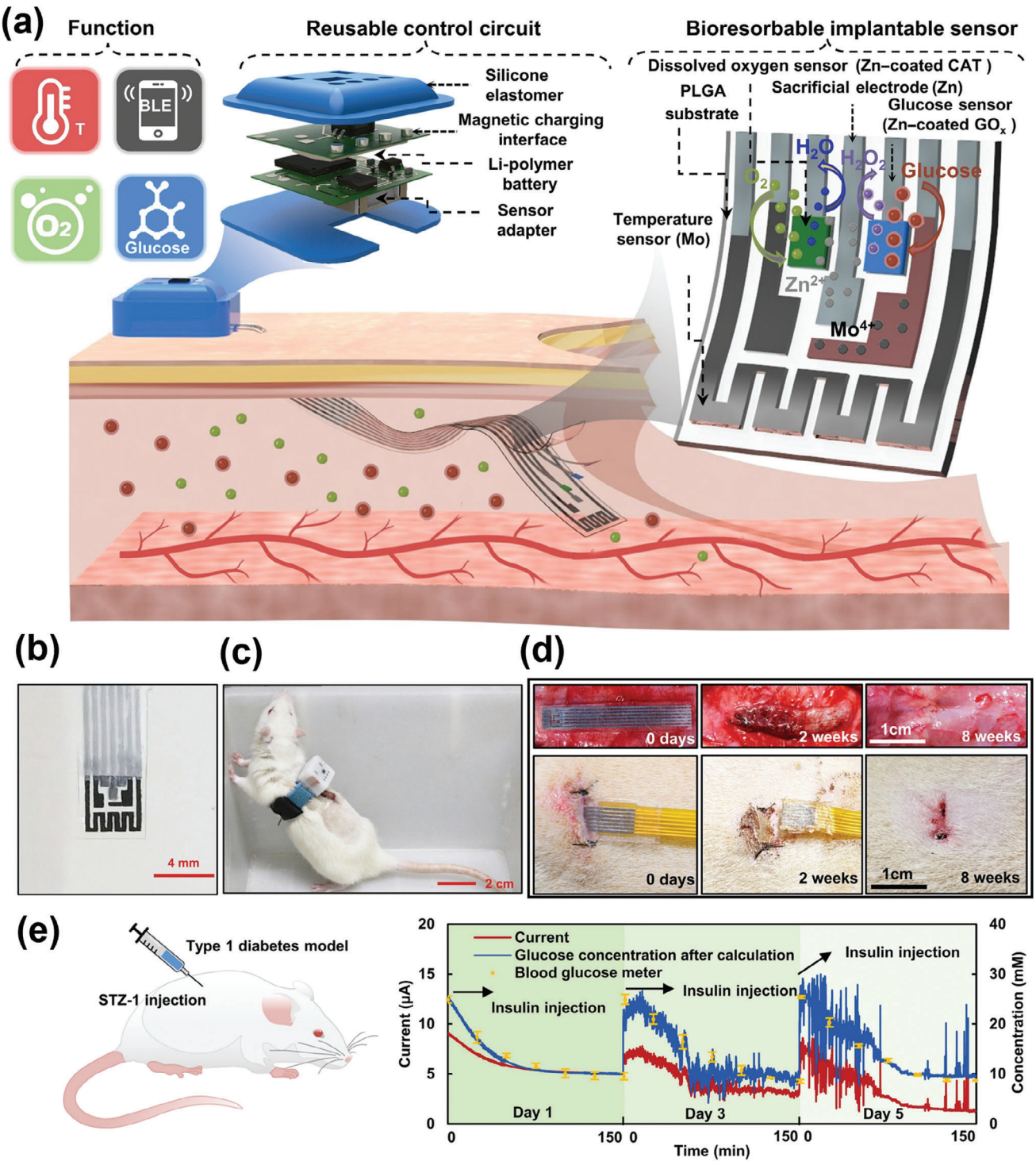


Figure 6. a) Schematic illustration of the hybrid device including wearable part for data reading and implantable part for glucose measuring. b) Optical image of the developed biodegradable and implantable glucose sensor. c) Optical image of the device attached to the dorsal skin of a rat. d) Optical image of the glucose sensor during implantation during the in vivo experiments. e) In vivo demonstration of device operation by injection of Streptozotocin and glucose monitoring for 5 days. Reproduced with permission.[196] Available under a Creative Commons CC BY license. Copyright 2020, American Association for the Advancement of Science.

© 2024 The Author(s). Advanced Functional Materials published by Wiley-VCH GmbH

16163028, 2025, 3, Downloaded from https://advanced.onlinelibrary.wiley.com/doi/10.1002/adfm.202413324 by Koc University, Wiley Online Library on [22/05/2025]. See the Terms and Conditions (https://onlinelibrary.wiley.com/terms-and-conditions) on Wiley Online Library for rules of use; OA articles are governed by the applicable Creative Commons License

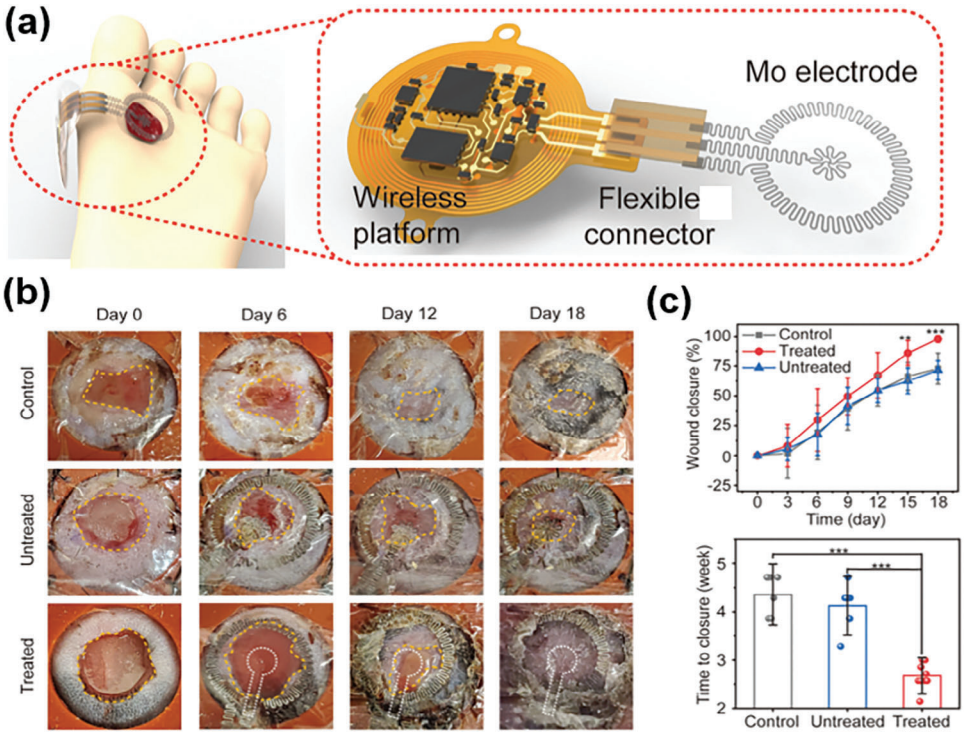


Figure 7. Developed electrotherapy system for wound healing application presented.[197] a) A schematic figure indicating the transient, battery-free wireless system for wound healing. b) Optical images indicating would closure as the result of electrotherapy by the proposed device compared to results from untreated and control images of wound closure. c) Quantification and comparison of wound closure after 18 days from electrostimulation. Reproduced with permission.[197] Available under a Creative Commons CC BY license. Copyright 2023, American Association for the Advancement of Science.

during its intended operational lifespan. After the therapeutic period concludes, the devices undergo complete resorption due to innate biological mechanisms. Employing resonant inductive coupling, the system harnesses wireless energy transfer. Such features empower complete intra-body implantation without the need for wire connection to the external hardware units or battery, reducing potential complications, such as infections or device displacement.

In the U.S., the vast diabetic population (≈at 30 million) struggles with the severe complication of diabetic foot ulcers (DFUs), manifesting in 15%–25% of these individuals.[197] Electrostimulation proved to be effective in wound healing by case studies, remains sparsely adopted in medical settings. Such restrained usage can be attributed to ambiguities surrounding optimal electrostimulation parameters (dosing, timing, stimulation type), clunky hardware (resulting in the need for in-hospital treatment and dampened patient adherence), and suboptimal, often cumbersome, user interfaces. Beyond these, an overall concern for any therapeutic or diagnostic apparatus interacting directly with the wound is potential soft tissue damage upon removal postusage.[245,246] Addressing these challenges, a bioresorbable electrotherapy system was introduced, without batteries, wirelessly operational, and capable of delivering electrostimulation while concurrently gauging wound impedance[197] (**Figure 7**). The device was composed of a wireless NFC-based electronic board, a detachable flexible electrical connection, and a stimulator fabricated from a Mo electrode pair designed in a serpentine structure for enhancing its flexibility and stretchability, without encapsulation for direct contact with the wound area. In vivo experiments were carried out to monitor wound dimensions and closures as the healing parameters.[247] Implementing electrostimulation with the described devices marked a roughly 30% acceleration in the healing of wounds concerning the outcomes from control and untreated groups.

Annually, more than 20 million hernia repairs are performed globally, involving the implantation of various surgical meshes.[248] These include 1) synthetic nonabsorbable meshes, often made from materials like polypropylene (PP),[249,250] expanded polytetrafluoroethylene (ePTFE),[251,252] and polyester (PET);[253] 2) synthetic resorbable meshes; and 3) biological meshes.[252,254] Nonabsorbable meshes are preferred for their affordability and mechanical strength.[254] Yet, they often lead to complications like foreign body reactions, adhesions (over 15%),[255] infections, and fibrosis, causing chronic pain and physical limitations[256] Conversely, resorbable meshes, such as PLGA, PCL, PLLA, PDO, and PGA facilitate tissue integration but their rapid degradation raises hernia recurrence risks.[257,258] Biological meshes, made from extracellular matrix-based scaffolds derived from various sources like human and animal tissues, offer better biocompatibility and tissue regrowth.[259] However, they are costly, mechanically weak, and less elastic, resulting in high hernia recurrence rates (about 29%).[260,261] A recent study showcased a bioresorbable electronic surgical mesh for wireless pressure monitoring and on-demand drug delivery for hernia

© 2024 The Author(s). Advanced Functional Materials published by Wiley-VCH GmbH

16163028, 2025, 3, Downloaded from https://advanced.onlinelibrary.wiley.com/doi/10.1002/adfm.202413324 by Koc University, Wiley Online Library on [22/05/2025]. See the Terms and Conditions (https://onlinelibrary.wiley.com/terms-and-conditions) on Wiley Online Library for rules of use; OA articles are governed by the applicable Creative Commons License

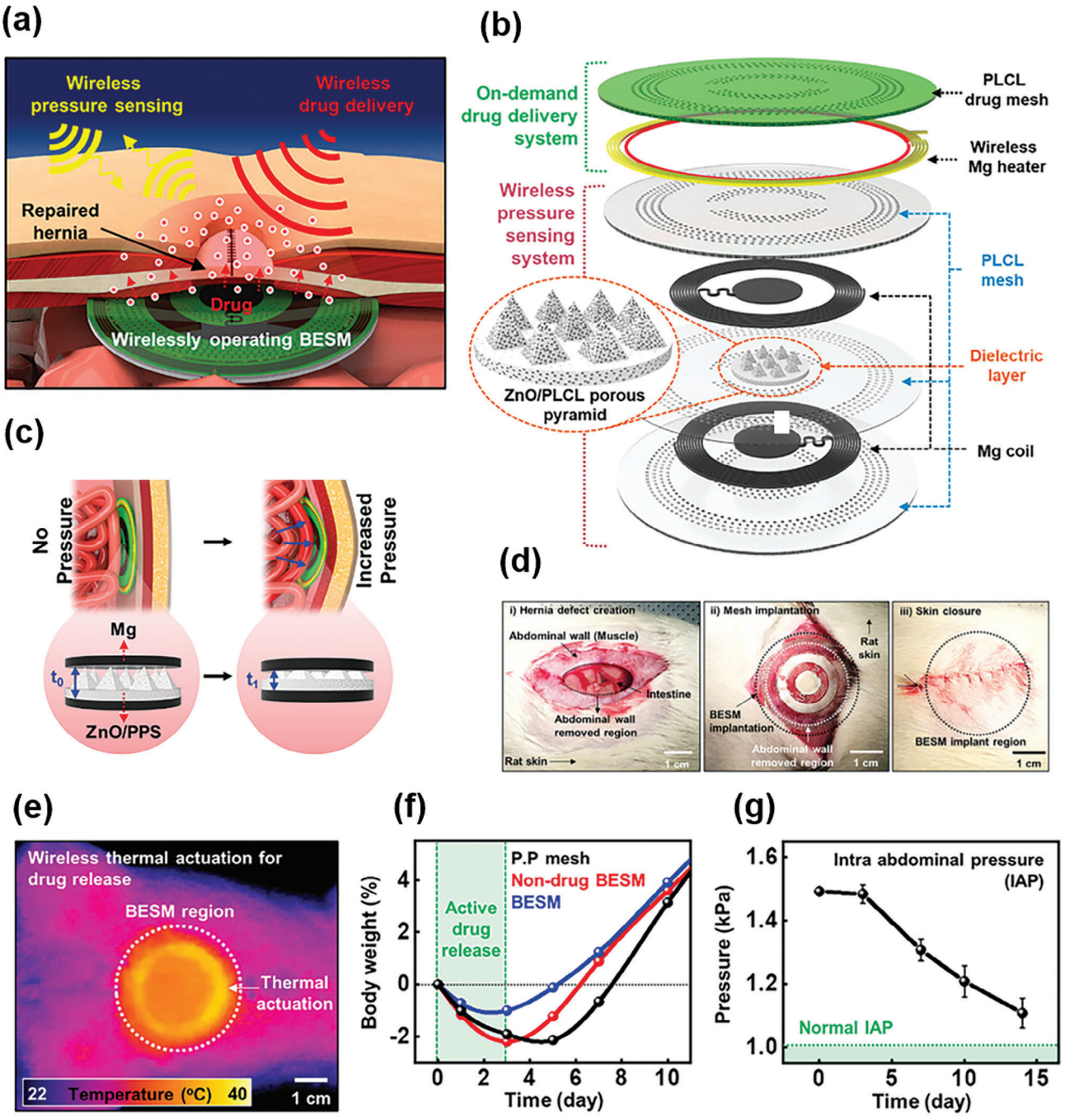


Figure 8. a) A schematic illustration indicating the operation mechanism of the hernia monitoring device. b) Schematic illustration indicating different structural layers of the device. c) Operation mechanism of the device for real-time pressure monitoring. d) Optical images indicating implantation process of the device and preparation for in vivo experiments. e) Thermal image of the device after implantation into the animal and actuation of the thermal actuator through an external antenna. The figure indicates uniform heat distribution on the structure. f) Body weight measurement of the rats during the in vivo experiments after device implantation, and g) pressure variations in intra-abdominal pressure during the recovery process after device implantation. Reproduced with permission.[262] Copyright 2023, John Wiley & Sons.

repair[262] (**Figure 8**). The device has a bioresorbable mesh structure made from poly(L-lactide-*co*-ε-caprolactone) (PLCL) polymer, known for its robust mechanical strength and durability, essential for hernioplasty recovery. A zinc oxide (ZnO)/PLCL composite with a spongy structure was employed to provide high-pressure sensitivity for wireless monitoring of hernia repairs. A wirelessly triggered drug delivery system tailored for controlled inflammation management and healing acceleration was employed. The device's wireless pressure sensor was made up of layered magnesium (Mg) double-coils (15 μm thick), separated

© 2024 The Author(s). Advanced Functional Materials published by Wiley-VCH GmbH

16163028, 2025, 3, Downloaded from https://advanced.onlinelibrary.wiley.com/doi/10.1002/adfm.202413324 by Koc University, Wiley Online Library on [22/05/2025]. See the Terms and Conditions (https://onlinelibrary.wiley.com/terms-and-conditions) on Wiley Online Library for rules of use; OA articles are governed by the applicable Creative Commons License

by a 50 µm thick PLCL interlayer and topped with a 150 µm thick ZnO/PLCL porous pyramid sponge (PPS) for improved detection sensitivity. The drug delivery system comprised a wireless thermal actuator, consisting of an RF inductive coil (Mg, 15 µm thick), a microheater (Mg, 500 nm thick), and a layered capacitor ($Mg/SiO_2/Mg$), all encapsulated in a PLCL layer (100 µm). The slow-degrading PLCL maintains the mesh's structure for over 25 weeks and fully dissolves after 60 weeks, offering long-term support to minimize hernia recurrence risks.

The opioid epidemic in the United States reached a critical point in 2019, with opioid-related fatalities accounting for 50 000 lives and an economic toll estimated at $100 billion.[263] This urgent situation has catalyzed a surge in research into nonpharmacological pain relief methodologies. Notably, interventions employing electrical stimulation, thermal therapy,[264–266] ultrasonic applications,[267,268] and light-based treatments[269,270] are gaining traction as promising alternatives for modulating or obstructing pain signals along peripheral nerve channels. In a study conducted by Lee et al.,[189] it was demonstrated that utilizing localized electrical stimulation on peripheral nerves can impede action potential propagation, offering a compelling substitute to drugs in addressing acute pain (**Figure 9a**). This technology can be an alternative to the conventional counterpart for temporary pain alleviation equipment as it brings economic and medical challenges due to subsequent surgical extraction necessities.[271] The design provides immediate electrode-nerve interaction for rapid, comprehensive functionality, and leverages natural bioresorption processes, eliminating surgical extraction needs. Their presented configurations synergize the benefits of both Mo and Mg, integrating them into woven designs. Mo electrodes, incorporated within the cuff architecture, establish a connection with the designated nerve during blocking stimulus administration. Meanwhile, Mg extension electrodes, enveloped by a bioresorbable polymer, ensure electrical insulation from neighboring biofluids and reduce their dissolution rates, functioning as links to an external power source.

While effective, passive biodegradable systems can impose unwanted side effects on patients, as prolonged remnants may trigger inflammation or tissue toxicity.[272] In response, the concept of an active operation system, which operates precisely upon specific triggering events, has emerged. This approach allows for comprehensive device management aligned with a clinical timeline and has been recognized for enhancing clinical safety by reducing the risk of prolonged residue-related harm.[272] A recent study[273] introduced an on-demand bioresorbable neurostimulator that works without a battery utilizing triboelectric energy harvesting from standard medical ultrasound sources (Figure 9b). The device comprises two main components: an acoustically triggerable transient triboelectric nanogenerator (ACT–TENG), and a bioresorbable cuff electrode. The ACT–TENG represents a biocompatible, bioresorbable energy harvester, designed for noninvasive degradation via ultrasound. The cuff electrode, made of Mg electrodes and poly(3-hydroxybutyrate-*co*-3-hydroxyvalerate) membranes, transmits electric impulses from the ACT–TENG to the sciatic nerve. The ACT–TENG generates high-frequency triboelectric signals (20 kHz, AC waveform) for effective peripheral neuropathy treatment. During treatment, a low-intensity ultrasonic wave ($\leq$1.0 W cm^{-2}) from an external probe activates the ACT–TENG, transmitting signals through the Mg lead to the nerve. Post-treatment, a high-intensity ultrasound (HIU, $\geq$3.0 W cm^{-2}) accelerates the neurostimulator's mechanical breakdown and dissolution.

Injuries to the peripheral nerves rank as some of the primary culprits behind sensorimotor impairments, stemming from disruptions in axonal connections, neuronal cell mortality, and the impact of denervation on motor, sensory, and autonomic activities.[274,275] Addressing these injuries typically necessitates surgical interventions, which repair the nerve gaps either through stitching or by employing nerve grafts or conduits as bridges. Despite incorporating these surgical methods, possibly in conjunction with drug treatments, the recovery trajectories can remain uncertain, leading to suboptimal functional results.[276] This inconsistency arises primarily because; i) the affiliated muscle clusters progressively suffer from denervation-induced shrinkage, reaching a point where they become unresponsive to the regenerating axons bridging the discontinuity,[277] and ii) nerve regeneration speeds from injury sites to the denervated targets are sluggish, at $\approx$1 mm day^{-1}.[278] This translates to extended recuperation durations and a bleaker functional outlook for nerve damages situated closer to the body's core.[279] Clinical studies suggest electrifying denervated muscles through surface electrodes or implanted devices may enhance muscle retention and overall results.[193,280,281] In this regard, Choi et al., introduced a combination of materials, device layouts, and integration approaches, forming the foundation of an implantable, bioresorbable electric stimulator for severe peripheral nerve injuries[193] (**Figure 10**). This platform showcases flexible, rubber-like mechanics, and durable materials powered by an external antenna through inductive coupling. Additionally, the stimulation method, tested on rodents, counteracts muscle shrinkage from denervation by deploying a bioresorbable cuff electrode interface, positioned after the nerve damage site. A bioresorbable dynamic covalent polyurethane (b-DCPU) was used as the top and bottom layer of the device providing flexibility and minimal biofluid absorption, allowing effective performance in moving tissues, and alleviating the operational lifespan constraints of prior bioresorbable nerve stimulators.[282–284]

3.3. Drug Delivery

Although micropumps might only require partial implantation, drug-delivering microchips are typically fully implantable. Hence, the materials used in their construction, especially those in direct contact with bodily fluids or tissues, must ensure biocompatibility. However, biodegradability is not always a crucial factor, as these devices often reside inside the body indefinitely or for extended periods. However, recently the trend has shifted toward creating biodegradable electroactive microchips.[191] Lee et al. introduced an instance of such implantable microchips[285–287] (**Figure 11a**). They harnessed a biological lipid membrane to achieve wireless drug delivery via bioresorbable electronic implants.[285] In the study, drug release was facilitated by inducing a voltage between a metallic anode membrane and cathode, which subsequently led to the electrochemical dissolution of a drug reservoir cover made from PLGA. This implant was subjected to in vitro testing, wherein it was evaluated for DOX and dextran release and monitored for

© 2024 The Author(s). Advanced Functional Materials published by Wiley-VCH GmbH

16163028, 2025, 3, Downloaded from https://advanced.onlinelibrary.wiley.com/doi/10.1002/adfm.202413324 by Koc University, Wiley Online Library on [22/05/2025]. See the Terms and Conditions (https://onlinelibrary.wiley.com/terms-and-conditions) on Wiley Online Library for rules of use; OA articles are governed by the applicable Creative Commons License

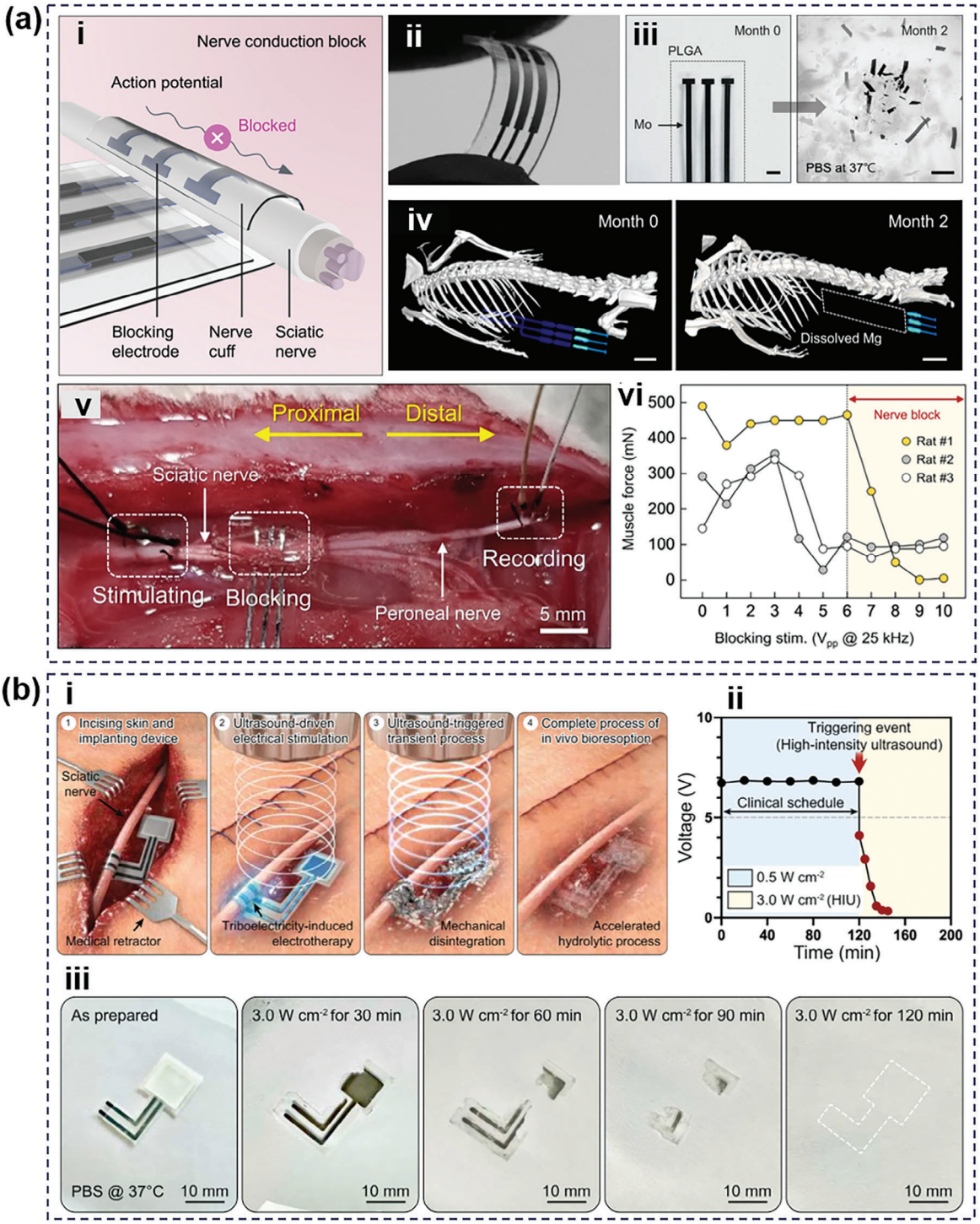


Figure 9. a) Nerve conduction blockage device presented.[189] i) Schematic illustration of the proposed device, ii) optical image of the device indicating its flexibility and Mo traces in the structure, iii) optical image of the device during the in vitro degradation process, iv) CT images of mice taken 2 months after implantation of the device, v) implantation of the electrodes for in vivo studies, vi) effect of the device on muscle force during in vivo studies as the result of application of AC signal with frequency of 25 kHz various amplitudes. Reproduced with permission.[189] Available under a Creative Commons CC BY license. Copyright 2022, American Association for the Advancement of Science. b) The on-demand wireless bioresorbable neurostimulator device utilizing triboelectric energy harvesting from a standard medical ultrasound source presented.[273] i) The schematic illustration of the proposed device and its clinical protocol for peripheral nerve electrotherapy, ii) operational plots of the device during the clinical schedule planned for a duration of 120 min indicating an output voltage of more than 5 V. The plot also indicates that the output of the device rapidly drops to near zero after triggering effect, iii) dissolution timeframes of the device after HIU-triggering. Reproduced with permission.[273] Available under a Creative Commons CC BY license. Copyright 2022, Springer Nature.

© 2024 The Author(s). Advanced Functional Materials published by Wiley-VCH GmbH

16163028, 2025, 3, Downloaded from https://advanced.onlinelibrary.wiley.com/doi/10.1002/adfm.202413324 by Koc University, Wiley Online Library on [22/05/2025]. See the Terms and Conditions (https://onlinelibrary.wiley.com/terms-and-conditions) on Wiley Online Library for rules of use; OA articles are governed by the applicable Creative Commons License

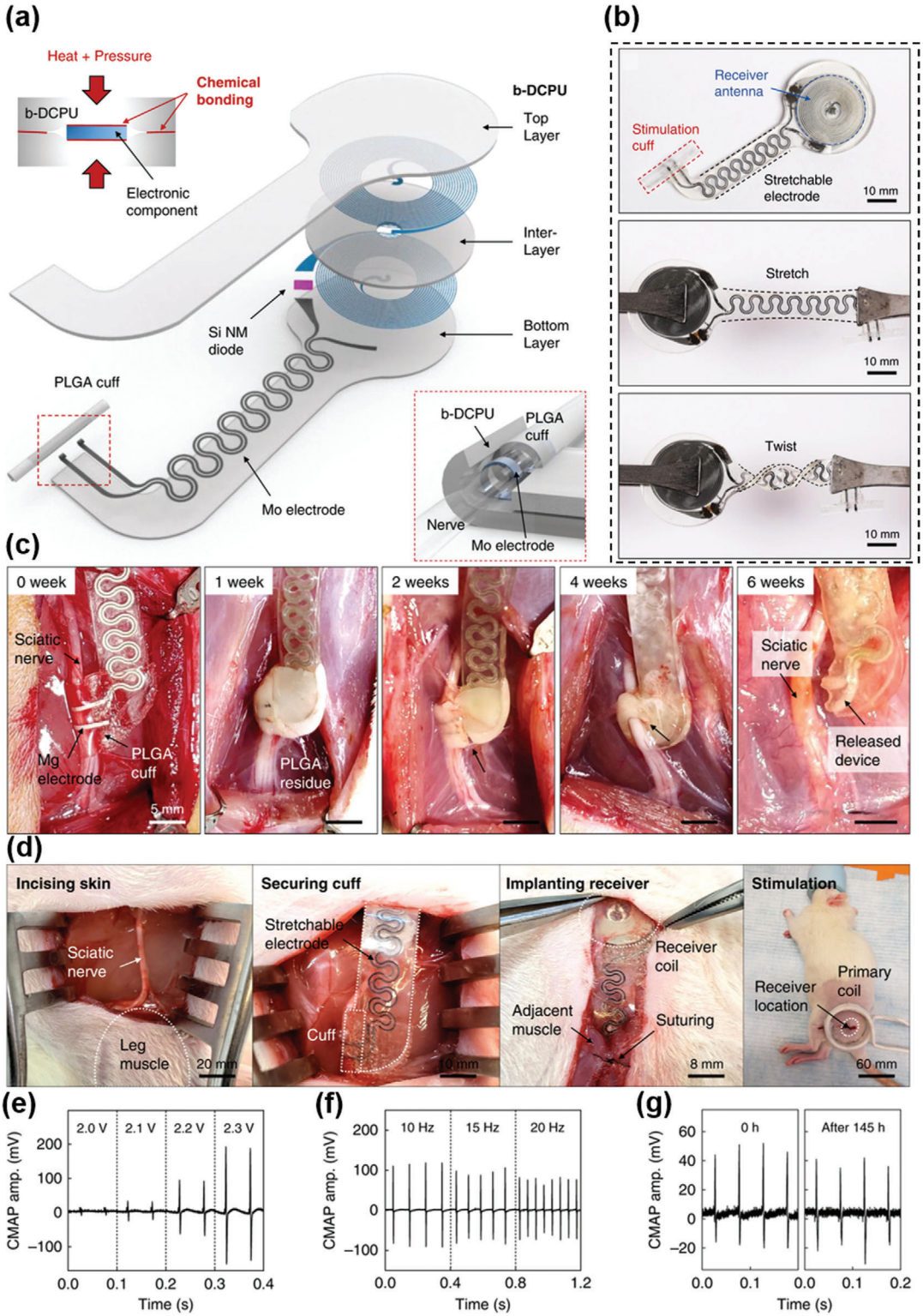
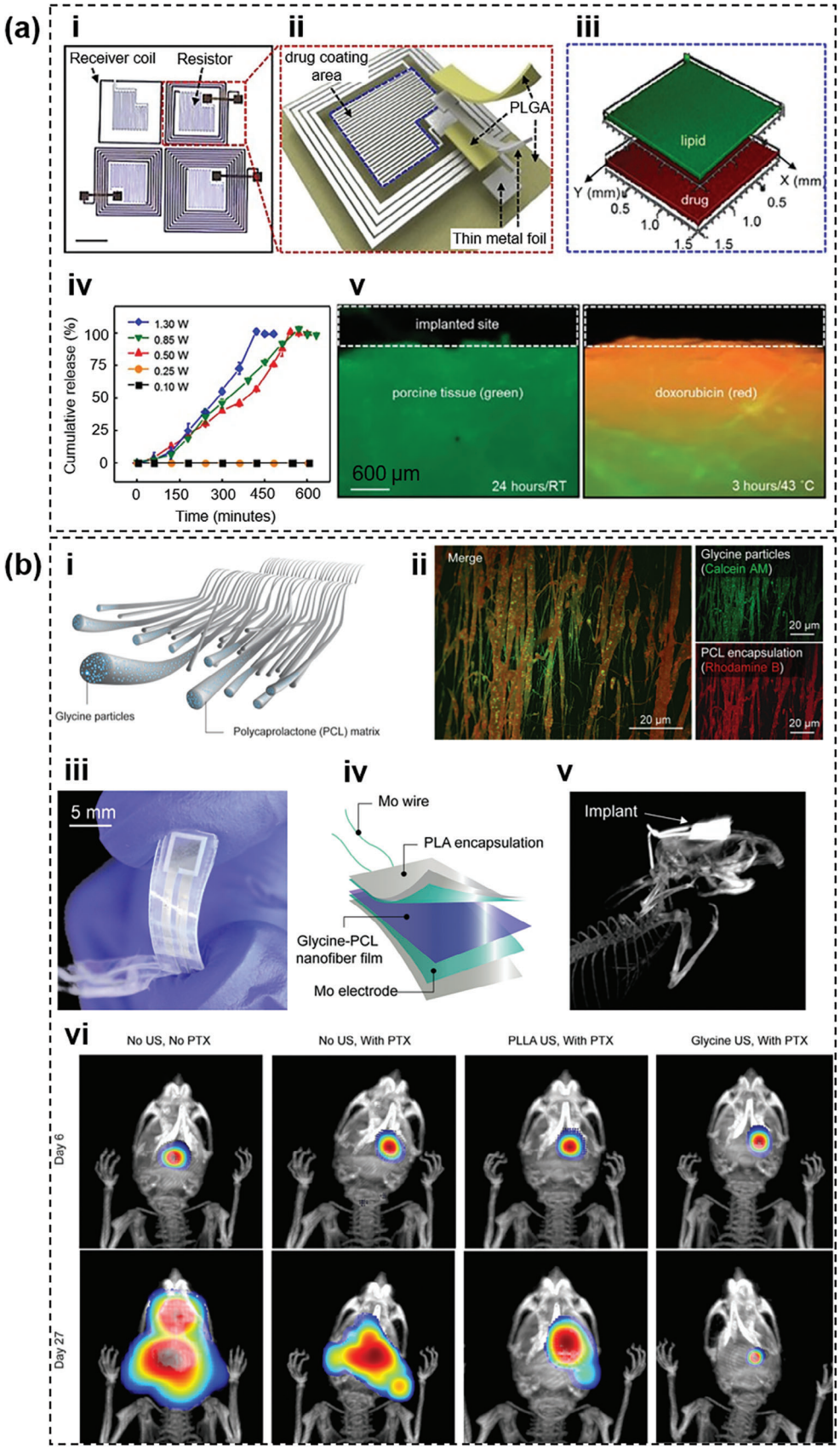


Figure 10. a) Schematic illustration of the bioresorbable electronic stimulator designed for neuromuscular regeneration. The figure indicates different layers in the device structure and their materials.[193] b) Optical images of the final fabricated device indicating its stretchability and flexibility. c) Optical images of PLGA cuff electrodes on the sciatic nerve after 6 weeks. The figures indicate the release of the sciatic nerve from the device after a specific period. d) Surgical procedure for implanting the device. e,f) Muscle action potential amplitude measured from the gastrocnemius muscle when the sciatic nerve was stimulated by voltages ranging from 2.0 to 2.3 V at the frequency of 20 Hz and frequencies of 10, 15, 20 Hz with an applied voltage of 2.2 V. g) Measured changes in the device amplitude generated by electrical stimulation at a frequency of 20 Hz after surgery (0 h) and after 145 h of implantation. Reproduced with permission.[193] Available under a Creative Commons CC BY license. Copyright 2020, Springer Nature.

© 2024 The Author(s). Advanced Functional Materials published by Wiley-VCH GmbH

16163028, 2025, 3, Downloaded from https://advanced.onlinelibrary.wiley.com/doi/10.1002/adfm.202413324 by Koc University, Wiley Online Library on [22/05/2025]. See the Terms and Conditions (https://onlinelibrary.wiley.com/terms-and-conditions) on Wiley Online Library for rules of use; OA articles are governed by the applicable Creative Commons License



© 2024 The Author(s). Advanced Functional Materials published by Wiley-VCH GmbH

16163028, 2025, 3, Downloaded from https://advanced.onlinelibrary.wiley.com/doi/10.1002/adfm.202413324 by Koc University, Wiley Online Library on [22/05/2025]. See the Terms and Conditions (https://onlinelibrary.wiley.com/terms-and-conditions) on Wiley Online Library for rules of use; OA articles are governed by the applicable Creative Commons License

biodegradation across a span of 30 days. Furthermore, the device's cytotoxicity was assessed in an in vivo porcine model, which indicated no detrimental consequences. As already discussed, materials with piezoelectric properties offer substantial promise in implantable microdevices.[288] Their capability to harness power during the device's in vivo functioning within the body eliminates the need for potentially harmful batteries typically associated with medical implants. Traditional piezoelectric ceramics, such as lead zirconate titanate (PZT), and polymers like polyvinylidene fluoride (PVDF) pose challenges due to their nondegradable nature and potentially toxic components, such as lead in PZT.[289,290] In response to these challenges, Chorsi and colleagues developed a biodegradable, flexible, user-friendly, stable, and highly piezoelectric nanofiber film composed of glycine crystals encased in a polycaprolactone (PCL) polymer matrix[291] (Figure 11b). Utilizing these glycine/polymer nanofibers, they crafted an ultrasonic transducer designed for brain implantation, aiming to enhance drug delivery across the blood–brain barrier, ultimately targeting the treatment of neurological conditions. Through the electrospinning technique, nanofibers comprising glycine-PCL with highly aligned glycine crystals were fabricated on a broad scale. This arrangement of piezoelectric glycine showcased an actuation surpassing conventional solvent-cast glycine crystal films.

4. Powering Techniques

4.1. Self-Sustained Implants

Designing sensors for use within the body poses challenges, particularly concerning foreign body reactions and potential toxicity. While many studies have focused on creating passive biocompatible sensors, these typically rely on an external power source. This dependence can pose risks, as the exhaustion of harmful electrolytes (wires) could result in health issues. Traditional batteries also fall short for in-body, flexible, or downsized sensors due to their large size, rigidity, toxicity, and nondegradability. Renewable energy sources like triboelectric nanogenerators or piezoelectric nanogenerators stand out as they transform biomechanical energy from living organisms into electrical energy.

4.1.1. Triboelectric Nanogenerators Energy Harvesting Implants

Triboelectric energy harvesters operate on a similar principle of converting mechanical energy into electrical energy, yet they circumvent the necessity for piezoelectric materials. Instead, these devices harness static polarized charges produced through the interaction of two distinct materials, a process known as contact electrification. The application of mechanical force to separate these two materials creates a potential difference, which in turn prompts electrons to migrate between the electrodes situated on the upper and lower surfaces of the materials.[292,293] The Wimshurst machine introduced around 1880, and the Van de Graaff generator, developed approximately in 1929, stand as quintessential examples of early triboelectric generators.[294] These devices, also known as triboelectric nanogenerators (TENGs), are capable of producing alternating current (AC) electrical outputs through cycles of contact and separation. Fundamentally, a TENG is constructed with just two electrodes and two dielectric materials, often separated by an air gap. An instance of a bioresorbable device within this category employs electrospun PLA alongside nanostructured gelatin as the triboelectric components, integrating magnesium plates for electrodes[295] (**Figure 12a**). Such a device, measuring 4 × 4 cm^2, is capable of producing an open-circuit voltage reaching 500 V, along with a short-circuit current density of 10.6 mA m^{-2}, and achieves a peak power density exceeding 5 W m^{-2}. Further examples of bioresorbable triboelectric nanogenerators (TENGs) encompass materials like a carrageenan−agar composite paired with PCL and chitosan/hyaluronic acid (HA) hydrogel films, both utilizing magnesium electrodes.[296,297] Various materials, both natural and synthetic, can be utilized in the fabrication of triboelectric nanogenerators. Wang and colleagues developed a synthetic biodegradable triboelectric nanogenerator.[298] They selected biodegradable polymers, specifically poly(L-lactide-*co*-glycolide) (PLGA), poly(3-hydroxybutyric acid-*co*-3-hydroxyvaleric acid) (PHB/V), poly(caprolactone) (PCL), and PVA, based on their electron transfer properties. These polymers allowed for diverse combinations, providing different electrical outputs. Computed tomography scans showed significant biodegradation of these polymers post-9-week implantation in the subdermal dorsal region of SD rats. Jiang and colleagues, in their research,[299] assessed the triboelectric sequence of five distinct biodegradable polymers, namely cellulose, chitin, silk fibroin, rice paper, and egg white (Figure 12b). For all their experiments, Kapton film served as the benchmark friction layer. Their findings positioned the triboelectric series as follows: egg white as the most positive, followed by silk fibroin, chitin, cellulose, and rice paper as the most negative. The peak outputs observed for voltage, current, and power density were 55 V, 0.6 μA, and 21.6 mW m^{-2}, meeting the critical electrical output criteria while

Figure 11. a) A wireless and implantable device for drug delivery to internal body organs.[285] i) Optical image of a 2 × 2 array of inductive coils coupled to serpentine thermal actuator fabricated on a fully biodegradable substrate, ii) 3D exploded schematic view of the fabricated devices indicating different layers of the device and materials, iii) 3D confocal microscopy images of the drug molecules loaded over the lipid membrane, iv) percentage cumulative doxorubicin release from the wireless device activated by an external power of between 0.1 and 1.3 W. v) Fluorescent optical images of the implanted device after 24 h (left) and after heat application for a duration of 3 h. Reproduced with permission.[285] Available under a Creative Commons CC BY license. Copyright 2015, Springer Nature. b) An implantable and biodegradable piezoelectric amino acid nanofiber for brain tumor treatment application.[291] i) A schematic illustration of the PCL matrix filled with glycine crystals for the development of glycine-PCL nanofibers, ii) fluorescent microscopy images of glycine particles (green stained) and PCL matrix (red stained). The figure indicates a uniform distribution of glycine particles over the PCL matrix. iii) An optical image of the fabricated glycine-PCL as an ultrasound transducer, iv) a schematic illustration of the fabricated device indicating the layers and materials of the device, v) in vivo examination of the glycine-PCL ultrasonic transducer operation for enhanced chemotherapeutic drug delivery to the brain for GBM tumor treatment. The position of the glycine-PCL device is revealed by the Micro-CT image. vi) Bioluminescence images during the in vivo experiment (day 27) demonstrating the effect of drug administration by glycine-PCL device on GBM tumor growth. Reproduced with permission.[291] Available under a Creative Commons CC BY license. Copyright 2020, American Association for the Advancement of Science.

© 2024 The Author(s). Advanced Functional Materials published by Wiley-VCH GmbH

16163028, 2025, 3, Downloaded from https://advanced.onlinelibrary.wiley.com/doi/10.1002/adfm.202413324 by Koc University, Wiley Online Library on [22/05/2025]. See the Terms and Conditions (https://onlinelibrary.wiley.com/terms-and-conditions) on Wiley Online Library for rules of use; OA articles are governed by the applicable Creative Commons License

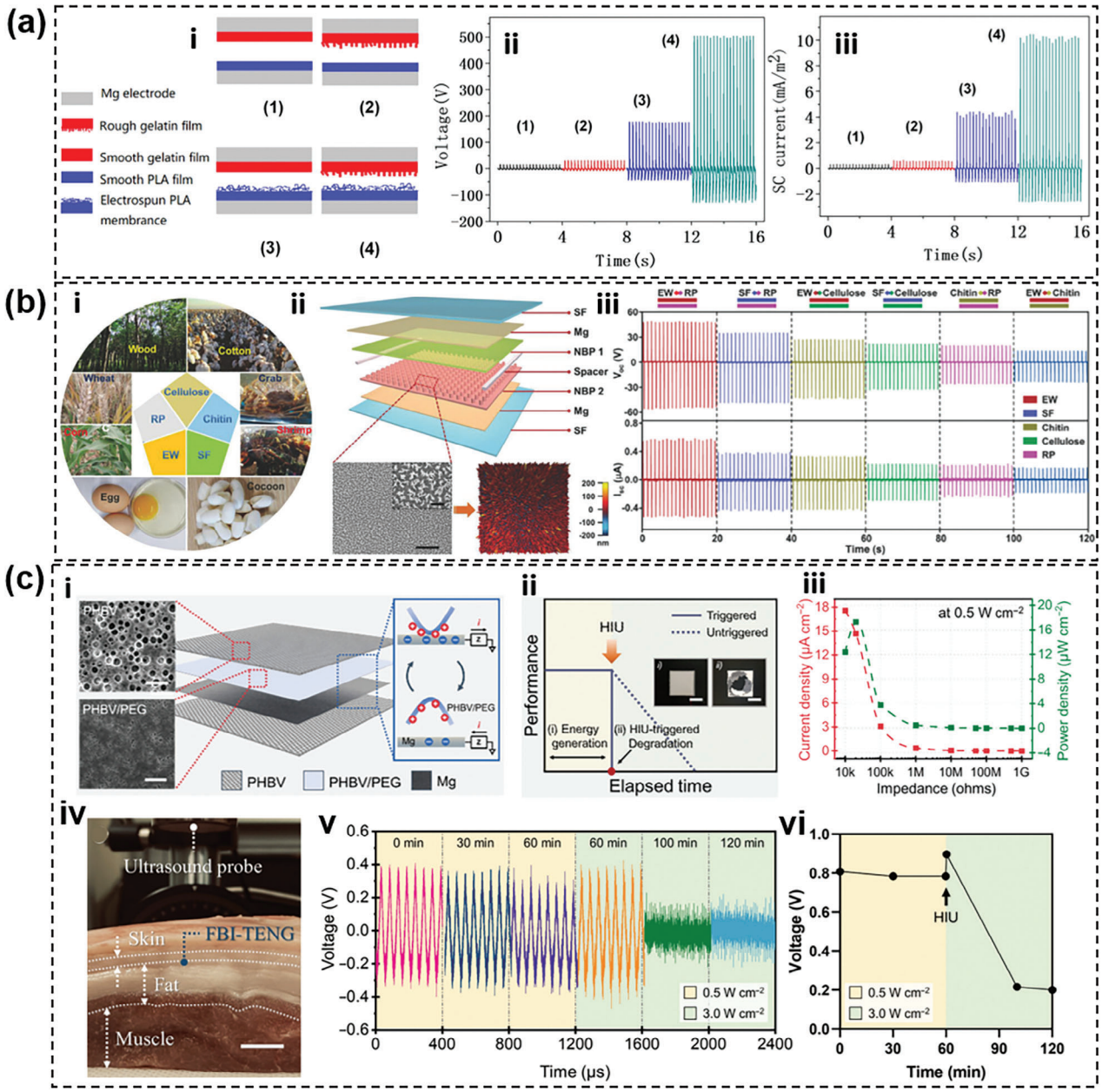


Figure 12. a-i) Schematic illustration and layers of the TENGs presented.[295] a-ii) Open circuit voltage and a-iii) short circuit current density of the presented TENG devices with various structure combinations shown in (a-i). Reproduced with permission.[295] Copyright 2018, Elsevier. b-i) Natural Biomass Particles extracted from different raw materials. b-ii) Schematic illustration of the fabricated device along with various layers incorporated in the structure. b-iii) Open circuit voltage and short circuit current density of the TENG developed by various materials.[299] Reproduced with permission.[299] Copyright 2018, John Wiley & Sons. c-i) Schematic illustration, materials used, and operation mechanism of the proposed TENG.[300] c-ii) Schematic illustration of the transience mechanism, indicating how HIU starts the degradation process of the device. c-iii) Power and current density of the device measurement as a function of electrical impedance. c-iv) Optical image of the device during ex vivo experiments implanted 0.5 cm under porcine skin. c-v) Triggered transient performance of the device and stable output generation at a lower probe power and lower output voltage after application of higher external power. c-vi) Summation of the output voltage presented in (c-v). Reproduced with permission.[300] Available under a Creative Commons CC BY license. Copyright 2022, American Association for the Advancement of Science.

maintaining minimal power consumption.[299] In vivo experiments on Sprague–Dawley rats revealed that these triboelectric nanogenerators, fabricated from natural materials, underwent complete degradation and resorption. Similar to piezoelectric energy harvesters, triboelectric devices can also be triggered by ultrasound. In one example, a device incorporates a magnesium (Mg) electrode as the base triboelectric layer, a composite membrane of poly(3-hydroxybutyrate-*co*-3-hydroxyvalerate) (PHBV) and polyethylene glycol (PEG) as the upper triboelectric layer, enveloped in PHBV.[300] This setup achieves stable electrical

© 2024 The Author(s). Advanced Functional Materials published by Wiley-VCH GmbH

16163028, 2025, 3, Downloaded from https://advanced.onlinelibrary.wiley.com/doi/10.1002/adfm.202413324 by Koc University, Wiley Online Library on [22/05/2025]. See the Terms and Conditions (https://onlinelibrary.wiley.com/terms-and-conditions) on Wiley Online Library for rules of use; OA articles are governed by the applicable Creative Commons License

output under ultrasound exposure at a low intensity of 0.5 W cm^{-2}, leading to voltage and current levels of 4.51 V and 27.86 µA, respectively, at a frequency of 20 kHz. At higher ultrasound intensities of 3.0 W cm^{-2}, the mechanical breakdown of the PHBV encapsulation is induced, which accelerates bioresorption[300] (Figure 12c). Another bioresorption activation method involves using gold (Au) nanorods as optical absorbers for photothermally induced bioresorption.[301] Exposure to near-infrared light diminishes the device's performance to zero within 24 h and ensures its complete bioresorption in 14 days.

4.2. Externally Powered Implants

4.2.1. Piezoelectric Energy Harvesting Implants

Piezoelectric energy harvesting devices transform kinetic energy into electrical energy, manifested as vibrations, shock waves, or various mechanical motions. This conversion process leverages the piezoelectric effect, capitalizing on the inherent polarization characteristics of the material involved.[302–304] In the context of a piezoelectric energy harvester, the application of mechanical stresses on its piezoelectric element leads to the generation of electrical charges on the component's surfaces. This, in turn, can initiate the flow of electrical current once the system is connected to an external load. Yang and colleagues[305] introduced wafer-scale heterostructured piezoelectric films derived from glycine. Utilizing a self-assembly approach, they crafted a film with γ-glycine crystals enveloped by PVA layers. The conformality of the PVA layers offsets the rigidity of the γ-glycine crystals, rendering the film both flexible and responsive to piezoelectric stimuli. In vivo evaluations revealed that this film can function as a temporary force detector in rats, exhibiting complete biodegradability in the dorsal area of Sprague–Dawley rats within a day. To prolong the film's lifespan and delay its rapid degradation, the device was encapsulated with a 30 µm thick PLA layer, exhibiting a progressive signal output as the solution permeated the encapsulation. Cheng and colleagues[306] developed a degradable device employing isoleucine film (**Figure 13a**). The device was adept at tracking various physiological actions, such as muscle movements and lung breathing, showcasing a vast detection spectrum with impressive sensitivity (below 1 kPa). Although 60% of its initial weight diminished over 6 weeks, the device retained its operational capabilities for up to 4 weeks. Through the application of ultrasound, mechanical vibrations can be generated, which can then be transformed into electrical power utilizing piezoelectric devices.[307] Devices engineered with this functionality can facilitate electrical stimulation techniques driven by ultrasound, thereby providing rapid healing processes of peripheral nerve injuries[304] and spinal cord damage.[118] The concept revolves around designing electroactive biomaterials for tissue engineering that simultaneously function as a degradable scaffold for regeneration and a controllable source of electrical stimulation. The use of biodegradable materials with piezoelectric properties, capable of producing electrical currents when subjected to mechanical forces, holds significant potential for enabling in vivo electrical stimulation (ES) in the area of tissue engineering. As an illustrative example, PLLA which is recognized as a biodegradable piezoelectric polymer, has been documented in numerous studies for its potential in tissue engineering. Specifically, Das et al. introduced a scaffold made of piezoelectric PLLA fibers, harnessing electrical stimulation to augment tissue regeneration[308] (Figure 13b). The in vitro assessments revealed an augmented tendency of stem cells to mature into osteoblasts. The in vivo experiments indicated an enhancement in bone development within a calvarial defect. Observations under the fluorescent microscope indicated a higher cell proliferation on the piezoelectric PLLA nanofiber films in comparison to their less piezoelectric or nonpiezoelectric counterparts. In another implementation, Chen et al., presented a method for ultrasound (US)-driven, wirelessly controlled electrical stimulation (ES) using a biodegradable and highly efficient 3D piezoelectric scaffold, aimed at facilitating the healing of spinal cord injuries in rats[118] (Figure 13c). The application of programmable US treatments enables the targeted delivery of in vivo ES, with customizable schedules, durations, and intensities, through the 3D piezoelectric scaffold. Such capabilities surpass those of current in vivo ES methods, like biofuel cell and galvanic cell techniques. The piezoelectric composite nanofibers' ability to drive wireless ES has been shown to encourage the differentiation of neural stem cells into neurons in laboratory conditions. With specific US exposure, the complex multichannel scaffolds composed of PLA/KNN@polydopamine (PLA/KNN@PDA) piezoelectric composite nanofibers significantly speed up the restoration of motor skills and contribute to the repair of spinal cord injuries (SCI). Immunohistofluorescence studies have revealed that combining the 3D piezoelectric scaffolds with in situ ES fosters the differentiation of neural stem cells and natural angiogenesis at the injury site. Furthermore, piezoelectric nanofibers have demonstrated their efficacy in enhancing cartilage regeneration. A study by Liu et al. introduced a biodegradable piezoelectric PLLA nanofiber scaffold, crafted using an electrospinning technique.[309] Serving as an intrinsic stimulator in vivo, this nanofibrous structure promotes cell migration, triggers endogenous TGF-signaling pathways, and aids in both chondrogenesis and cartilage restoration. Such findings spotlight the potential of biodegradable piezoelectric PLLA nanofibrous scaffolds in addressing osteoarthritis and repairing other tissue damages.

4.2.2. Radio Frequency Energy Harvesting Implants

The use of radio frequency (RF) electromagnetic transmission between transmitting and receiving antennas offers an alternative method to ultrasound and triboelectric generators for achieving wireless power delivery, especially effective for targeting deep tissue locations.[195] This energy transfer can be executed through either near-field[15,61,64,191,193,195] or far-field[310–312] mechanisms. Near-field transfer relies on magnetic inductive coupling by coils to efficiently transfer power across relatively short distances, utilizing RF frequencies that are minimally absorbed by biological tissues.[313] On the other hand, far-field transfer employs electromagnetic coupling, which allows for power transmission over greater distances, although it is more susceptible to the orientation of the antennas and uses frequencies that may be more readily absorbed by biological materials. In both strategies, the antennas play a crucial role, as do the rectifying electronics in many instances, which are necessary for converting the alternating

© 2024 The Author(s). Advanced Functional Materials published by Wiley-VCH GmbH

16163028, 2025, 3, Downloaded from https://advanced.onlinelibrary.wiley.com/doi/10.1002/adfm.202413324 by Koc University, Wiley Online Library on [22/05/2025]. See the Terms and Conditions (https://onlinelibrary.wiley.com/terms-and-conditions) on Wiley Online Library for rules of use; OA articles are governed by the applicable Creative Commons License

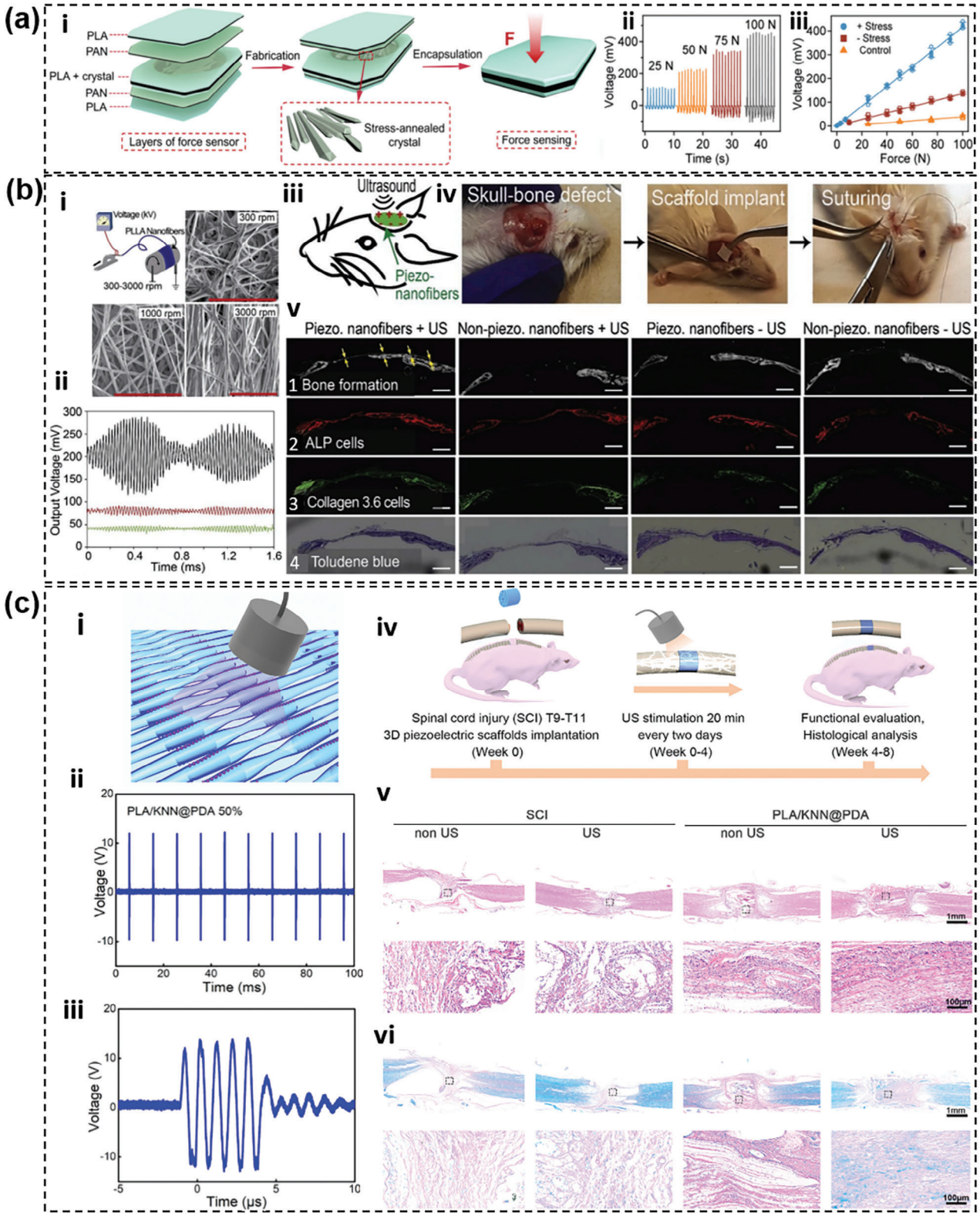


Figure 13. a-i) Schematic illustration of the proposed device[306] along with different layers and materials. a-ii) The open circuit voltage of the device measured at different applied forces of 25, 50, 75, and 100 N. a-iii) The linear relationship between the open-circuit voltage and the applied force to the device. Reproduced with permission.[306] Available under a Creative Commons CC BY license. Copyright 2023, John Wiley & Sons. b-i) The schematic illustration of the setup developed for the fabrication of PLLA films along with their SEM images. b-ii) The open circuit voltage at the output of the PLLA sensor under an applied ultrasound frequency of 40 kHz. b-iii) Schematic illustration of the implantation site and device actuation during in vivo

© 2024 The Author(s). Advanced Functional Materials published by Wiley-VCH GmbH

16163028, 2025, 3, Downloaded from https://advanced.onlinelibrary.wiley.com/doi/10.1002/adfm.202413324 by Koc University, Wiley Online Library on [22/05/2025]. See the Terms and Conditions (https://onlinelibrary.wiley.com/terms-and-conditions) on Wiley Online Library for rules of use; OA articles are governed by the applicable Creative Commons License

current received into a direct current output.[195,314,315] Antennas play an essential role in wireless power transmission for various biomedical applications, including implantable devices and ingestible and wearable electronics.[312,316–318] Ingestible devices rely on antennas to transmit data from inside the body to external receivers, enabling real-time monitoring of physiological conditions.[319,320] For instance, ultrahigh-frequency RF antennas have been shown to work effectively in the gastrointestinal tract, transmitting signals from ingestible sensors to external monitors, even in the presence of varying pH and humidity levels.[26,321–326] In wearable technologies, antennas facilitate continuous wireless communication between sensors embedded in clothing or skin patches and external systems.[310,311] When integrated into implantable electronics, antennas, particularly those utilizing RF transmission, offer significant advantages, including noninvasive energy harvesting and data transmission from deep within the body.[36] RF antennas' flexibility and compact design also make them ideal for biomedical devices, where minimizing size and optimizing patient comfort are crucial. In biomedical applications, antennas need to be flexible, biocompatible, and, in some cases, biodegradable to reduce long-term risks associated with permanent implants.[327] Recent advancements have pushed the development of bioresorbable antennas, which degrade safely after their functional lifetime, eliminating the need for removal surgeries.[61,328,329] A straightforward instance of a bioresorbable antenna is showcased by linear-dipole structures made of Mg, which are 500 nm in thickness and feature two quarter-wavelength arms along with wideband quasilog-periodic dipoles, situated on silk fibroin films. These were fabricated using physical vapor deposition through shadow masks[64] (**Figure 14a**). It has been demonstrated that by an applied power of 20 W, the proposed antenna was able to transfer power of 54 mW to a distance of around 2 m at a frequency of 950 MHz. In another implementation, a bioresorbable RF energy harvester was designed for near-field operations including a disk-shaped coil.[61] In this design, the near-field harvester antenna was constructed from two layers of Mg coil, separated by a dielectric interlayer made from poly(lactic-*co*-glycolic acid). A Si NM was utilized in the structure of the design as an RF diode for the rectification process, coupled to a Mg/SiO2/Mg capacitor for signal smoothing. The device was designed for neurostimulation applications, operating at a resonance frequency of around 5 MHz. In another implementation, Choi et al.,[195] utilized a wireless power harvesting system for cardiac pacing. Alternatively, a low-frequency PIN diode with significant parasitic capacitance has been utilized in a capacitor-free harvester design, featuring a disk-shaped coil of 17 turns and a 25 mm diameter. In more sophisticated versions, the use of multiple receiving coils, each tuned to different resonance frequencies, lays the groundwork for frequency-selective energy harvesting. This method is applicable either for powering various components within a single device or for selectively energizing multiple devices located within the same area[330] (Figure 14b). Such a technique finds practical application in the programmed release of drugs from multiple, independently managed reservoirs[328,331] (Figure 14c).

4.3. Energy Storage Devices

Batteries in implantable devices are often rigid and bulky and occupy significant space. Moreover, since they are not biodegradable, they pose risks to the body and necessitate a second surgery for removal. Although significant efforts have recently focused on harnessing ambient energy sources, such as body movements,[332] glucose oxidation,[333] and wirelessly transmitting energy through methods like electromagnetic/acoustic waves,[334,335] or solar radiation to power implantable devices,[336] these approaches still face various challenges.[337] Consequently, biodegradable energy storage components for medical implants are becoming increasingly necessary, even as energy harvesting technologies like piezoelectric energy harvesting implants and triboelectric nanogenerators offer renewable energy sources. When external or harvested energy is unavailable, these devices can store and supply energy to bioresorbable medical equipment. Because of their high energy/power density and flexibility to be deployed independently, biodegradable energy storage devices—such as batteries and supercapacitors—have been highlighted in recent publications as a viable alternative to conventional energy sources.[338–345] In recent years, transition-metal-based metal–organic frameworks (MOFs), particularly those incorporating metals like iron, cobalt, and nickel, have emerged as promising materials for biodegradable energy storage devices due to their high porosity, tunable structures, and the ability to facilitate efficient ion transport.[346] Despite their potential, these devices also have certain drawbacks that limit their use in implantable bioelectronics.[339] For example, more adequate contact between the active material and the current collector is often needed. The ion transport pathways are long and inefficient, resulting in poor electrochemical performance, including lower output voltage, energy, and power density. Moreover, their large size and mechanical rigidity make them unsuitable for implantable devices' compact and flexible design needs. Research in this field is ongoing to develop energy storage devices that are small, have sufficient capacity, and possess mechanical flexibility to integrate with soft biological tissues fully.

4.3.1. Bioabsorbable Batteries

Bioabsorbable batteries have been developed to power transient medical devices without the need for surgical removal.[347] These

experiments. b-iv) Optical images of the implantation process of the device before in vivo experiment. b-v) Aperture contrast images, fluorescent images, microscopic fluorescent images, and microscopic optical images were taken for characterization of the mineral formation in the defect, presence of ALP producing cells in the defect, the migration of Collagen 3.6 gene positive cells in the defect, the bone formation in the defect, respectively. Reproduced with permission.[308] Copyright 2020, Elsevier. c-i) Schematic illustration of the device and its output as the result of ultrasound actuation. c-ii) Open circuit voltage generated by the device after application of acoustic pressure of 150 kPa at the frequency of 1 MHz and pulse width of 5 µs. c-iv) Schematic illustration for the in vivo protocol for spinal cord injury repair by the aid of an ultrasound activation. c-v) Histological images of spinal cords prepared after 8 weeks. c-vi) Luxol fast blue staining of myelin sheaths on longitudinal sections of spinal cords collected after 8 weeks. Reproduced with permission.[118] Copyright 2022, American Chemical Society.

© 2024 The Author(s). Advanced Functional Materials published by Wiley-VCH GmbH

16163028, 2025, 3, Downloaded from https://advanced.onlinelibrary.wiley.com/doi/10.1002/adfm.202413324 by Koc University, Wiley Online Library on [22/05/2025]. See the Terms and Conditions (https://onlinelibrary.wiley.com/terms-and-conditions) on Wiley Online Library for rules of use; OA articles are governed by the applicable Creative Commons License

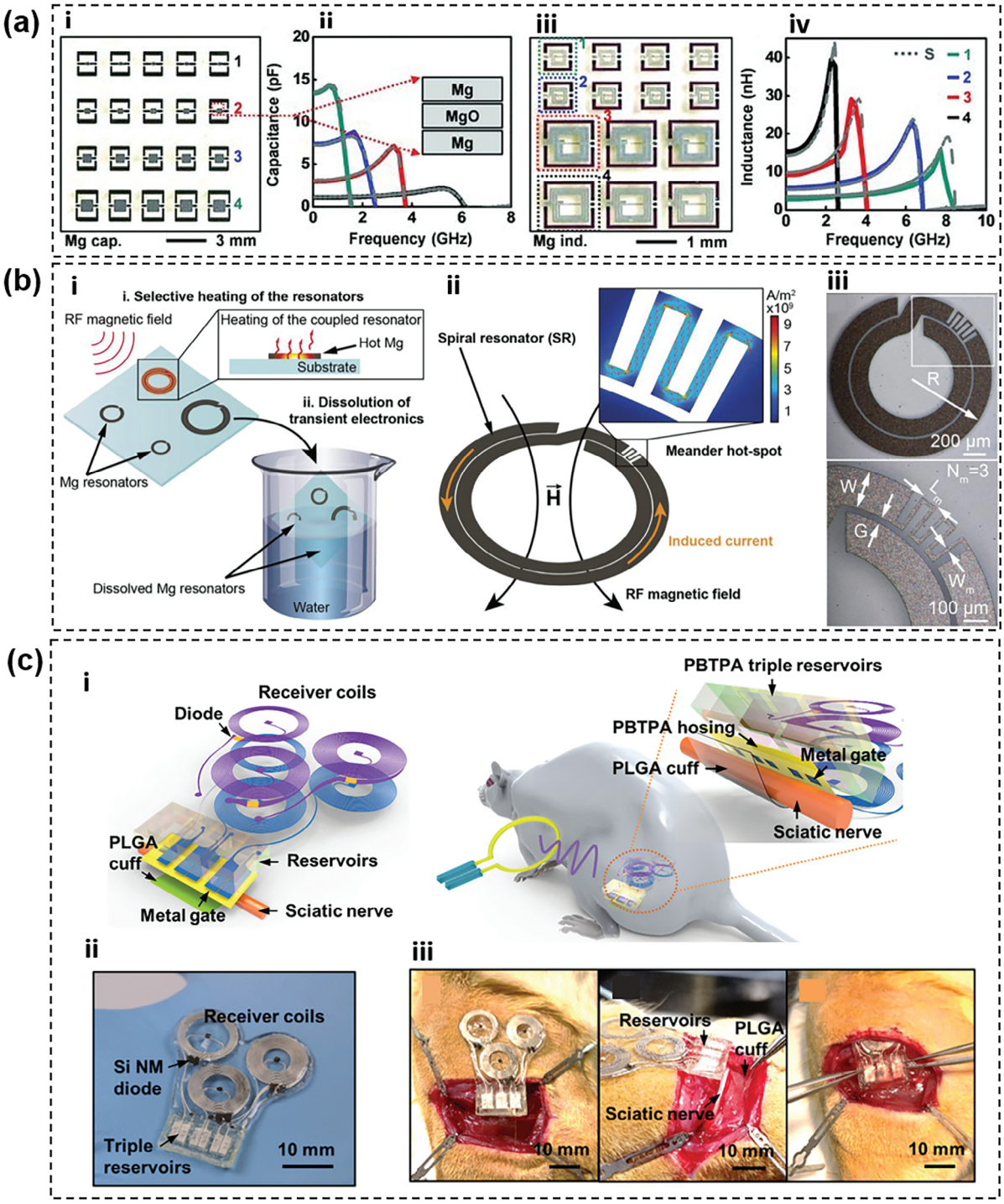


Figure 14. a-i) Optical images indicating capacitors of varying dimensions fabricated with Mg electrodes and MgO dielectrics. a-ii) Capacitance measurements resulting up to the frequency of 6 GHz. a-iii) Optical images indicating a series of inductors fabricated from Mg electrodes and MgO for interlayer dielectrics. a-iv) The measured results of the inductors as a function of frequency up to ≈8 GHz. Reproduced with permission.[64] Available under a Creative Commons CC BY license. Copyright 2013, John Wiley & Sons. b-i) Conceptual illustration indicating frequency-selective, biodegradable microresonators as power receivers and microheaters for transient electronics. b-ii) Finite element simulation of a spiral resonator (SR) with a meander hot spot, engineered to increase the induced current density by one to two orders of magnitude. b-iii) Optical image of the fabricated spiral antenna and microheater and related dimensions. Reproduced with permission.[330] Available under a Creative Commons CC BY license. Copyright 2013, John Wiley & Sons. c-i) Schematic illustration of the system with triple reservoirs and a cuff structure interfacing with the sciatic nerve. The figure also indicates the design details of the nerve interface and the layers and used materials. c-ii) An optical image of the developed device, and c-iii) optical images of the device during the implantation process and in vivo experiments. Reproduced with permission.[331] Available under a Creative Commons CC BY license. Copyright 2020, The American Association for the Advancement of Science.

© 2024 The Author(s). Advanced Functional Materials published by Wiley-VCH GmbH

16163028, 2025, 3, Downloaded from https://advanced.onlinelibrary.wiley.com/doi/10.1002/adfm.202413324 by Koc University, Wiley Online Library on [22/05/2025]. See the Terms and Conditions (https://onlinelibrary.wiley.com/terms-and-conditions) on Wiley Online Library for rules of use; OA articles are governed by the applicable Creative Commons License

batteries should degrade safely in the body after use, avoiding complications associated with permanent implants.[36,348,349] The development of such batteries is focused on materials that can deliver sufficient energy for short-term applications while being biocompatible and degradable.

In a study, Huang et al. developed a high-performance dual-electrolyte magnesium-iodine battery that is fully biodegradable, offering a safe and eco-friendly solution for both biomedical implants and environmental sensors.[340] The battery is designed to completely resorb in the body or environment, addressing the growing concern of waste from conventional batteries. This battery utilizes magnesium as the anode and iodine as the cathode, with a dual-electrolyte system combining ionic liquid and aqueous electrolytes. This setup has reached high voltage (up to 1.8 V) and improved energy density. The battery's areal capacity reaches 10 mAh cm^{-2} with a volumetric energy density of 93 mWh cm^{-3}. The dual-electrolyte design significantly reduces the rate of iodine leaching, enabling the battery to retain 87% of its capacity after 7 days of immersion in PBS at 37 °C. The in vivo degradation studies showed that the Mg anode corroded as expected, and the iodine dissolution rate remained within safe limits. The battery was implanted in rats, where it maintained stable operation for 5 days, with minimal impact on surrounding tissues.

4.3.2. Bioabsorbable Capacitors and Supercapacitors

Recent advances in bioabsorbable supercapacitors and capacitors have opened up new possibilities for powering transient implantable medical devices. Research has focused on developing flexible, high-performance devices that meet the stringent requirements of implantable medical electronics.

Li et al. developed a biodegradable capacitor designed to serve as a temporary energy storage device for implantable medical electronics.[341] The capacitor features a layer-by-layer structure consisting of a PLA substrate with nanopillar arrays, a nanoporous zinc oxide (ZnO) layer for energy storage, and a PVA and PBS hydrogel as the electrolyte and separator. The capacitor demonstrated a high voltage of 1.5 V and acceptable capacitive performance, with 70% capacitance retention after 3000 charge/discharge cycles. It operated stably for up to 30 days in vitro in PBS and up to 50 days in vivo in rats. The capacitor's operation time could be adjusted by altering the encapsulation, allowing for tunable work durations ranging from days to weeks. Sheng et al. further advanced the field by creating a fully biodegradable supercapacitor that is lightweight, flexible, and capable of storing significant energy.[350] Constructed with 2D amorphous molybdenum oxide (MoOx) flakes on water-soluble molybdenum foil, the supercapacitor exhibited an areal capacitance of 112.5 mF cm^{-2} and an energy density of 15.64 μWh cm^{-2}. Its mechanical flexibility allows it to conform to soft tissues, making it suitable for implantable electronics. The device demonstrated biocompatibility and bioabsorption, with stable performance during degradation, retaining 86.7% of its capacitance after 2000 cycles. Encapsulation adjustments with biodegradable materials like PLA and sodium alginate could also control its degradation timeline. In another study, Sheng and colleagues introduced a wireless charging system integrated with Zn-ion hybrid supercapacitors.[342] This soft, flexible power supply featured molybdenum sulfide (MoS_2) nanosheets as the cathode, an ion-crosslinked alginate gel electrolyte, and a zinc foil anode. The device demonstrated high energy storage performance with a capacitance of 93.5 mF cm^{-2} and a voltage of 1.3 V. A biodegradable magnesium (Mg) coil and rectifier circuit allow wireless energy transmission, providing sustained power.

5. Conclusions and Perspectives

The area of implantable electronics stands as a captivating domain rich with potential for medical applications. Within this area, bioresorbable materials interact deliberately with the surrounding biological medium. This interaction is orchestrated through a spectrum of potential metabolic pathways involving enzymatic reactions, hydrolysis, or alternative processes. Occasionally, these processes occur concurrently with physical disintegration or fragmentation mechanisms. In this review, we draw attention to the latest breakthroughs in bioresorbable electronics, with a specific emphasis on their utilization within implantable platforms designed for continuous and real-time measurement and monitoring of postsurgery vital signals. The content of this review encompasses illustrations of various components that incorporate diagnostic or therapeutic functionalities, aligning seamlessly with clinical requirements. Beyond this, we also touch upon some emerging prospects and the accompanying challenges, which we briefly introduce in the following, illustrated in **Figure 15**.

5.1. Challenges

5.1.1. Biocompatibility

Navigating the challenges of biocompatibility in biodegradable microdevices for postoperative monitoring is pivotal in harnessing their potential to revolutionize patient care.[351,352] These devices, designed for intimate biological interaction, must meet rigorous biocompatibility standards to ensure patient safety and device efficacy. A primary concern is the body's immune response, which can interpret the implanted device as a foreign entity, initiating a cascade of reactions from mild inflammation to severe, chronic immune attacks. Such responses can culminate in fibrous encapsulation, impairing the device's function and the body's healing process. In addition to immune responses, safety concerns arise when biodegradable implants are exposed to external electromagnetic fields, such as RF waves or MRI environments. A key factor in ensuring patient safety is the specific absorption rate (SAR), which represents the amount of RF power absorbed per unit of mass of body tissues indicated in W kg^{-1}.[353] The SAR is governed by the equation[354]

$$SAR = \frac{\sigma}{2\rho} \left|E^2\right| \quad (1)$$

where σ is the conductivity of the material (S m^{-1}), ρ is material density (kg m^{3-1}), and E is the electric field. When biodegradable materials are exposed to MRI or RF radiation, it is

© 2024 The Author(s). Advanced Functional Materials published by Wiley-VCH GmbH

16163028, 2025, 3, Downloaded from https://advanced.onlinelibrary.wiley.com/doi/10.1002/adfm.202413324 by Koc University, Wiley Online Library on [22/05/2025]. See the Terms and Conditions (https://onlinelibrary.wiley.com/terms-and-conditions) on Wiley Online Library for rules of use; OA articles are governed by the applicable Creative Commons License

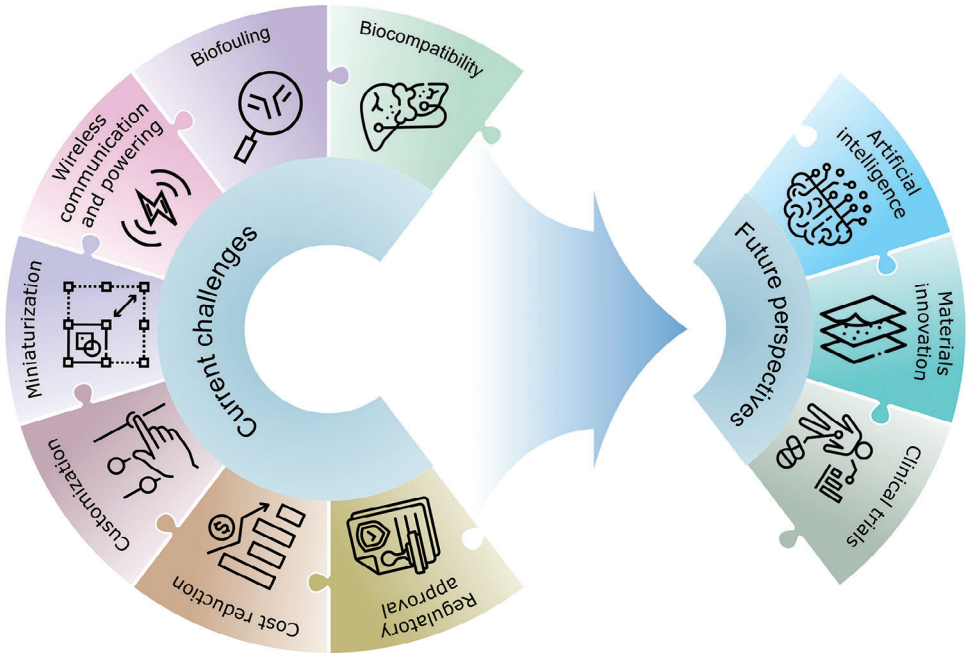


Figure 15. A systematic delineation of the current challenges and future perspectives for biodegradable and implantable platforms for postsurgery applications. The near-term obstacles and forthcoming tasks are depicted on the left, whereas long-term goals and issues for resolution are illustrated on the right.

important to make sure they do not induce excessive tissue heating. Certain biodegradable implants, especially those composed of polymers or magnesium, may react to RF waves in different ways.[354,355] These implants' direct contact with MRI fields may cause regional heating issues, even though their eventual breakdown in the body may lower long-term exposure hazards. The SAR can assist in determining whether biodegradable implants meet safety requirements and whether there is a risk of tissue heating. Addressing this necessitates research into bioactive coatings or surface modifications encouraging biointegration and mitigating the body's defensive reflex. The cornerstone of these devices, the biodegradable materials, presents another challenge. These substances must degrade predictably into harmless byproducts, maintaining structural integrity until their mission concludes. The degradation process, including corrosion control and managing degradation byproducts, requires meticulous attention to prevent adverse biological reactions. Moreover, the risk of infection due to implantation procedures necessitates exploration into antibacterial coatings or materials. However, introducing such substances complicates the biocompatibility landscape, as they must not provoke further inflammatory responses or hinder the healing trajectory. A notable gap in current research is understanding the long-term physiological implications of these biodegradable materials postdegradation. Extended studies and postmarket monitoring are essential for uncovering potential chronic issues, demanding robust, long-term clinical trials. Looking forward, the field is ripe for innovation. Novel research lines could explore the intersection of nanotechnology with immunomodulatory therapies, devising ways to manipulate the immune response at the molecular level. Another promising avenue is integrating real-time monitoring systems within these devices, capable of tracking inflammation markers or infection indicators, thereby providing immediate alerts regarding biocompatibility issues. The journey toward seamlessly biocompatible implantable microdevices is complex, demanding a symbiotic balance between biological acceptance and technological advancement.

5.1.2. Biofouling

The signal stability of implantable biosensors can be augmented by mitigating biofouling occurrences and reducing the body's foreign object reactions. A wealth of studies has been dedicated to exploring various passive and active approaches for tackling biofouling within biological systems. Passive strategies involve the use of advanced materials, including hydrophilic, biomimetic, drug-releasing, and zwitterionic polymers, designed to inherently resist biofouling. In contrast, active methods include the application of stimulus-responsive materials as well as electromechanical and electromagnetic transducers that actively combat biofouling. However, many of these strategies have been investigated in isolation, primarily demonstrating their effectiveness in vitro, with limited focus on comprehensive system integration or prolonged in vivo evaluation. This gap presents extensive opportunities to exhibit the long-term in vivo efficacy of antibiofouling biosensors using these techniques or more innovative solutions. For example, the development of a more reliable biosensor that integrates both passive and active antibiofouling measures could potentially 1) delay the initial phase of biofouling and 2) eliminate bioaccumulation when necessary, ensuring more consistent and durable functionality within the host. The potential also exists to harness various assortments of materials, structures, and transducers to enhance long-term dependability. Undoubtedly, other

© 2024 The Author(s). Advanced Functional Materials published by Wiley-VCH GmbH

16163028, 2025, 3, Downloaded from https://advanced.onlinelibrary.wiley.com/doi/10.1002/adfm.202413324 by Koc University, Wiley Online Library on [22/05/2025]. See the Terms and Conditions (https://onlinelibrary.wiley.com/terms-and-conditions) on Wiley Online Library for rules of use; OA articles are governed by the applicable Creative Commons License

challenges unique to specific applications and production hurdles must be addressed when adapting these innovative methods for clinical implementation. For passive antibiofouling strategies, an exhaustive study into the stability, scalability, and production feasibility of the material or surface is crucial. Furthermore, for active antibiofouling methods, examining the frequency and duty cycle necessary for removing biofouling is essential. Indeed, several critical engineering challenges must be confronted to improve the reliability of implantable biosensors, including stabilizing biorecognition elements and understanding diverse nonbiological degradation pathways. Nevertheless, addressing the complications associated with biofouling constitutes a substantial advancement, paving the way for biosensors characterized by enhanced consistency and extended operational lifespan.

5.1.3. Wireless Communication and Powering

In terms of wireless communication, future research efforts are poised to focus on the development of a completely biodegradable wireless system. This involves engineering a wireless transmission circuit that facilitates the communication of captured signals across the skin barrier. An integral hurdle in this endeavor is pinpointing an optimal operating frequency to ensure efficient functionality. Utilizing high frequencies is crucial for transmitting significant energy, yet this practice also increases the absorption of energy within the human body. Conversely, employing lower frequencies leads to a reduction in sensor sensitivity. At present, magnetic field power transfer, specifically through resonant inductive coupling, stands as the dominant strategy for wireless power transfer. This method garners preference, particularly in scenarios where the distance between the interrogating instrument and the embedded sensor is relatively small. In such scenarios, near-field technology exhibits appealing attributes, such as elevated energy transfer efficiency. It achieves this without necessitating excessively high operation frequencies that might lead to heightened power absorption within living tissue. Additionally, the achieved miniaturization of these sensors ensures their seamless integration within the body, offering a level of convenience. While microwave power transfer, often referred to as far-field technology, is still in its nascent stages when applied to medical diagnosis, it exhibits significant promise. The support for extreme sensor miniaturization is a distinctive advantage of this technology. While higher operational frequencies may not present the most efficient power transfer currently, they enhance the operational range of these sensors, offering extended working distance capabilities compared to those achievable with resonant inductive coupling methods.

5.1.4. Miniaturization

Ongoing research in implantable sensor technology also focuses on miniaturization. To be effective in postsurgery scenarios, these sensors must achieve a high degree of miniaturization and lightness, rendering them suitable for both wearable and implantable applications. Achieving this level of miniaturization necessitates the development of innovative fabrication techniques and the utilization of advanced materials to reduce the device's size while preserving its functionality. Moreover, the adoption of flexible and stretchable materials, such as polymers and elastomers, plays a pivotal role in the miniaturization process. These materials enable the sensors to conform seamlessly to the skin's surface or internal organs, ensuring comfortable and inconspicuous integration while maintaining efficient functionality.

5.1.5. Customization

An essential benefit offered by patient-centered care lies in its capacity to deliver treatment that is personalized and individualized. Analytical microdevices can be crafted to align precisely with the unique needs of each patient, facilitating the creation of highly tailored therapeutic interventions. Scientists are actively investigating multiple strategies for tailoring these devices, which encompass employing machine learning algorithms to fine-tune the design according to individual patient requirements. Furthermore, the utilization of flexible and stretchable materials further enhances customization by allowing the device to seamlessly adapt to the contours of the internal organs.

5.1.6. Cost Reduction

The affordability of producing transient biosensors for implantable applications presents a notable challenge to their widespread adoption. This stems primarily from the considerable expenses associated with materials and manufacturing techniques, especially when custom or miniature devices are involved. Consequently, scientists are investigating several strategies to mitigate these costs. One strategy entails the utilization of economical and readily available materials, such as polymers and metals. Another approach involves the development of scalable and high-throughput manufacturing processes, aimed at cost reduction. For instance, researchers are exploring techniques like 3D printing, laser cutting, and roll-to-roll printing to create large-scale sensors more economically. Furthermore, integrating biosensors with other technologies, such as sensors and wireless communication, offers an avenue to decrease the overall system cost by enabling more efficient and targeted treatment.

5.1.7. Regulatory Approval

Securing regulatory clearance for bioanalytical microdevices, particularly those designed for implantation, is essential for their broad acceptance within clinical environments. The pathway to regulatory approval necessitates rigorous testing and assessment of these devices to ascertain their safety and effectiveness. This, in turn, mandates the establishment of standardized testing protocols and methodologies that facilitate a uniform and replicable evaluation process. Furthermore, the attainment of regulatory approval demands the creation of manufacturing methods and quality control protocols that guarantee the safety and dependability of transient devices. These measures are integral to ensuring the overall quality and reliability of the devices in question.

© 2024 The Author(s). Advanced Functional Materials published by Wiley-VCH GmbH

16163028, 2025, 3, Downloaded from https://advanced.onlinelibrary.wiley.com/doi/10.1002/adfm.202413324 by Koc University, Wiley Online Library on [22/05/2025]. See the Terms and Conditions (https://onlinelibrary.wiley.com/terms-and-conditions) on Wiley Online Library for rules of use; OA articles are governed by the applicable Creative Commons License

16163028, 2025, 3, Downloaded from https://advanced.onlinelibrary.wiley.com/doi/10.1002/adfm.202413324 by Koc University, Wiley Online Library on [22/05/2025]. See the Terms and Conditions (https://onlinelibrary.wiley.com/terms-and-conditions) on Wiley Online Library for rules of use; OA articles are governed by the applicable Creative Commons License

5.2. Future perspectives

5.2.1. Artificial Intelligence Integration

Many existing implantable devices primarily focus on either sensing or stimulation functions, accompanied by a wireless connection for energy provision or data transfer to an external apparatus. Yet, there is a pressing demand for systems offering integrated closed-loop therapeutic capabilities. These systems utilize continuous biofeedback to modify treatment parameters autonomously, be it drug delivery or stimulation, targeting the preservation or attainment of a specific physiological condition. Closed-loop soft bioelectronic systems typically encompass three fundamental components: 1) a module dedicated to monitoring physiological signals, 2) electronic components for the assimilation and analysis of data, and 3) a feedback-responsive therapeutic module, as depicted in Figure 13. Enhancing therapeutic results through tailored treatment necessitates that these closed-loop constructs satisfy a multitude of criteria. Among these, the capacity for self-powering is critical, given that reliance on external power sources could impose limitations, cause discomfort, or inflict potential harm on the biological host system. Furthermore, a closed-loop system should facilitate tailored therapies (be they pharmacological or through stimulation) grounded in precise health monitoring. This objective necessitates the incorporation of machine learning algorithms calibrated in accordance with the unique physiological landscape of each individual. Such an approach is crucial for devising an efficacious, personalized medication regimen that is congruent with the patient's daily routine and specific health circumstances.[356] Most contemporary closed-loop mechanisms rely on algorithms grounded in predefined rules for their regulatory functions. Essential to the data processing core of these bioelectronic systems is the development of precise and sensitive acquisition techniques capable of handling signals of various modalities, including biophysical, chemical, and electrical characteristics. Utilization of mathematical analyses is imperative for isolating intended signals amidst background interference. To enhance treatment effectiveness, recent advancements have seen the formulation of diverse training strategies, such as artificial neural networks and intelligent algorithms. These methods are designed to amalgamate data from multiple biomarkers, enabling an exhaustive analytical process.[357] The analysis of extensive datasets, spanning various timelines and demographics, will connect patterns of disease with prospective treatment modalities. This connection paves the way for predictive algorithms that bolster both diagnosis and treatment procedures. When fused with Artificial Intelligence (AI) technologies, these intelligent closed-loop systems possess the potential to enhance precision in diagnosis and treatment. By expediting the decision-making pathway, they offer a novel therapeutic framework for comprehensive disease management.[358] For instance, Ward and colleagues introduced a sophisticated wound dressing patch operating on a closed-loop system, integrating a pyocyanin detection mechanism, a platform predicting antibiotic toxicity aided by artificial neural networks, and modules allowing regulated medication dosing.[359] Employed in multiple evaluations, this sensor system could identify pyocyanin levels, subsequently triggering the targeted release of antimicrobial medications as required, thereby facilitating enhanced wound recovery processes. Nonetheless, several obstacles in this realm persist, necessitating further exploration and resolution. For instance, the implementation of AI-driven control mechanisms capable of self-calibration presents challenges, particularly in the intricate tasks of biosignal identification, categorization, and consequential decision-making.[360] Furthermore, there is an imperative need to develop platforms capable of rendering medical data, sourced from bioelectronics, visually comprehensible. Such advancements are crucial in meeting patients' growing needs for independent oversight of their health status and medical conditions. Additionally, aspects such as system miniaturization, strategies for signal capture and interpretation, precise timing, and meticulous material selection warrant attention to ensure the efficacy of a high-performance therapeutic closed-loop system.[361,362]

5.2.2. Materials Innovation

Advancements in bioresorbable materials chemistry will persist as the foundational driver of progress in this technology. An avenue for further research with significant potential lies in exploring chemical techniques that offer precise mastery over the mechanisms and pace of bioresorption. As an illustration, existing materials support applications that can function for days or several weeks, but achieving the requisite enduring stability for chronic applications remains unattainable. To overcome this constraint, advanced materials must serve as effective shields against biofluid infiltration and undergo gradual dissolution primarily through surface erosion mechanisms. Aside from the materials used for encapsulation, it is imperative to develop techniques for effectively bonding biofluid barrier materials and securely sealing bioresorbable electronics. Sturdy conductive composites are vital to the integration process that establishes connections between various electronic components. Furthermore, in numerous systems, the timeframes required for complete bioresorption extend significantly beyond the durations associated with operational stability. To narrow this gap, there is an interest in chemical processes that facilitate quicker resorption rates when triggered by an external stimulus. The flexible nature of many implantable and wearable devices presents another material-related challenge, particularly when dealing with components like antennas and coils. Flexibility can lead to resonance frequency shifts, affecting the efficiency and stability of wireless communication. However, advancements in substrate materials, such as dielectro-elastic elastomers, which exhibit tunable dielectric properties, offer a promising solution to maintain stable operating frequencies.[363] By controlling the relative permittivity of the substrate, such materials help ensure that resonance frequency remains consistent, even under dynamic conditions. These materials also show potential for integration into future biodegradable devices, where flexibility and reliable performance are critical. A comprehensive understanding of the long-term consequences of bioresorbable devices and the byproducts generated as they undergo degradation within the biological environment is still an ongoing effort. Presently, most evaluations for implantable microdevices are conducted either using artificial bodily fluids or during in vivo experiments on small animal models. More investigation is required, especially employing large animal models

 © 2024 The Author(s). Advanced Functional Materials published by Wiley-VCH GmbH

during in vivo experiments to characterize the degradation mechanism and any possible biological effects.

5.2.3. Clinical Trials

Clinical trials play a crucial role in assessing the effectiveness of analytical microdevices for implantable and other medical applications. The results from these trials provide essential insights to guide the development and clinical use of such devices. Additionally, they offer a key opportunity to validate the personalized approach to disease diagnosis enabled by the proposed technology. Currently, there are few clinical trials involving implantable biosensors used for postsurgery monitoring and other applications. This highlights the urgent need for more extensive and rigorous clinical investigations to evaluate their safety and efficacy. These trials should include a diverse patient population with varying health conditions, ages, and medical histories. Moreover, it is essential that these trials thoroughly assess the long-term safety and effectiveness of these devices. The outcomes of these studies could provide valuable insights into the efficacy of temporary implants, significantly influencing precise diagnostic procedures and shaping the future of medical device technologies and therapeutic guidelines.

In summary, the journey toward creating entirely biodegradable implants for medical use remains extensive, particularly considering the medical community's familiarity with non-biodegradable sensors, backed by a more extended usage history. However, the pursuit is undeniably warranted due to the prospective enhanced patient comfort and safety. Despite various challenges, continuous advancements have marked significant milestones in the past decade. With major technological hurdles now overcome, there's optimistic anticipation for the prevalent adoption of active, biodegradable, and implantable platforms in human healthcare. Their successful integration into clinical practice could dramatically elevate patient health outcomes.

5.3. Commercialization

The process of bringing transient/biodegradable electronic implants from concept to clinical use is a lengthy, intricate, and expensive endeavor, often taking 3–7 years to reach clinical validation and regulatory approval.[364,365] The financial burden is significant, with premarket approval costing around $100 million.[366] Due to the novel nature of biodegradable implants, there are no established, standardized manufacturing processes for large-scale production, leading to increased costs and added complexities in regulatory compliance.[356] To successfully compete in the medical market, new devices must offer a notable cost reduction, show clear clinical advantages over current solutions, or address unmet medical needs.[356]

Commercialization becomes more appealing when these devices can serve dual purposes in clinical and commercial markets. For instance, biodegradable implants initially designed for cardiovascular monitoring may have potential applications in other areas, such as wound healing or orthopedic treatments, thus increasing their market potential. The rise of start-ups specializing in biodegradable electronics, such as Neurosoft Bioelectronics and BeFC, further drives the rapid development of these technologies, pushing patient-centric solutions more swiftly toward clinical adoption.

Nonetheless, biodegradable implants face significant regulatory and ethical challenges that can delay their market entry.[367–369] To streamline the approval process and improve the quality of these devices, adopting frameworks like IDEAL-D (idea, development, exploration, assessment, and long-term follow-up) can help create a structured path for evaluating and validating new technologies[370] The process involves rigorous in vitro and in vivo testing for transient implants, typically starting with animal models and followed by human trials to ensure safety, functionality, and predictable degradation.[371]

Understanding patient and clinician perspectives is also crucial for successfully commercializing these implants.[372] Gathering feedback through surveys or focus groups can help assess patient concerns about comfort, safety, and overall experience with the devices. On the other hand, clinicians must evaluate the ease of use, including the ergonomics of implantation and any additional training requirements.[373] A thorough economic evaluation is also necessary to understand the broader impact on healthcare costs, ensuring the technology is both practical and economically viable for widespread adoption.[372,373]

By navigating these challenges with a clear roadmap that includes rigorous testing, regulatory planning, scalable manufacturing, and economic assessments, biodegradable electronic implants have the potential to transform healthcare across various applications while meeting the expectations of both patients and the market.[367,368,373]

Acknowledgements

This work has been supported by a Marie Skłodowska-Curie Post-doctoral Fellowship (No. H2020-MSCA-IF-2021-101068646, HAMP).

Conflict of Interest

The authors declare no conflict of interest.

Keywords

biodegradable, biosensors, electronics, wireless communication

Received: July 24, 2024
Revised: September 23, 2024
Published online: October 23, 2024

[1] J. Y. Chyou, E. Barkoudah, J. W. Dukes, L. B. Goldstein, A. M. Lee, S. A. Lubitz, K. A. Marill, K. B. Sneed, M. M. Streur, G. C. Wong, R. Gopinathannair, *Circulation* **2023**, *147*, e676.
[2] S.-W. Hwang, H. Tao, D.-H. Kim, H. Cheng, J.-K. Song, E. Rill, M. A. Brenckle, B. Panilaitis, S. M. Won, J. A. Rogers, *Science* **2012**, *337*, 1640.
[3] K. J. Yu, D. Kuzum, S.-W. Hwang, B. H. Kim, H. Juul, N. H. Kim, S. M. Won, K. Chiang, M. Trumpis, A. G. Richardson, H. Cheng, H. Fang, M. Thompson, H. Bink, D. Talos, K. J. Seo, H. N. Lee, S.-K. Kang, J.-H. Kim, J. Y. Lee, Y. Huang, F. E. Jensen, M. A. Dichter, T. H. Lucas, J. Viventi, B. Litt, J. A. Rogers, *Nat. Mater.* **2016**, *15*, 782.

© 2024 The Author(s). Advanced Functional Materials published by Wiley-VCH GmbH

16163028, 2025, 3, Downloaded from https://advanced.onlinelibrary.wiley.com/doi/10.1002/adfm.202413324 by Koc University, Wiley Online Library on [22/05/2025]. See the Terms and Conditions (https://onlinelibrary.wiley.com/terms-and-conditions) on Wiley Online Library for rules of use; OA articles are governed by the applicable Creative Commons License

[4] D. Dobrev, M. Aguilar, J. Heijman, J.-B. Guichard, S. Nattel, *Nat. Rev. Cardiol.* **2019**, *16*, 417.
[5] M. Gaudino, A. Di Franco, L. Q. Rong, J. Piccini, M. Mack, *Eur. Heart J.* **2023**, *44*, 1020.
[6] P. Rimington, P. Dasgupta, *Nat. Clin. Pract. Urol.* **2007**, *4*, 414.
[7] J. Hah, S. C. Mackey, P. Schmidt, R. McCue, K. Humphreys, J. Trafton, B. Efron, D. Clay, Y. Sharifzadeh, G. Ruchelli, S. Goodman, J. Huddleston, W. J. Maloney, F. M. Dirbas, J. Shrager, J. G. Costouros, C. Curtin, I. Carroll, *JAMA Surg.* **2018**, *153*, 303.
[8] J. A. Kellum, P. Romagnani, G. Ashuntantang, C. Ronco, A. Zarbock, H.-J. Anders, *Nat. Rev. Dis. Primers* **2021**, *7*, https://doi.org/10.1038/s41572-021-00284-z.
[9] T. R. Harring, N. S. Deal, D. C. Kuo, *Emerg. Med. Clin.* **2014**, *32*, 379.
[10] A. Kiourti, K. S. Nikita, *IEEE Antennas Propag. Mag.* **2012**, *54*, 190.
[11] A. Sani, M. Rajab, R. Foster, Y. Hao, *Proc. IEEE* **2010**, *98*, 1648.
[12] J. Dean, N. Sulke, *Br. Med. J.* **2016**, *352*, i228.
[13] A. L. Chamis, G. E. Peterson, C. H. Cabell, G. R. Corey, R. A. Sorrentino, R. A. Greenfield, T. Ryan, L. B. Reller, V. G. Fowler, Jr, *Circulation* **2001**, *104*, 1029.
[14] L. Hall-Stoodley, J. W. Costerton, P. Stoodley, *Nat. Rev. Microbiol.* **2004**, *2*, 95.
[15] G. Lee, M. D. Does, R. Avila, J. Kang, K. D. Harkins, Y. Wu, W. E. Banks, M. Park, Di Lu, X. Yan, J. U. Kim, S. M. Won, A. G. Evans, J. T. Joseph, C. L. Kalmar, A. C. Pollins, H. Karagoz, W. P. Thayer, Y. Huang, J. A. Rogers, *Adv. Sci.* **2023**, *11*, 2301232.
[16] H. Ryu, X. Wang, Z. Xie, J. Kim, Y. Liu, W. Bai, Z. Song, J. W. Song, Z. Zhao, J. Kim, Q. Yang, J. J. Xie, R. Keate, H. Wang, Y. Huang, I. R. Efimov, G. A. Ameer, J. A. Rogers, *Adv. Sci.* **2023**, *10*, 2303429.
[17] Y. Zhang, G. Lee, S. Li, Z. Hu, K. Zhao, J. A. Rogers, *Chem. Rev.* **2023**, *123*, 11722.
[18] Y. Bai, H. Meng, Z. Li, Z. L. Wang, *Med. Mat.* **2024**, *1*, 40.
[19] H. Ouyang, Z. Liu, N. Li, B. Shi, Y. Zou, F. Xie, Y. Ma, Z. Li, H. Li, Q. Zheng, X. Qu, Y. Fan, Z. L. Wang, H. Zhang, *Nat. Commun.* **2019**, *10*, 1821.
[20] Z. U. Abdin, A. Basir, S. A. A. Shah, I. A. Shah, Y. Cho, H. Yoo, *Adv. Mater. Technol.* **2024**, https://doi.org/10.1002/admt.202400342.
[21] Y. Shen, C. Tang, B. Sun, Y. Wu, X. Yu, J. Cui, M. Zhang, M. El-Newehy, H. El-Hamshary, P. Barlis, W. Wang, X. Mo, *Adv. Healthcare Mater.* **2024**, *13*, 2304293.
[22] Z. Wang, J. Song, Y. Peng, *J. Alloys Compd.* **2024**, *1002*, 175313.
[23] D. Bian, Z. Tong, G. Gong, H. Huang, L. Fang, H. Yang, W. Gu, H. Yu, Y. Zheng, *Adv. Mater.* **2024**, *36*, 2401614.
[24] S. Lounansa, H. Ameddah, H. Mazouz, E. A. A. Alkebsi, *Aust. J. Mech. Eng.* **2024**, *22*, 642.
[25] M. He, Y.-I. Hsu, H. Uyama, *Appl. Mater. Today* **2024**, *36*, 102057.
[26] H. Mirzajani, C. Cheng, J. Wu, C. S. Ivanoff, E. N. Aghdam, H. B. Ghavifekr, *Sens. Actuators, B* **2016**, *235*, 330.
[27] W. H. Lee, G. D. Cha, D.-H. Kim, *Curr. Opin. Biotechnol.* **2021**, *72*, 13.
[28] A. Samir, F. H. Ashour, A. A. Hakim, M. Bassyouni, *Npj Mater. Degrad.* **2022**, *6*, 68.
[29] M. Sang, K. Kim, J. Shin, K. J. Yu, *Adv. Sci.* **2022**, *9*, 2202980.
[30] Y. Liu, Q. Yu, L. Yang, Y. Cui, *Adv. Mater. Technol.* **2023**, *8*, 2200853.
[31] Z. Zhai, X. Du, Y. Long, H. Zheng, *Front. Electron.* **2022**, *3*, 985681.
[32] G. Liu, Z. Lv, S. Batool, M.-Z. Li, P. Zhao, L. Guo, Y. Wang, Y. Zhou, S.-T. Han, *Small* **2023**, *19*, 2207879.
[33] W. B. Han, T.-M. Jang, B. Shin, V. R. Naganaboina, W.-H. Yeo, S.-W. Hwang, *Biosens. Bioelectron.* **2024**, *261*, 116472.
[34] Ž. Janićijević, T. Huang, D. I. S. Bojórquez, T. H. Tonmoy, S. Pané, D. Makarov, L. Baraban, *Adv. Sci.* **2024**, *11*, 2307232.
[35] H. Kim, B. Rigo, G. Wong, Y. J. Lee, W.-H. Yeo, *Nano-Micro Lett.* **2024**, *16*, 52.
[36] H. Mirzajani, M. Kraft, *ACS Sens.* **2024**, *9*, 4328.
[37] C. Godavitarne, A. Robertson, J. Peters, B. Rogers, *Biodegrad. Mater. Orthop. Trauma* **2017**, *31*, 316.
[38] X. Huang, L. Li, T. Liu, N. Hao, H. Liu, D. Chen, F. Tang, *ACS Nano* **2011**, *5*, 5390.
[39] M. Nishita, S.-Y. Park, T. Nishio, K. Kamizaki, Z. Wang, K. Tamada, T. Takumi, R. Hashimoto, H. Otani, G. J. Pazour, V. W. Hsu, Y. Minami, *Sci. Rep.* **2017**, *7*, https://doi.org/10.1038/s41598-016-0028-x.
[40] H. Zhuang, Y. Han, A. Feng, *Mater. Sci. Eng., C* **2008**, *28*, 1462.
[41] R. Pantani, A. Sorrentino, *Polym. Degrad. Stab.* **2013**, *98*, 1089.
[42] S. Virtanen, *Mater. Sci. Eng., B* **2011**, *176*, 1600.
[43] H.-S. Han, S. Loffredo, I. Jun, J. Edwards, Y.-C. Kim, H.-K. Seok, F. Witte, D. Mantovani, S. Glyn-Jones, *Mater. Today* **2019**, *23*, 57.
[44] C. Li, C. Guo, V. Fitzpatrick, A. Ibrahim, M. J. Zwierstra, P. Hanna, A. Lechtig, A. Nazarian, S. J. Lin, D. L. Kaplan, *Nat. Rev. Mater.* **2020**, *5*, 61.
[45] H. Ryu, M. H. Seo, J. A. Rogers, *Adv. Healthcare Mater.* **2021**, *10*, 2002236.
[46] G. Lee, S. K. Kang, S. M. Won, P. Gutruf, Y. R. Jeong, J. Koo, S.-S. Lee, J. A. Rogers, J. S. Ha, *Adv. Energy Mater.* **2017**, *7*, 1700157.
[47] D. Lu, T. L. Liu, J. K. Chang, D. Peng, Y. Zhang, J. Shin, T. Hang, W. Bai, Q. Yang, J. A. Rogers, *Adv. Mater.* **2019**, *31*, 1902739.
[48] S.-K. Kang, R. K. Murphy, S.-W. Hwang, S. M Lee, D. V. Harburg, N. A. Krueger, J. Shin, P. Gamble, H. Cheng, S. Yu, Z. Liu, J. G. McCall, M. Stephen, H. Ying, J. Kim, G. Park, R. C. Webb, C. H. Lee, S. Chung, D. S. Wie, A. D. Gujar, B. Vemulapalli, A. H. Kim, K.-M. Lee, J. Cheng, Y. Huang, S. H. Lee, P. V. Braun, W. Z. Ray, J. A. Rogers, *Nature* **2016**, *530*, 71.
[49] J. Y. Lee, C. A. Bashur, A. S. Goldstein, C. E. Schmidt, *Biomaterials* **2009**, *30*, 4325.
[50] J.-f. Zhou, Y.-g. Wang, L. Cheng, Z. Wu, X.-d. Sun, J. Peng, *Neural Regener. Res.* **2016**, *11*, 1644.
[51] D. Mawad, K. Gilmore, P. Molino, K. Wagner, P. Wagner, D. L. Officera, G. G. Wallace, *J. Mater. Chem.* **2011**, *21*, 5555.
[52] M. Xie, L. Wang, B. Guo, Z. Wang, Y. E. Chen, P. X. Ma, *Biomaterials* **2015**, *71*, 158.
[53] J. Chen, R. Dong, J. Ge, B. Guo, P. X. Ma, *ACS Appl. Mater. Interfaces* **2015**, *7*, 28273.
[54] Y. K. Lee, K. J. Yu, E. Song, A. B. Farimani, F. Vitale, Z. Xie, Y. Yoon, Y. Kim, A. Richardson, H. Luan, Y. Wu, X. Xie, T. H. Lucas, K. Crawford, Y. Mei, X. Feng, Y. Huang, B. Litt, N. R. Aluru, L. Yin, O. A. Rogers, *ACS Nano* **2017**, *11*, 12562.
[55] S.-K. Kang, G. Park, K. Kim, S.-W. Hwang, H. Cheng, J. Shin, S. Chung, M. Kim, L. Yin, J. C. Lee, K.-M. Lee, J. A. Rogers, *ACS Appl. Mater. Interfaces* **2015**, *7*, 9297.
[56] J.-K. Chang, M. B. Emon, C.-S. Li, Q. Yang, H.-P. Chang, Z. Yang, C.-I. Wu, M. T. Saif, J. A. Rogers, *ACS Nano* **2018**, *12*, 9721.
[57] S.-W. Hwang, G. Park, C. Edwards, E. A. Corbin, S.-K. Kang, H. Cheng, J.-K. Song, J.-H. Kim, S. Yu, J. Ng, J. E Lee, J. Kim, C. Yee, B. Bhaduri, Y. Su, F. G. Omennetto, Y. Huang, R. Bashir, L. Goddard, G. Popescu, K.-M. Lee, J. A. Rogers, *ACS Nano* **2014**, *8*, 5843.
[58] W. Park, V. P. Nguyen, Y. Jeon, B. Kim, Y. Li, J. Yi, H. Kim, J. W. Leem, Y. L. Kim, D. R. Kim, Y. M. Paulus, C. H. Lee, *Sci. Adv.* **2022**, *8*, eabn1772.
[59] L. Yin, A. B. Farimani, K. Min, N. Vishal, J. Lam, Y. K. Lee, N. R. Aluru, J. A. Rogers, *Adv. Mater.* **2015**, *27*, 1857.
[60] H. Zhao, Z. Xue, X. Wu, Z. Wei, Q. Guo, M. Xu, C. Qu, C. You, Y. Mei, M. Zhang, Z. Di, Q. Guo, *npj Flexible Electron.* **2022**, *6*, 63.
[61] J. Koo, M. R. MacEwan, S.-K. Kang, S. M. Won, M. Stephen, P. Gamble, Z. Xie, Y. Yan, Y.-Y. Chen, J. Shin, N. Birenbaum, S. Chung, S. B. Kim, J. Khalifeh, D. V. Harburg, K. Bean, M. Paskett, J. Kim, Z. S. Zohny, S. M. Lee, R. Zhang, K. Luo, B. Ji, A. Banks, H. M. Lee, Y. Huang, W. Z. Ray, J. A. Rogers, *Nat. Med.* **2018**, *24*, 1830.

© 2024 The Author(s). Advanced Functional Materials published by Wiley-VCH GmbH

16163028, 2025, 3, Downloaded from https://advanced.onlinelibrary.wiley.com/doi/10.1002/adfm.202413324 by Koc University, Wiley Online Library on [22/05/2025]. See the Terms and Conditions (https://onlinelibrary.wiley.com/terms-and-conditions) on Wiley Online Library for rules of use; OA articles are governed by the applicable Creative Commons License

[62] S. W. Hwang, D. H. Kim, H. Tao, T. Kim, S. Kim, K. J. Yu, B. Panilaitis, J.-W. Jeong, J.-K. Song, F. G. Omenetto, J. A. Rogers, *Adv. Funct. Mater.* **2013**, *23*, 4087.
[63] S. Walther, S. Polster, B. Meyer, M. Jank, H. Ryssel, L. Frey, *J. Vac. Sci. Technol. B* **2011**, *29*, https://doi.org/10.1116/1.3524291.
[64] S. W. Hwang, X. Huang, J. H. Seo, J.-K. Song, S. Kim, S. Hage-Ali, H.-J. Chung, H. Tao, F. G. Omenetto, Z. Ma, J. A. Rogers, *Adv. Mater.* **2013**, *25*, 3526.
[65] Q. Yang, S. Lee, Y. Xue, Y. Yan, T.-L. Liu, S.-K. Kang, Y. J. Lee, S. H. Lee, M.-H. Seo, D. Lu, J. Koo, M. R. MacEwan, R. T. Yin, W. Z. Ray, Y. Huang, J. A. Rogers, *Adv. Funct. Mater.* **2020**, *30*, 1910718.
[66] S. K. Kang, S. W. Hwang, H. Cheng, S. Yu, B. H. Kim, J.-H. Kim, Y. Huang, J. A. Rogers, *Adv. Funct. Mater.* **2014**, *24*, 4427.
[67] J. C. Middleton, A. J. Tipton, *Biomaterials* **2000**, *21*, 2335.
[68] L. S. Nair, C. T. Laurencin, *Prog. Polym. Sci.* **2007**, *32*, 762.
[69] L. Yin, H. Cheng, S. Mao, R. Haasch, Y. Liu, X. Xie, S.-W. Hwang, H. Jain, S.-K. Kang, Y. Su, R. Li, Y. Huang, J. A. Rogers, *Adv. Funct. Mater.* **2014**, *24*, 645.
[70] N. Kirkland, N. Birbilis, M. Staiger, *Acta Biomater.* **2012**, *8*, 925.
[71] L. Aljihmani, L. Alic, Y. Boudjemline, Z. M. Hijazi, B. Mansoor, E. Serpedin, K. Qaraqe, *J. Bio-and Tribo-Corros.* **2019**, *5*, 26.
[72] A. P. M. Saad, A. Syahrom, *Corros. Sci.* **2018**, *131*, 45.
[73] V. Herber, B. Okutan, G. Antonoglou, N. G. Sommer, M. Payer, *J. Clin. Med.* **2021**, *10*, 1842.
[74] S.-K. Kang, R. K. J. Murphy, S.-W. Hwang, S. M. Lee, D. V. Harburg, N. A. Krueger, J. Shin, P. Gamble, H. Cheng, S. Yu, Z. Liu, J. G. McCall, M. Stephen, H. Ying, J. Kim, G. Park, R. C. Webb, C. H. Lee, S. Chung, D. S. Wie, A. D. Gujar, B. Vemulapalli, A. H. Kim, K.-M. Lee, J. Cheng, Y. Huang, S. H. Lee, P. V. Braun, W. Z. Ray, J. A. Rogers, *Nature* **2016**, *530*, 71.
[75] W. Park, J. Baik, T.-Y. Kim, K. Cho, W.-K. Hong, H.-J. Shin, T. Lee, *ACS Nano* **2014**, *8*, 4961.
[76] C. Fernandes, I. Taurino, *Sensors* **2022**, *22*, 3062.
[77] C. Redlich, P. Quadbeck, M. Thieme, B. Kieback, *Acta Biomater.* **2020**, *104*, 241.
[78] H. Deng, Z. Xie, Y. Wang, R. Liu, T. Zhang, T. Hao, X. P. Wang, Q. F. Fang, C. S. Liu, *Mater. Sci. Eng., A* **2018**, *715*, 117.
[79] R. Gorejová, L. Haverová, R. Oriňaková, A. Oriňak, M. Oriňak, *J. Mater. Sci.* **2019**, *54*, 1913.
[80] F. Zivic, N. Grujovic, E. Pellicer, J. Sort, S. Mitrovic, D. Adamovic, M. Vulovic, *Biodegradable Metals as Biomaterials for Clinical Practice: Iron-Based Materials*. Biomaterials in Clinical Practice: Advances in Clinical Research and Medical Devices **2018**, pp. 225–280.
[81] J. Min, Y. Jung, J. Ahn, J. G. Lee, J. Lee, S. H. Ko, *Adv. Mater.* **2023**, *35*, 2211273.
[82] P. K. Bowen, J. Drelich, J. Goldman, *Adv. Mater.* **2013**, *25*, 2577.
[83] J. Li, J. Liu, W. Huo, J. Yu, X. Liu, M. J. Haslinger, M. Muehlberger, P. Kulha, X. Huang, *Mater. Today Nano* **2022**, *18*, 100201.
[84] W. B. Han, J. H. Lee, J. W. Shin, S. W. Hwang, *Adv. Mater.* **2020**, *32*, 2002211.
[85] L. Wang, Y. Gao, F. Dai, S. Gong, D. T. Lai, Y. Wang, L. W. Yap, K. J. Si, Q. Shi, N. N. Jason, T. Sridhar, H. Uddin, W. Cheng, *ACS Appl. Mater. Interfaces* **2019**, *11*, 18013.
[86] M. Sang, K. Kang, Y. Zhang, H. Zhang, K. Kim, M. Cho, J. Shin, J.-H. Hong, T. Kim, S. K. Lee, W.-H. Yeo, J. W. Lee, T. Lee, B. Xu, K. J. Yu, *Adv. Mater.* **2022**, *34*, 2105865.
[87] C. Xu, Y. Huang, G. Yepez, Z. Wei, F. Liu, A. Bugarin, L. Tang, Y. Hong, *Sci. Rep.* **2016**, *6*, 34451.
[88] F. Chen, O. R. Teniola, C. T. Laurencin, *J. Mater. Res.* **2022**, *37*, 1417.
[89] G. Rodríguez-Roldán, A. Cruz-Orea, E. Suaste-Gómez, *Int. J. Thermophys.* **2019**, *40*, 16.
[90] X. Jia, C. Wang, C. Zhao, Y. Ge, G. G. Wallace, *Adv. Funct. Mater.* **2016**, *26*, 1454.
[91] I. S. Romero, M. L. Schurr, J. V. Lally, M. Z. Kotlik, A. R. Murphy, *ACS Appl. Mater. Interfaces* **2013**, *5*, 553.
[92] L. B. Kenry, *Biomacromolecules* **2018**, *19*, 1783.
[93] C. J. Bettinger, J. P. Bruggeman, A. Misra, J. T. Borenstein, R. Langer, *Biomaterials* **2009**, *30*, 3050.
[94] T. Eom, J. Jeon, S. Lee, A. M. El-Naggar, K. H. Zein, A. M. Kamal, E. A. Khalid, H. Abd-E. Omar, B. M. Mohamed, *Part. Part. Syst. Charact.* **2019**, *36*, 1900166.
[95] N. Madkhali, H. R. Alqahtani, S. Alterary, H. A. Albrithen, A. Laref, A. Hassib, *Arabian J. Chem.* **2020**, *13*, 4987.
[96] A. E. Franke, J. M. Heck, T.-J. King, R. T. Howe, *J. Microelectromech. Syst.* **2003**, *12*, 160.
[97] Q. Shabir, A. Pokale, A. Loni, D. R. Johnson, L. T. Canham, R. Fenollosa, M. Tymczenko, I. Rodríguez, F. Meseguer, A. Cros, A. Cantarero, *Silicon* **2011**, *3*, 173.
[98] R. Li, L. Wang, D. Kong, L. Yin, *Bioact. Mater.* **2018**, *3*, 322.
[99] S.-W. Hwang, C. H. Lee, H. Cheng, H. Cheng, J.-W. Jeong, S.-K. Kang, J.-H. Kim, J. Shin, J. Yang, Z. Liu, G. A. Ameer, Y. Huang, J. A. Rogers, *Nano Lett.* **2015**, *15*, 2801.
[100] A. Sarkar, Y. Lee, J.-H. Ahn, *Nano Res.* **2021**, *14*, 3010.
[101] C. Dagdeviren, S.-W. Hwang, Y. Su, S. Kim, H. Cheng, O. Gur, R. Haney, F. G. Omenetto, Y. Huang, J. A. Rogers, *Small* **2013**, *9*, 3398.
[102] T. Lei, M. Guan, J. Liu, H.-C. Lin, R. Pfattner, L. Shaw, A. F. McGuire, T.-C. Huang, L. Shao, K.-T. Cheng, J. B.-H. Tok, Z. Bao, *Proc. Natl. Acad. Sci. USA* **2017**, *114*, 5107.
[103] J.-S. Shim, J. A. Rogers, S.-K. Kang, *Mater. Sci. Eng.: R* **2021**, *145*, 100624.
[104] J. Shin, Y. Yan, W. Bai, Y. Xue, P. Gamble, L. Tian, I. Kandela, C. R. Haney, W. Spees, Y. Lee, M. Choi, J. Ko, H. Ryu, J.-K. Chang, M. Pezhouh, S.-K. Kang, S. M. Won, K. J. Yu, J. Zhao, Y. K. Lee, M. R. MacEwan, S.-K. Song, Y. Huang, W. Z. Ray, J. A. Rogers, *Nat. Biomed. Eng.* **2019**, *3*, 37.
[105] N. Vidakis, M. Petousis, N. Michailidis, V. Papadakis, N. Mountakis, A. Argyros, E. Dimitriou, C. Charou, A. Moutsopoulou, *Biomed. Eng. Adv.* **2023**, *6*, 100103.
[106] J. Olofsson, T. M. Grehk, T. Berlind, C. Persson, S. Jacobson, H. Engqvist, *Biomatter* **2012**, *2*, 94.
[107] J. Hwangbo, H. Seo, G. Sim, R. Avila, M. Nair, B. Kim, Y. Choi, *Cell Rep. Phys. Sci.* **2024**, *5*, 102099.
[108] A. Petritz, A. Wolfberger, A. Fian, M. Irimia-Vladu, A. Haase, H. Gold, T. Rothländer, T. Griesser, B. Stadlober, *Appl. Phys. Lett.* **2013**, *103*, 153303.
[109] A. Sannino, C. Demitri, M. Madaghiele, *Materials* **2009**, *2*, 353.
[110] R. K. Pal, A. A. Farghaly, C. Wang, M. M. Collinson, S. C. Kundu, V. K. Yadavalli, *Biosens. Bioelectron.* **2016**, *81*, 294.
[111] L.-D. Koh, Y. Cheng, C.-P. Teng, Y.-W. Khin, X.-J. Loh, S.-Y. Tee, M. Low, E. Ye, H.-D. Yu, Y.-W. Zhang, M.-Y. Han, *Prog. Polym. Sci.* **2015**, *46*, 86.
[112] N. Thombare, S. Kumar, U. Kumari, P. Sakare, R. K. Yogi, N. Prasad, K. K. Sharma, *Int. J. Biol. Macromol.* **2022**, *215*, 203.
[113] S. Chen, Z. Wu, C. Chu, Y. Ni, R. E. Neisiany, Z. You, *Adv. Sci.* **2022**, *9*, 2105146.
[114] R. Singh, M. J. Bathaei, E. Istif, L. Beker, *Adv. Healthcare Mater.* **2020**, *9*, 2000790.
[115] R. T. Tran, P. Thevenot, D. Gyawali, J.-C. Chiao, L. Tang, J. Yang, *Soft Matter* **2010**, *6*, 2449.
[116] B. L. Turner, S. Ramesh, S. Menegatti, M. Daniele, in *44th Annual International Conference of the IEEE Engineering in Medicine & Biology Society, (EMBC)*, IEEE, New York **2022**, p. 4860.
[117] L. Aliotta, M. Seggiani, A. Lazzeri, V. Gigante, P. Cinelli, *Polymers* **2022**, *14*, 844.
[118] P. Chen, C. Xu, P. Wu, K. Liu, F. Chen, Y. Chen, H. Dai, Z. Luo, *ACS Nano* **2022**, *16*, 16513.

© 2024 The Author(s). Advanced Functional Materials published by Wiley-VCH GmbH

16163028, 2025, 3, Downloaded from https://advanced.onlinelibrary.wiley.com/doi/10.1002/adfm.202413324 by Koc University, Wiley Online Library on [22/05/2025]. See the Terms and Conditions (https://onlinelibrary.wiley.com/terms-and-conditions) on Wiley Online Library for rules of use; OA articles are governed by the applicable Creative Commons License

[119] N. Goonoo, A. Bhaw-Luximon, I. Rodriguez, D. Wesner, H. Schönherr, G. L. Bowlin, D. Jhurry, *J. Mater. Chem. B* **2015**, *3*, 673.
[120] S. Eshraghi, S. Das, *Acta Biomater.* **2010**, *6*, 2467.
[121] M. Abedalwafa, F. Wang, L. Wang, C. Li, *Rev. Adv. Mater. Sci.* **2013**, *34*, 123.
[122] N. Kumar, R. S. Langer, A. J. Domb, *Adv. Drug Delivery Rev.* **2002**, *54*, 889.
[123] C. Verma, M. Quraishi, *Corros. Eng., Sci. Technol.* **2022**, *57*, 796.
[124] C. S. Kong, W. S. Yoo, K. Y. Lee, H. S. Kim, *J. Mater. Sci.* **2009**, *44*, 1107.
[125] L. Yu, Y. Zhang, W. Tong, J. Shang, B. Shen, F. Lv, P. K. Chub, *RSC Adv.* **2012**, *2*, 8793.
[126] N. A. Althubiti, N. Al-Harbi, R. K. Sendi, A. Atta, A. M. Henaish, *Inorganics* **2023**, *11*, 74.
[127] J. Bhaiswar, M. Salunkhe, S. Dongre, *Int.J. Compos. Mater.* **2013**, *3*, 115.
[128] C. Qi, J. Lin, L.-H. Fu, P. Huang, *Chem. Soc. Rev.* **2018**, *47*, 357.
[129] C.-H. Park, E. K. Kim, L. D. Tijing, A. Amarjargal, H. R. Pant, C. S. Kim, H. K Shon, *Ceram. Int.* **2014**, *40*, 5049.
[130] M. Bohner, B. L. G. Santoni, N. Döbelin, *Acta Biomater.* **2020**, *113*, 23.
[131] Y. Y. Li, D. A. Yang, H. Zhao, *Key Eng. Mater.* **2007**, *336*, 1650.
[132] E. Song, J. Li, J. A. Rogers, *APL Mater.* **2019**, *7*, 050902.
[133] D. Yu, Y.-Q. Yang, Z. Chen, Y. Tao, Y.-F. Liu, *Opt. Commun.* **2016**, *362*, 43.
[134] S. W. Kim, M. M. Rehman, M. Sajid, M. M. ur Rehman, J. Gul, J. D Jo, K. H Choi, *Thin Solid Films* **2019**, *673*, 44.
[135] C. M. Boutry, A. Nguyen, Q. O. Lawal, A. Chortos, S. Rondeau-Gagné, Z. Bao, *Adv. Mater.* **2015**, *27*, 6954.
[136] J. Borges, J. Zeng, X. Q. Liu, X. Q. Liu, H. Chang, C. Monge, C. Garot, K. Ren, P. Machillot, N. E. Vrana, P. Lavalle, T. Akagi, M. Matsusaki, J. Ji, M. Akashi, J. F. Mano, V. Gribova, C. Picart, *Adv. Healthcare Mater.* **2024**, *13*, 2302713.
[137] Z. Shi, L. Liu, H. Chen, C. Tang, J. Yu, Y. Fan, *Carbohydr. Polym.* **2024**, *323*, 121369.
[138] B.-S. Kim, S. W. Park, P. T. Hammond, *ACS Nano* **2008**, *2*, 386.
[139] D. Ji, Y. Lin, X. Guo, B. Ramasubramanian, R. Wang, N. Radacsi, R. Jose, X. Qin, S. Ramakrishna, *Nat. Rev. Methods Primers* **2024**, *4*, https://doi.org/10.1038/s43586-023-00278-z.
[140] A. Rogina, *Appl. Surf. Sci.* **2014**, *296*, 221.
[141] W. Peng, L. Wang, M. Zhang, D. G. Yu, X. Li, *J. Appl. Polym. Sci.* **2024**, *141*, e55433.
[142] Y. Yang, M. Zhong, W. Wang, N. Lu, Y. Gou, W. Cai, J. Huang, Y. Lai, *Sep. Purif. Technol.* **2025**, *352*, 128143.
[143] X. Liang, A. W. Weimer, *Curr.Opin.Solid State Mater. Sci.* **2015**, *19*, 115.
[144] R. Suntornnond, J. An, W. Y. Yeong, C. K. Chua, *Macromol. Mater. Eng.* **2015**, *300*, 858.
[145] E. E. Ekanem, S. A. Nabavi, G. T. Vladisavljevic´, S. Gu, *ACS Appl. Mater. Interfaces* **2015**, *7*, 23132.
[146] T. Y. Lee, M. Ku, B. Kim, S. Lee, J. Yang, S. H. Kim, *Small* **2017**, *13*, 1700646.
[147] K. Wang, K. Huang, L. Wang, X. Lin, M. Tan, W. Su, *J. Agric. Food Chem.* **2024**, *72*, 15092.
[148] Y. Xia, G. M. Whitesides, *Angew. Chem., Int. Ed.* **1998**, *37*, 550.
[149] C. J. Brinker, G. W. Scherer, *Sol-Gel Science: The Physics and Chemistry of Sol-Gel Processing*, Academic Press, New York **2013**.
[150] F. Bollino, M. Catauro, *Photoenergy and Thin Film Materials*, Wiley, New York **2019**, p. 321.
[151] E. Bourgeat-Lami, E. Duguet, *Functional Coatings: By Polymer Microencapsulation*, Wiley, Hoboken, NJ **2006**, p. 85.
[152] S. Wintzheimer, L. Luthardt, K. L. A. Cao, I. Imaz, D. Maspoch, T. Ogi, A. Bück, D. P. Debecker, M. Faustini, K. Mandel, *Adv. Mater.* **2023**, *35*, 2306648.
[153] T. Yoshioka, T. Ando, M. Shikida, K. Sato, *Sens. Actuators, A* **2000**, *82*, 291.
[154] L. Adler-Abramovich, N. Kol, I. Yanai, C. Rameshan, W. Stadlmayr, C. Weilach, S. Penner, H. Lorenz, M. Hävecker, R. Blume, T. Rocha, D. Teschner, A. Knop-Gericke, R. Schlögl, N. Memmel, D. Zemlyanov, G. Rupprechter, B. Klötzer, *Angew. Chem., Int. Ed.* **2010**, *49*, 9788.
[155] T. L. da Silva, D. B. Arellano, S. Martini, *J. Am. Oil Chem. Soc.* **2018**, *95*, 797.
[156] J. F. Toro-Vazquez, J. Morales-Rueda, V. A. Mallia, R. G. Weiss, *Food Biophys.* **2010**, *5*, 193.
[157] S. H. Kim, H. J. Lee, J.-C. Yoo, H. J. Park, J. Y. Jeong, Y. B. Seo, T. Sultan, S. H. Kim, O. J. Lee, C. H. Park, *J. Biomater. Sci.* **2018**, *29*, 997.
[158] K. Phooplub, J. Meesane, N. Muensit, *Biomed. Phys. Eng. Exp.* **2018**, *4*, 055022.
[159] J. Sarasua, A. L. Arraiza, P. Balerdi, I. Maiza, *Polym. Eng. Sci.* **2005**, *45*, 745.
[160] M. A. Woodruff, D. W. Hutmacher, *Prog. Polym. Sci.* **2010**, *35*, 1217.
[161] H. Doyle, S. Lohfeld, P. McHugh, *Ann. Biomed. Eng.* **2014**, *42*, 661.
[162] M. Bartnikowski, T. R. Dargaville, S. Ivanovski, D. W. Hutmacher, *Prog. Polym. Sci.* **2019**, *96*, https://doi.org/10.1016/j.progpolymsci.2019.05.004.
[163] M. Mehrasa, M. A. Asadollahi, K. Ghaedi, H. Salehi, A. Arpanaei, *Int. J. Biol. Macromol.* **2015**, *79*, 687.
[164] P. In Pyo Park, S. Jonnalagadda, *J. Appl. Polym. Sci.* **2006**, *100*, 1983.
[165] Y. Huang, Y. Cui, H. Deng, J. Wang, R. Hong, S. Hu, H. Hou, Y. Dong, H. Wang, J. Chen, L. Li, Y. Xie, P. Sun, X. Fu, L. Yin, W. Xiong, S.-H. Shi, M. Luo, S. Wang, X. Li, X. Sheng, *Nat. Biomed. Eng.* **2023**, *7*, 486.
[166] Y.-H. Na, Y. He, T. Nishiwaki, Y. Inagawa, Y. Osanai, S. Matsumura, T. Saito, Y. Doi, Y. Inoue, *Polym. Degrad. Stab.* **2003**, *79*, 535.
[167] Y. S. Choi, J. Koo, Y. J. Lee, G. Lee, R. Avila, H. Ying, J. Reeder, L. Hambitzer, K. Im, J. Kim, K.-M. Lee, J. Cheng, Y. Huang, S.-K. Kang, J. A. Rogers, *Adv. Funct. Mater.* **2020**, *30*, 2000941.
[168] K. Leong, B. Brott, R. Langer, *J. Biomed. Mater. Res.* **1985**, *19*, 941.
[169] D. J. Liaw, *J. Appl. Polym. Sci.* **1997**, *66*, 1251.
[170] Z. Wang, L. Yu, M. Ding, H. Tan, J. Li, Q. Fu, *Polym. Chem.* **2011**, *2*, 601.
[171] A. Kumar, Y. S. Negi, V. Choudhary, N. K. Bhardwaj, *Cellulose* **2014**, *21*, 3409.
[172] P. B. Bhargav, B. Sarada, A. Sharma, V. N. Rao, *J. Macromol. Sci., Part A* **2009**, *47*, 131.
[173] M. De Santis, I. Cacciotti, *Nanotechnology* **2020**, *31*, 252001.
[174] J. Min, Y. Jung, J. Ahn, J. G. Lee, J. Lee, S. H. Ko, *Adv. Mater.* **2023**, *35*, 2211273.
[175] S. K. Ghosh, J. Park, S. Na, M. P. Kim, H. Ko, *Adv. Sci.* **2021**, *8*, 2005010.
[176] T. A. Baldo, L. F. de Lima, L. F. Mendes, W. R. de Araujo, T. R. Paixao, W. K. Coltro, *ACS Appl. Electron. Mater.* **2020**, *3*, 68.
[177] H. Tai, Z. Duan, Y. Wang, S. Wang, Y. Jiang, *ACS Appl. Mater. Interfaces* **2020**, *12*, 31037.
[178] C. M. Boutry, H. Chandrahalim, P. Streit, M. Schinhammer, A. C. Hänzi, C. Hierold, *Philos. Trans. R. Soc., A* **2012**, *370*, 2418.
[179] Q. Yang, Z. Hu, M.-H. Seo, Y. Xu, Y. Yan, Y.-H. Hsu, J. Berkovich, K. Lee, T.-L. Liu, S. McDonald, H. Nie, H. Oh, M. Wu, J.-T. Kim, S. A. Miller, Y. Jia, S. Butun, W. Bai, H. Guo, J. Choi, A. Banks, W. Z. Ray, Y. Kozorovitskiy, M. L. Becker, M. A. Pet, M. R. MacEwan, J.-K. Chang, H. Wang, Y. Huang, J. A. Rogers, *Nat. Commun.* **2022**, *13*, 6518.
[180] A. A. Mendelson, C. Gillis, W. R. Henderson, J. J. Ronco, V. Dhingra, D. E. Griesdale, *Can. J. Neurol. Sci.* **2012**, *39*, 571.
[181] C. Heck, *Crit. Care Nurs. Clin.* **2023**, *35*, 83.
[182] C. He, C. Teng, Z. Xiong, X. Lin, H. Li, X. Li, *Chin. Neurosurg. J.* **2023**, *9*, 14.

© 2024 The Author(s). Advanced Functional Materials published by Wiley-VCH GmbH

16163028, 2025, 3, Downloaded from https://advanced.onlinelibrary.wiley.com/doi/10.1002/adfm.202413324 by Koc University, Wiley Online Library on [22/05/2025]. See the Terms and Conditions (https://onlinelibrary.wiley.com/terms-and-conditions) on Wiley Online Library for rules of use; OA articles are governed by the applicable Creative Commons License

[183] S. Chatterjee, R. K. Joshi, S. Bhaskara, R. Hari, S. Datta, K. S. Girishan, H. J. Pandya, *bioRxiv* **2023**, 566132.
[184] D. Whitmer, C. De Solages, B. Hill, H. Yu, J. M. Henderson, H. Bronte-Stewart, *Front. Human Neurosci.* **2012**, *6*, 155.
[185] B. Litt, R. Esteller, J. Echauz, M. D'Alessandro, R. Shor, T. Henry, P. Pennell, C. Epstein, R. Bakay, M. Dichter, G. Vachtsevanos, *Neuron* **2001**, *30*, 51.
[186] W. C. Stacey, B. Litt, *Nat. Clin. Pract. Neurol.* **2008**, *4*, 190.
[187] S. M. Yang, J. H. Shim, H. U. Cho, T.-M. Jang, G.-J. Ko, J. Shim, T. H. Kim, J. Zhu, S. Park, Y. S. Kim, S.-Y. Joung, J. C. Choe, J.-W. Shin, J. H. Lee, Y. M. Kang, H. Cheng, Y. Jung, C.-H. Lee, D. P. Jang, S.-W. Hwang, *Adv. Mater.* **2022**, *34*, 2108203.
[188] H. S. Kim, S. M. Yang, T. M. Jang, N. Oh, H. S. Kim, S. W. Hwang, *Adv. Healthcare Mater.* **2018**, *7*, 1801071.
[189] G. Lee, E. Ray, H.-J. Yoon, S. Genovese, Y. S. Choi, M.-K. Lee, S. Şahin, Y. Yan, H.-Y. Ahn, A. J. Bandodkar, J. Kim, M. Park, H. Ryu, S. S. Kwak, Y. H Jung, A. Odabas, U. Khandpur, W. Z. Ray, M. R. MacEwan, J. A. Rogers, *Sci. Adv.* **2022**, *8*, eabp9169.
[190] E. J. Curry, T. T. Le, R. Das, K. Ke, E. M. Santorella, D. Paul, M. T. Chorsi, K. T. M. Tran, J. Baroody, E. R. Borges, B. Ko, A. Golabchi, X. Xin, D. Rowe, L. Yue, J. Feng, M. D. Morales-Acosta, Q. Wu, I.-P. Chen, X. T Cui, J. Pachter, T. D. Nguyen, *Proc. Natl. Acad. Sci. USA* **2020**, *117*, 214.
[191] J. Lee, H. R. Cho, G. D. Cha, H. Seo, S. Lee, C.-K. Park, J. W. Kim, S. Qiao, L. Wang, D. Kang, T. Kang, T. Ichikawa, J. Kim, H. Lee, W. Lee, S. Kim, S.-T. Lee, N. Lu, T. Hyeon, S. H. Choi, D.-H. Kim, *Nat. Commun.* **2019**, *10*, 5205.
[192] S. Senapati, A. K. Mahanta, S. Kumar, P. Maiti, *Signal Transduction Targeted Ther.* **2018**, *3*, 7.
[193] Y. S. Choi, Y.-Y. Hsueh, J. Koo, Q. Yang, R. Avila, B. Hu, Z. Xie, G. Lee, Z. Ning, C. Liu, Y. Xu, Y. J. Lee, W. Zhao, J. Fang, Y. Deng, S. M. Lee, A. Vázquez-Guardado, I. Stepien, Y. Yan, J. W. Song, C. Haney, Y. S. Oh, W. Liu, H.-J. Yoon, A. Banks, M. R. MacEwan, G. A. Ameer, W. Z. Ray, Y. Huang, T. Xie, et al., *Nat. Commun.* **2020**, *11*, 5990.
[194] C. M. Boutry, L. Beker, Y. Kaizawa, C. Vassos, H. Tran, A. C. Hinckley, R. Pfattner, S. Niu, J. Li, J. Claverie, Z. Wang, J. Chang, P. M. Fox, Z. Bao, *Nat. Biomed. Eng.* **2019**, *3*, 47.
[195] Y. S. Choi, R. T. Yin, A. Pfenniger, J. Koo, R. Avila, K. Benjamin Lee, S. W. Chen, G. Lee, G. Li, Y. Qiao, A. Murillo-Berlioz, A. Kiss, S. Han, S. Min Lee, C. Li, Z. Xie, Y.-Y. Chen, A. Burrell, B. Geist, H. Jeong, J. Kim, H.-J. Yoon, A. Banks, S.-K. Kang, Z. Jenny Zhang, C. R. Haney, A. V. Sahakian, D. Johnson, T. Efimova, Y. Huang, et al., *Nat. Biotechnol.* **2021**, *39*, 1228.
[196] J. Li, J. Liu, Z. Wu, X. Shang, Y. Li, W. Huo, X. Huang, *Sci. Adv.* **2023**, *9*, eadi3839.
[197] J. W. Song, H. Ryu, W. Bai, Z. Xie, X. A. Vázquez-Guardado, K. Nandoliya, R. Avila, G. Lee, Z. Song, J. Kim, M.-K. Lee, Y. Liu, M. Kim, H. Wang, Y. Wu, H.-J. Yoon, S. S. Kwak, J. Shin, K. Kwon, W. Lu, X. Chen, Y. Huang, G. A. Ameer, J. A. Rogers, *Sci. Adv.* **2023**, *9*, eade4687.
[198] H. Tao, S.-W. Hwang, B. Marelli, B. An, J. E. Moreau, M. Yang, M. A. Brenckle, S. Kim, D. L. Kaplan, J. A. Rogers, F. G. Omenetto, *Proc. Natl. Acad. Sci. USA* **2014**, *111*, 17385.
[199] C. M. Boutry, Y. Kaizawa, B. C. Schroeder, A. Chortos, A. Legrand, Z. Wang, J. Chang, P. Fox, Z. Bao, *Nat. Electron.* **2018**, *1*, 314.
[200] R. Li, H. Qi, Y. Ma, Y. Deng, S. Liu, Y. Jie, J. Jing, J. He, X. Zhang, L. Wheatley, C. Huang, X. Sheng, M. Zhang, L. Yin, *Nat. Commun.* **2020**, *11*, 3207.
[201] J. Lee, S. J. Ihle, G. S. Pellegrino, H. Kim, J. Yea, C.-Y. Jeon, H.-C. Son, C. Jin, D. Eberli, F. Schmid, B. L. Zambrano, A. F. Renz, C. Forró, H. Choi, K.-I. Jang, R. Küng, J. Vörös, *Nat. Electron.* **2021**, *4*, 291.
[202] G. Yao, L. Kang, C. Li, S. Chen, Q. Wang, J. Yang, Y. Long, J. Li, K. Zhao, W. Xu, W. Cai, Y. Lin, X. Wang, *Proc. Natl. Acad. Sci. USA* **2021**, *118*, 2100772118.
[203] P. Roriz, L. Carvalho, O. Frazão, J. L. Santos, J. A. Simões, *J. Biomech.* **2014**, *47*, 1251.
[204] S. Bogaerts, H. Desmet, P. Slagmolen, K. Peers, *J. Biomech.* **2016**, *49*, 1411.
[205] Y. Shan, E. Wang, X. Cui, Y. Xi, J. Ji, J. Yuan, L. Xu, Z. Liu, Z. Li, *Adv. Funct. Mater.* **2024**, *34*, 2400295.
[206] H. Ouyang, Z. Li, M. Gu, Y. Hu, L. Xu, D. Jiang, S. Cheng, Y. Zou, Y. Deng, B. Shi, W. Hua, Y. Fan, Z. Li, Z. Wang, *Adv. Mater.* **2021**, *33*, 2102302.
[207] G. Jiang, *Front. Neurosci.* **2010**, *4*, 1340.
[208] A. J. Sit, *J. Glaucoma* **2009**, *18*, 272.
[209] L. Yu, B. J. Kim, E. Meng, *Sensors* **2014**, *14*, 20620.
[210] E. J. Curry, K. Ke, M. T. Chorsi, K. S. Wrobel, A. N. Miller III, A. Patel, I. Kim, J. Feng, L. Yue, Q. Wu, C.-L. Kuo, K. W.-H. Lo, C. T. Laurencin, H. Ilies, P. K. Purohit, T. D. Nguyen, *Proc. Natl. Acad. Sci. USA* **2018**, *115*, 909.
[211] S. W. Hwang, J. K. Song, X. Huang, H. Cheng, S. Kang, B. H. Kim, J.-H. Kim, S. Yu, Y. Huang, J. A. Rogers, *Adv. Mater.* **2014**, *26*, 3905.
[212] S. K. Kang, S. W. Hwang, S. Yu, J.-H. Seo, E. A. Corbin, J. Shin, D. S. Wie, R. Bashir, Z. Ma, J. A. Rogers, *Adv. Funct. Mater.* **2015**, *25*, 1789.
[213] J. Shin, Z. Liu, W. Bai, Y. Liu, Y. Yan, Y. Xue, I. Kandela, M. Pezhouh, M. R. MacEwan, Y. Huang, W. Z. Ray, W. Zhou, J. A. Rogers, *Sci. Adv.* **2019**, *5*, eaaw1899.
[214] V. Calabrese, C. Mancuso, M. Calvani, E. Rizzarelli, D. A. Butterfield, A. M. Giuffrida Stella, *Nat. Rev. Neurosci.* **2007**, *8*, 766.
[215] U. Förstermann, W. C. Sessa, *Eur. Heart J.* **2012**, *33*, 829.
[216] C. Bogdan, *Nat. Immunol.* **2001**, *2*, 907.
[217] C. Farah, L. Y. Michel, J.-L. Balligand, *Nat. Rev. Cardiol.* **2018**, *15*, 292.
[218] B. Prendergast, D. Scott, P. Mankad, *Eur. J. Cardio-Thoracic Surg.* **1998**, *14*, 488.
[219] R. Li, L. Wang, L. Yin, *Materials* **2018**, *11*, 2108.
[220] S. Shafaei, S. Akbari Nakhjavani, G. S. Kanberoglu, B. Khalilzadeh, R. Mohammad-Rezaei, *Anal. Lett.* **2022**, *55*, 2418.
[221] H. Beyrampour-Basmenj, M. Pourhassan-Moghamddam, S. A. Nakhjavani, N. Faraji, M. Alivand, N. Zarghami, *IEEE Trans. NanoBiosci.* **2022**, *22*, 155.
[222] J. Wu, H. Liu, W. Chen, B. Ma, H. Ju, *Nat. Rev. Bioeng.* **2023**, *1*, 346.
[223] S. Papamatthaiou, U. Zupancic, C. Kalha, A. Regoutz, P. Estrela, D. Moschou, *Sci. Rep.* **2020**, *10*, 17152.
[224] J. Aleman, T. Kilic, L. S. Mille, S. R. Shin, Y. S. Zhang, *Nat. Protoc.* **2021**, *16*, 2564.
[225] L. Guo, Y. Zhao, Q. Huang, J. Huang, Y. Tao, J. Chen, H.-Y. Li, H. Liu, *Microsyst. Nanoeng.* **2024**, *10*, 65.
[226] R. Li, H. Qi, Y. Ma, Y. Deng, S. Liu, Y. Jie, J. Jing, J. He, X. Zhang, L. Wheatley, C. Huang, X. Sheng, M. Zhang, L. Yin, *Nat. Commun.* **2020**, *11*, 3207.
[227] X. Jia, C. Wang, V. Ranganathan, B. Napier, C. Yu, Y. Chao, M. Forsyth, F. G. Omenetto, D. R. MacFarlane, G. G. Wallace, *ACS Energy Lett.* **2017**, *2*, 831.
[228] G.-J. Ko, S. D. Han, J.-K. Kim, J. Zhu, W. B. Han, J. Chung, S. M. Yang, H. Cheng, D.-H. Kim, C.-Y. Kang, S.-W. Hwang, *NPG Asia Mater.* **2020**, *12*, 71.
[229] G. L. Long, J. D. Winefordner, *Anal. Chem.* **1983**, *55*, 712A.
[230] M. Xu, V. K. Yadavalli, *ACS Sens.* **2019**, *4*, 1040.
[231] R. Freeman, J. Girsh, A. Fang-ju Jou, J. A. Ho, T. Hug, J. Dernedde, I. Willner, *Anal. Chem.* **2012**, *84*, 6192.
[232] S.-W. Hwang, S.-K. Kang, X. Huang, M. A. Brenckle, F. G. Omenetto, J. A. Rogers, *Adv. Mater.* **2015**, *27*, 47.
[233] S. A. Nakhjavani, H. Mirzajani, S. Cararra, M. C. Onbaşlı, *TrAC, Trends Anal. Chem.* **2024**, *180*, 117979.
[234] H. Mirzajani, C. Cheng, J. Wu, J. Chen, S. Eda, E. N. Aghdam, H. B. Ghavifekr, *Biosens. Bioelectron.* **2017**, *89*, 1059.
[235] R. A. Gross, B. Kalra, *Science* **2002**, *297*, 803.

© 2024 The Author(s). Advanced Functional Materials published by Wiley-VCH GmbH

16163028, 2025, 3, Downloaded from https://advanced.onlinelibrary.wiley.com/doi/10.1002/adfm.202413324 by Koc University, Wiley Online Library on [22/05/2025]. See the Terms and Conditions (https://onlinelibrary.wiley.com/terms-and-conditions) on Wiley Online Library for rules of use; OA articles are governed by the applicable Creative Commons License

[236] H. Mirzajani, H. Urey, *IEEE Sens. Lett.* **2023**, *8*, https://doi.org/10.1109/LSENS.2023.3335887.
[237] T. Abbasiasl, F. Mirlou, H. Mirzajani, M. J. Bathaei, E. Istif, N. Shomalizadeh, R. E. Cebecioğlu, E. E. Özkahraman, U. C. Yener, L. Beker, *Adv. Mater.* **2024**, *36*, 2304704.
[238] Z. Wang, J. Luan, A. Seth, L. Liu, M. You, P. Gupta, P. Rathi, Y. Wang, S. Cao, Q. Jiang, X. Zhang, R. Gupta, Q. Zhou, J. J. Morrissey, E. L. Scheller, J. S. Rudra, S. Singamaneni, *Nat. Biomed. Eng.* **2021**, *5*, 64.
[239] F. Tehrani, H. Teymourian, B. Wuerstle, J. Kavner, R. Patel, A. Furmidge, R. Aghavali, H. Hosseini-Toudeshki, C. Brown, F. Zhang, K. Mahato, Z. Li, A. Barfidokht, L. Yin, P. Warren, N. Huang, Z. Patel, P. P. Mercier, J. Wang, *Nat. Biomed. Eng.* **2022**, *6*, 1214.
[240] Y. Wang, Z. Chen, B. Davis, W. Lipman, S. Xing, L. Zhang, T. Wang, P. Hafiz, W. Xie, Z. Yan, Z. Huang, J. Song, W. Bai, *Nat. Commun.* **2024**, *15*, 511.
[241] M. Zheng, T. Sheng, J. Yu, Z. Gu, C. Xu, *Nat. Rev. Bioeng.* **2024**, *2*, 324.
[242] L. K. Vora, A. H. Sabri, P. E. McKenna, A. Himawan, A. R. J. Hutton, U. Detamornrat, A. J. Paredes, E. Larrañeta, R. F. Donnelly, *Nat. Rev. Bioeng.* **2024**, *2*, 64.
[243] C. Meyer, S. OConnor, *Diabetes* **2016**, https://drbarnaistvan.hu/first-series-leadless-pacing-percutaneous-implantable-transcatheter-pacemaker-background-technical-aspects-possible-pitfalls/.
[244] A. L. Waldo, J. L. Wells Jr., T. B. Cooper, W. A. MacLean, *Prog. Cardiovasc. Dis.* **1981**, *23*, 451.
[245] D.-W. Park, J. P. Ness, S. K. Brodnick, C. Esquibel, J. Novello, F. Atry, D.-H. Baek, H. Kim, J. Bong, K. I. Swanson, A. J. Suminski, K. J. Otto, R. Pashaie, J. C. Williams, Z. Ma, *ACS Nano* **2018**, *12*, 148.
[246] M. R. MacEwan, E. R. Zellmer, J. J. Wheeler, H. Burton, D. W. Moran, *Front. Neurosci.* **2016**, *10*, 557.
[247] P. Sheehan, P. Jones, A. Caselli, J. M. Giurini, A. Veves, *Diabetes Care* **2003**, *26*, 1879.
[248] J. A. Deprest, A. Benachi, E. Gratacos, K. H. Nicolaides, C. Berg, N. Persico, M. Belfort, G. J. Gardener, Y. Ville, A. Johnson, F. Morini, M. Wielgoś, B. V. Calster, P. L. J. DeKoninck, *N. Engl. J. Med.* **2021**, *385*, 119.
[249] Y. Mao, Y. Meng, S. Li, Y. Li, R. Guidoin, F. Wang, Y. Qiao, G. Brochu, Z. Zhang, J. Tang, L. Wang, *Composites, Part B* **2022**, *235*, 109761.
[250] U. A. Sezer, V. Sanko, M. Gulmez, B. Aru, E. Sayman, A. Aktekin, F. V Aker, G. Y. Demirel, S. Sezer, *Mater. Sci. Eng., C* **2019**, *99*, 1141.
[251] A. M. Ibrahim, C. R. Vargas, S. Colakoglu, J. T. Nguyen, S. J. Lin, B. T. Lee, *J. Reconstruct. Microsurg.* **2015**, *31*, 083.
[252] K. Baylón, P. Rodríguez-Camarillo, A. Elías-Zúñiga, J. A. Díaz-Elizondo, R. Gilkerson, K. Lozano, *Membranes* **2017**, *7*, 47.
[253] M. J. Rosen, D. M. Krpata, C. C. Petro, A. Carbonell, J. Warren, B. K. Poulose, A. Costanzo, C. Tu, J. Blatnik, A. S. Prabhu, *JAMA Surg.* **2022**, *157*, 293.
[254] T. Kim, C. W. See, X. Li, D. Zhu, *Eng. Regener.* **2020**, *1*, 6.
[255] E. Chelala, Y. Debardemaeker, B. Elias, F. Charara, M. Dessily, J.-L. Allé, *Hernia* **2010**, *14*, 123.
[256] K. J. Sowards, M. K. Liang, *Am. J. Surg.* **2022**, *224*, 177.
[257] F. Corduas, D. A. Lamprou, E. Mancuso, *Bio-Des. Manuf.* **2021**, *4*, 278.
[258] W. Liu, Y. Xie, Y. Zheng, W. He, K. Qiao, H. Meng, *Bioact. Mater.* **2021**, *6*, 420.
[259] M. Zhu, W. Li, X. Dong, X. Yuan, A. C. Midgley, H. Chang, Y. Wang, H. Wang, K. Wang, P. X. Ma, H. Wang, D. Kong, *Nat. Commun.* **2019**, *10*, 4620.
[260] A. Costa, S. Adamo, F. Gossetti, L. D'Amore, F. Ceci, P. Negro, P. Bruzzone, *Materials* **2019**, *12*, 2375.
[261] M. Sosin, M. Y. Nahabedian, P. Bhanot, *Plast. Reconstr. Surg.* **2018**, *142*, 107S.
[262] R. Kaveti, J. H. Lee, J. K. Youn, T.-M. Jang, W. Bae Han, S. M. Yang, J.-W. Shin, G.-J. Ko, D.-J. Kim, S. Han, H. Kang, A. J. Bandodkar, H.-Y. Kim, S.-W. Hwang, *Adv. Mater.* **2024**, *36*, 2307391.
[263] P. Seth, R. A. Rudd, R. K. Noonan, T. M. Haegerich, *Am. Pub. Health* **2018**, *108*, 500.
[264] N. Bhadra, E. Foldes, T. Vrabec, K. Kilgore, N. Bhadra, *J. Neural Eng.* **2018**, *15*, 016012.
[265] L. M. Roldan, T. E. Eggers, K. L. Kilgore, N. Bhadra, T. Vrabec, N. Bhadra, *J. Neurosci. Methods* **2019**, *315*, 48.
[266] K. L. Kilgore, N. Bhadra, *Neuromodulation: Technol. Neural Interface* **2014**, *17*, 242.
[267] Y. Lee, C. Lin, J. Cheng, G.-S. Chen, *Br. J. Anaesth.* **2015**, *114*, 840.
[268] V. Colucci, G. Strichartz, F. Jolesz, N. Vykhodtseva, K. Hynynen, *Ultrasound Med. Biol.* **2009**, *35*, 1737.
[269] E. H. Lothet, K. L. Kilgore, N. Bhadra, T. Vrabec, Y. T. Wang, E. D. Jansen, M. W. Jenkins, H. J. Chiel, *Neurophotonics* **2014**, *1*, 011010.
[270] S. M. Iyer, K. L. Montgomery, C. Towne, S. Y. Lee, C. Ramakrishnan, K. Deisseroth, S. L. Delp, *Nat. Biotechnol.* **2014**, *32*, 274.
[271] K.-I. Song, H. Seo, D. Seong, S. Kim, K.-J. Yu, Y.-C. Kim, J. Kim, S. J. Kwon, H.-S. Han, I. Youn, H. Lee, D. Son, *Nat. Commun.* **2020**, *11*, 4195.
[272] G. Lee, Y. S. Choi, H.-J. Yoon, J. A. Rogers, *Matter* **2020**, *3*, 1031.
[273] D.-M. Lee, M. Kang, I. Hyun, B.-J. Park, H. J. Kim, S. H. Nam, H.-J. Yoon, H. Ryu, H. Park, B.-O. Choi, S.-W. Kim, *Nat. Commun.* **2023**, *14*, 7315.
[274] I. Allodi, E. Udina, X. Navarro, *Prog. Neurobiol.* **2012**, *98*, 16.
[275] P. Sun, C. Li, C. Yang, M. Sun, H. Hou, Y. Guan, J. Chen, S. Liu, K. Chen, Y. Ma, Y. Huang, X. Li, H. Wang, L. Wang, S. Chen, H. Cheng, W. Xiong, X. Sheng, M. Zhang, J. Peng, S. Wang, Y. Wang, L. Yin, *Nat. Commun.* **2024**, *15*, 4721.
[276] I. K. Fox, M. J. Brenner, P. J. Johnson, D. A. Hunter, S. E. Mackinnon, *Microsurgery* **2012**, *32*, 552.
[277] K. Veltri, J. M. Kwiecien, W. Minet, M. Fahnestock, J. R. Bain, *J. Reconstruct. Microsurg.* **2005**, *21*, 57.
[278] S. Y. Fu, T. Gordon, *Mol. Neurobiol.* **1997**, *14*, 67.
[279] D. H. Kim, Y.-J. Cho, R. L. Tiel, D. G. Kline, *J. Neurosurg.* **2003**, *98*, 1005.
[280] S. Jones, W. D. C. Man, W. Gao, I. J. Higginson, A. Wilcock, M. Maddocks, *Cochrane Database Syst. Rev.* **2016**, https://doi.org/10.1002/14651858.CD009419.pub3.
[281] Z. Hong, M. Sui, Z. Zhuang, H. Liua, X. Zhenga, C. Caic, D. Jin, *Arch. Phys. Med. Rehabil.* **2018**, *99*, 1011.e1.
[282] Y. B. Hong, J. Joo, Y. S. Hyun, G. Kwak, Y.-R. Choi, H. K. Yeo, D. H. Jwa, E. J. Kim, W. M. Mo, S. H. Nam, S. M. Kim, J. H. Yoo, H. Koo, H. T. Park, K. W. Chung, B.-O. Choi, *PLoS Genet.* **2016**, *12*, 1005829.
[283] N. Ha, Y. I. Choi, N. Jung, J. Y. Song, D. K. Bae, M. C. Kim, Y. J. Lee, H. Song, G. Kwak, S. Jeong, S. Park, S. H. Nam, S.-C. Jung, B.-O. Choi, *Br. J. Pharmacol.* **2020**, *177*, 5096.
[284] S. Ozeri, D. Shmilovitz, S. Singer, C.-C. Wang, *Ultrasonics* **2010**, *50*, 666.
[285] C. H. Lee, H. Kim, D. V. Harburg, G. Park, Y. Ma, T. Pan, J. S. Kim, N. Y. Lee, B. H. Kim, K.-I. Jang, S.-K. Kang, Y. Huang, J. Kim, K.-M. Lee, C. Leal, J. A Rogers, *NPG Asia Mater.* **2015**, *7*, e227.
[286] A. C. R. Grayson, I. S. Choi, B. M. Tyler, P. P. Wang, H. Brem, M. J. Cima, R. Langer, *Nat. Mater.* **2003**, *2*, 767.
[287] X. Liu, G. J. Pettway, L. K. McCauley, P. X. Ma, *Biomaterials* **2007**, *28*, 4124.
[288] J. F. Hou, M. O. G. Nayeem, K. A. Caplan, E. A. Ruesch, A. Caban-Murillo, E. Criado-Hidalgo, S. B. Ornellas, B. Williams, A. A. Pearce, H. E. Dagdeviren, M. Surets, J. A. White, M. G. Shapiro, F. Wang, S. Ramirez, C. Dagdeviren, *Nat. Commun.* **2024**, *15*, 4601.
[289] E. S. Hosseini, S. Dervin, P. Ganguly, R. Dahiya, *ACS Appl. Bio Mater.* **2020**, *4*, 163.
[290] S. Guerin, S. A. Tofail, D. Thompson, *NPG Asia Mater.* **2019**, *11*, 10.

© 2024 The Author(s). Advanced Functional Materials published by Wiley-VCH GmbH

16163028, 2025, 3, Downloaded from https://advanced.onlinelibrary.wiley.com/doi/10.1002/adfm.202413324 by Koc University, Wiley Online Library on [22/05/2025]. See the Terms and Conditions (https://onlinelibrary.wiley.com/terms-and-conditions) on Wiley Online Library for rules of use; OA articles are governed by the applicable Creative Commons License

[291] M. T. Chorsi, T. T. Le, F. Lin, T. Vinikoor, R. Das, J. F. Stevens, C. Mundrane, J. Park, K. T. M. Tran, Y. Liu, J. Pfund, R. Thompson, W. He, M. Jain, M. D. Morales-Acosta, O. R. Bilal, K. Kazerounian, H. Ilies, T. D. Nguyen, *Sci. Adv.* **2023**, *9*, eadg6075.
[292] Z. L. Wang, L. Lin, J. Chen, S. Niu, Y. Zi, *Triboelectric Nanogenerator: Single-Electrode Mode*, Springer, Berlin **2016**.
[293] Q. Zheng, Q. Tang, Z. L. Wang, Z. Li, *Nat. Rev. Cardiol.* **2021**, *18*, 7.
[294] Z. L. Wang, *ACS Nano* **2013**, *7*, 9533.
[295] R. Pan, W. Xuan, J. Chen, S. Dong, H. Jin, X. Wang, H. Li, J. Luo, *Nano Energy* **2018**, *45*, 193.
[296] M. Kang, M. S. B. M. Khusrin, Y.-J. Kim, B. Kim, B. J. Park, I. Hyun, I. M. Imani, B.-O. Choi, S.-W. Kim, *Nano Energy* **2022**, *100*, 107480.
[297] H. Kim, S. Choi, Y. Hong, J. Chung, J. Choi, W.-K. Choi, I. W. Park, S. H. Park, H. Park, W.-J. Chung, K. Heo, M. Lee, *Appl. Mater. Today* **2021**, *22*, 100920.
[298] Q. Zheng, Y. Zou, Y. Zhang, Z. Liu, B. Shi, X. Wang, Y. Jin, H. Ouyang, Z. Li, Z. L. Wang, *Sci. Adv.* **2016**, *2*, 1501478.
[299] W. Jiang, H. Li, Z. Liu, Z. Li, J. Tian, B. Shi, Y. Zou, H. Ouyang, C. Zhao, L. Zhao, R. Sun, H. Zheng, Y. Fan, Z. Lin Wang, Z. Li, *Adv. Mater.* **2018**, *30*, 1801895.
[300] D.-M. Lee, N. Rubab, I. Hyun, W. Kang, Y.-J. Kim, M. Kang, B. O. Choi, S.-W. Kim, *Sci. Adv.* **2022**, *8*, eabl8423.
[301] Z. Li, H. Feng, Q. Zheng, H. Li, C. Zhao, H. Ouyang, S. Noreen, M. Yu, F. Su, R. Liu, L. Li, Z. L. Wang, Z. Li, *Nano Energy* **2018**, *54*, 390.
[302] T. Li, P. S. Lee, *Small Struct.* **2022**, *3*, 2100128.
[303] F. B. Sarıipek, İ. Özaytekin, F. Erci, *J. Appl. Polym. Sci.* **2023**, *140*, e53437.
[304] P. Wu, P. Chen, C. Xu, Q. Wang, F. Zhang, K. Yang, W. Jiang, J. Feng, Z. Luo, *Nano Energy* **2022**, *102*, 107707.
[305] F. Yang, J. Li, Y. Long, Z. Zhang, L. Wang, J. Sui, Y. Dong, Y. Wang, R. Taylor, X. Wan, *Science* **2021**, *373*, 337.
[306] Y. Cheng, J. Xu, L. Li, P. Cai, Y. Li, Q. Jiang, W. Wang, Y. Cao, B. Xue, *Adv. Sci.* **2023**, *10*, 2207269.
[307] M. Lin, Z. Zhang, X. Gao, Y. Bian, R. S. Wu, G. Park, Z. Lou, Z. Zhang, X. Xu, X. Chen, A. Kang, X. Yang, W. Yue, L. Yin, C. Wang, B. Qi, S. Zhou, H. Hu, H. Huang, M. Li, Y. Gu, J. Mu, A. Yang, A. Yaghi, Y. Chen, Y. Lei, C. Lu, R. Wang, J. Wang, S. Xiang, et al., *Nat. Biotechnol.* **2024**, *42*, 448.
[308] R. Das, E. J. Curry, T. T. Le, G. Awale, Y. Liu, S. Li, J. Contreras, C. Bednarz, J. Millender, X. Xin, D. Rowe, S. Emadi, K. W. H. Lo, T. D. Nguyen, *Nano Energy* **2020**, *76*, 105028.
[309] Y. Liu, G. Dzidotor, T. T. Le, T. Vinikoor, K. Morgan, E. J. Curry, R. Das, A. McClinton, E. Eisenberg, L. N. Apuzzo, K. T. M. Tran, P. Prasad, T. J. Flanagan, S.-W. Lee, H.-M. Kan, M. T. Chorsi, K. W. H. Lo, C. T. Laurencin, T. D. Nguyen, *Sci. Transl. Med.* **2022**, *14*, eabi7282.
[310] H. Mirzajani, T. Abbasiasl, F. Mirlou, E. Istif, M. J. Bathaei, Ç. Dağ, O. Deyneli, D. Yazıcı, L. Beker, *Biosens. Bioelectron.* **2022**, *213*, 114450.
[311] H. Mirzajani, E. Istif, T. Abbasiasl, F. Mirlou, E. E. Özkahraman, M. Hasanreisoglu, L. Beker, *Adv. Mater. Technol.* **2022**, *7*, 2101629.
[312] H. Mirzajani, F. Mirlou, E. Istif, R. Singh, L. Beker, *Biosens. Bioelectron.* **2022**, *197*, 113761.
[313] K. Kang, S. Ye, C. Jeong, J. Jeong, Y. Ye, J.-Y. Jeong, Y.-J. Kim, S. Lim, T. H. Kim, K. Y. Kim, J. U. Kim, G. I. Kim, D. H. Chun, K. Kim, J. Park, J.-H. Hong, B. Park, K. Kim, S. Jung, K. Baek, D. Cho, J. Yoo, K. Lee, H. Cheng, B.-W. Min, H. J. Kim, H. Jeon, H. Yi, T. Kim, K. J. Yu, et al., *Nat. Commun.* **2024**, *15*, 10.
[314] P. Gutruf, R. T. Yin, K. B. Lee, J. Ausra, J. A. Brennan, Y. Qiao, Z. Xie, R. Peralta, O. Talarico, A. Murillo, S. W. Chen, J. P. Leshock, C. R. Haney, E. A. Waters, C. Zhang, H. Luan, Y. Huang, G. Trachiotis, I. R. Efimov, J. A. Rogers, *Nat. Commun.* **2019**, *10*, 5742.
[315] H. Lyu, M. John, D. Burkland, B. Greet, A. Post, A. Babakhani, M. Razavi, *Sci. Rep.* **2020**, *10*, 2067.
[316] S. Rao, N. Llombart, E. Moradi, K. Koski, T. Bjorninen, L. Sydanheimo, *IEEE Antenn. Propag. Mag.* **2014**, *56*, 271.
[317] N. A. Malik, P. Sant, T. Ajmal, M. Ur-Rehman, *IEEE J. Electromagnet., RF Microwaves Med. Biol.* **2020**, *5*, 84.
[318] S. A. A. Shah, I. A. Shah, S. Hayat, H. Yoo, *IEEE Transac. Antenn. Propagat.* **2024**, *72*, https://doi.org/10.1109/TAP.2024.3349782.
[319] C. Steiger, A. Abramson, P. Nadeau, A. P. Chandrakasan, R. Langer, G. Traverso, *Nat. Rev. Mater.* **2019**, *4*, 83.
[320] A. Basir, Y. Cho, I. A. Shah, S. Hayat, S. Ullah, M. Zada, *IEEE Antenn. Propagat. Mag.* **2023**, *65*, 70.
[321] D. Nikolayev, M. Zhadobov, L. Le Coq, P. Karban, R. Sauleau, *IEEE Transac. Antenn. Propagat.* **2017**, *65*, 6107.
[322] L. Wang, T. D. Drysdale, D. R. Cumming, *IEEE Trans. Biomed. Eng.* **2007**, *54*, 2020.
[323] K. Kalantar-Zadeh, K. J. Berean, N. Ha, A. F. Chrimes, K. Xu, D. Grando, J. Z. Ou, N. Pillai, J. L. Campbell, R. Brkljača, K. M. Taylor, R. E. Burgell, C. K. Yao, S. A. Ward, C. S. McSweeney, J. G. Muir, P. R. Gibson, *Nat. Electron.* **2018**, *1*, 79.
[324] P. E. De la, N. H. Maganti, A. Trifonov, I. Jeerapan, K. Mahato, L. Yin, T. Sonsa-ard, N. Ma, W. Jung, R. Burns, A. Zarrinpar, J. Wang, P. P. Mercier, *Nat. Commun.* **2022**, *13*, 7405.
[325] S. S. You, A. Gierlach, P. Schmidt, G. Selsing, I. Moon, K. Ishida, J. Jenkins, W. A. M. Madani, S.-Y. Yang, H.-W. Huang, S. Owyang, A. Hayward, A. P. Chandrakasan, G. Traverso, *Nat. Electron.* **2024**, *7*, 497.
[326] A. Abdigazy, M. Arfan, G. Lazzi, C. Sideris, A. Abramson, Y. Khan, *Nat. Electron.* **2024**, *7*, 102.
[327] I. A. Shah, M. Zada, S. A. A. Shah, A. Basir, H. Yoo, *IEEE Trans. Microwave Theory Techniq.* **2024**, *72*, https://doi.org/10.1109/TMTT.2023.3319050.
[328] M. J. Bathaei, R. Singh, H. Mirzajani, E. Istif, M. J. Akhtar, T. Abbasiasl, L. Beker, *Adv. Mater.* **2023**, *35*, 2207081.
[329] K. Nan, K. Wong, D. Li, B. Ying, J. C. McRae, V. R. Feig, S. Wang, N. Du, Y. Liang, Q. Mao, E. Zhou, Y. Chen, L. Sang, K. Yao, J. Zhou, J. Li, J. Jenkins, K. Ishida, J. Kuosmanen, W. A. M. Madani, A. Hayward, K. B. Ramadi, X. Yu, G. Traverso, *Nat. Commun.* **2024**, *15*, 6749.
[330] M. Rüegg, R. Blum, G. Boero, J. Brugger, *Adv. Funct. Mater.* **2019**, *29*, 1903051.
[331] J. Koo, S. B. Kim, Y. S. Choi, Z. Xie, A. J. Bandodkar, J. Khalifeh, Y. Yan, H. Kim, M. K. Pezhouh, K. Doty, G. Lee, Y.-Y. Chen, S. M. Lee, D. D'Andrea, K. Jung, K. Lee, K. Li, S. Jo, H. Wang, J.-H. Kim, J. Kim, S.-G. Choi, W. J. Jang, Y. S. Oh, I. Park, S. S. Kwak, J.-H. Park, D. Hong, X. Feng, C.-H. Lee, et al., *Sci. Adv.* **2020**, *6*, eabb1093.
[332] H. Zhou, Y. Zhang, Y. Qiu, H. Wu, W. Qin, Y. Liao, Q. Yu, H. Cheng, *Biosens. Bioelectron.* **2020**, *168*, 112569.
[333] E. Katz, K. MacVittie, *Energy Environ. Sci.* **2013**, *6*, 2791.
[334] D. Jiang, B. Shi, H. Ouyang, Y. Fan, Z. L. Wang, Z. Li, *ACS Nano* **2020**, *14*, 6436.
[335] S. Yoo, J. Lee, H. Joo, S.-H. Sunwoo, S. Kim, D.-H. Kim, *Adv. Healthcare Mater.* **2021**, *10*, 2100614.
[336] K. Song, J. H. Han, T. Lim, N. Kim, S. Shin, J. Kim, H. Choo, S. Jeong, Y.-C. Kim, Z. L. Wang, J. Lee, *Adv. Healthcare Mater.* **2016**, *5*, 1572.
[337] Z. Gao, Y. Zhou, J. Zhang, J. Foroughi, S. Peng, R. H. Baughman, Z. L. Wang, C. H. Wang, *Adv. Mater.* **2024**, *36*, 2404492.
[338] M. Shao, H. Sheng, L. Lin, H. Ma, Q. Wang, J. Yuan, X. Zhang, G. Chen, W. Li, Q. Su, E. Xie, J. Wang, Z. Zhang, W. Lan, *Small* **2023**, *19*, 2205529.
[339] L. Yin, X. Huang, H. Xu, Y. Zhang, J. Lam, J. Cheng, J. A. Rogers, *Adv. Mater.* **2014**, *26*, 3879.
[340] I. Huang, Y. Zhang, H. M. Arafa, S. Li, A. Vazquez-Guardado, W. Ouyang, F. Liu, S. Madhvapathy, J. W. Song, A. Tzavelis, J. Trueb, Y. Choi, W. J. Jeang, V. Forsberg, E. Higbee-Dempsey, N. Ghoreishi-Haack, I. Stepien, K. Bailey, S. Han, Z. J. Zhang, C. Good, Y. Huang, A. J. Bandodkar, J. A. Rogers, *Energy Environ. Sci.* **2022**, *15*, 4095.

© 2024 The Author(s). Advanced Functional Materials published by Wiley-VCH GmbH

16163028, 2025, 3, Downloaded from https://advanced.onlinelibrary.wiley.com/doi/10.1002/adfm.202413324 by Koc University, Wiley Online Library on [22/05/2025]. See the Terms and Conditions (https://onlinelibrary.wiley.com/terms-and-conditions) on Wiley Online Library for rules of use; OA articles are governed by the applicable Creative Commons License

[341] H. Li, C. Zhao, X. Wang, J. Meng, Y. Zou, S. Noreen, L. Zhao, Z. Liu, H. Ouyang, P. Tan, M. Yu, Y. Fan, Z. L. Wang, Z. Li, *Adv. Sci.* **2019**, *6*, 1801625.
[342] H. Sheng, L. Jiang, Q. Wang, Z. Zhang, Y. Lv, H. Ma , H. Bi, J. Yuan, M. Shao, W. Lan, *Sci. Adv.* **2023**, *9*, eadh8083.
[343] K. Rajaram, S. M. Yang, H. S.-W. Transient, *Adv. Energy Sustainability Res.* **2022**, *3*, 2100223.
[344] M. Yu, Y. Peng, X. Wang, F. Ran, *Adv. Funct. Mater.* **2023**, *33*, 2301877.
[345] M. Shao, H. Sheng, L. Lin, H. Ma, Q. Wang, J. Yuan, X. Zhang, G. Chen, W. Li, Q. Su, E. Xie, J. Wang, Z. Zhang, W. Lan, *Small* **2023**, *19*, 2205529.
[346] S. Zheng, X. Li, B. Yan, Q. Hu, Y. Xu, X. Xiao, H. Xue, H. Pang, *Adv. Energy Mater.* **2017**, *7*, 1602733.
[347] T. Juqu, S. C. Willenberg, K. Pokpas, N. Ross, *Adv. Sensor Energy Mater.* **2022**, *1*, 100037.
[348] S.-H. Sunwoo, S. I. Han, C. S. Park, J. H. Kim, J. S. Georgiou, S.-P. Lee, D.-H. Kim, T. Hyeon, *Nat. Rev. Bioeng.* **2024**, *2*, 8.
[349] S. I. Han, S.-H. Sunwoo, C. S. Park, S.-P. Lee, T. Hyeon, D.-H. Kim, *ACS Nano* **2024**, *18*, 12025.
[350] H. Sheng, J. Zhou, B. Li, Y. He, X. Zhang, J. Liang, J. Zhou, Q. Su, E. Xie, C. Yu, *Sci. Adv.* **2021**, *7*, eabe3097.
[351] O. Böstman, H. Pihlajamäki, *Biomaterials* **2000**, *21*, 2615.
[352] L. Wang, X. Guo, J. Chen, Z. Zhen, B. Cao, W. Wan, Y. Dou, H. Pan, F. Xu, Z. Zhang, J. Wang, D. Li, Q. Guo, Q. Jiang, Y. Du, J. Yu, B. C. Heng, Q. Han, Z. Ge, *Bioact. Mater.* **2022**, *9*, 332.
[353] K. B. Baker, J. A. Tkach, J. A. Nyenhuis, M. Phillips, F. G. Shellock, J. Gonzalez-Martinez, A. R. Rezai, *J. Magn. Reson. Imaging* **2004**, *20*, 315.
[354] Z. U. Abdin, S. A. A. Shah, Y. Cho, H. Yoo, *Comput. Methods Programs Biomed.* **2024**, *244*, 107976.
[355] J. Espiritu, M. Meier, J.-M. Seitz, *Bioact. Mater.* **2021**, *6*, 4360.
[356] Y. Luo, M. R. Abidian, J.-H. Ahn, D. Akinwande, A. M. Andrews, M. Antonietti, Z. Bao, M. Berggren, C. A. Berkey, C. J. Bettinger, J. Chen, P. Chen, W. Cheng, X. Cheng, S.-J. Choi, A. Chortos, C. Dagdeviren, R. H. Dauskardt, C.-A. Di, M. D. Dickey, X. Duan, A. Facchetti, Z. Fan, Y. Fang, J. Feng, X. Feng, H. Gao, W. Gao, X. Gong, C. F. Guo, et al., *ACS Nano* **2023**, *17*, 5211.
[357] C. Wang, E. Shirzaei Sani, W. Gao, *Adv. Funct. Mater.* **2022**, *32*, 2111022.
[358] X. Yang, Y. Wang, R. Byrne, G. Schneider, S. Yang, *Chem. Rev.* **2019**, *119*, 10520.
[359] A. C. Ward, P. Dubey, P. Basnett, G. Lika, G. Newman, D. K. Corrigan, C. Russell, J. Kim, S. Chakrabarty, P. Connolly, I. Roy, *Front. Bioeng. Biotechnol.* **2020**, *8*, 1039.
[360] Q. Lyu, S. Gong, J. Yin, J. M. Dyson, W. Cheng, *Adv. Healthcare Mater.* **2021**, *10*, 2100577.
[361] C. Wang, C. Pan, Z. Wang, *ACS Nano* **2019**, *13*, 12287.
[362] Y. Jiang, A. A. Trotsyuk, S. Niu, D. Henn, K. Chen, C.-C. Shih, M. R. Larson, A. M. Mermin-Bunnell, S. Mittal, J.-C. Lai, A. Saberi, E. Beard, S. Jing, D. Zhong, S. R. Steele, K. Sun, T. Jain, E. Zhao, C. R. Neimeth, W. G. Viana, J. Tang, D. Sivaraj, J. Padmanabhan, M. Rodrigues, Z. Bao, *Nat. Biotechnol.* **2023**, *41*, 652.
[363] S. H. Kim, A. Basir, R. Avila, J. Lim, S. W. Hong, G. Choe, J. H. Shin, J. H. Hwang, S. Y. Park, J. Joo, C. Lee, J. Choi, B. Lee, K.-S. Choi, S. Jung, T.-I Kim, H. Yoo, Y. H. Jung, *Nature* **2024**, *15*, 927.
[364] A. E. Lottes, K. J. Cavanaugh, Y. Y.-F. Chan, V. J. Devlin, C. J. Goergen, R. Jean, J. C. Linnes, M. Malone, R. Peat, D. G. Reuter, K. Taylor, G. R. Wodicka, *J. Cardiovasc. Transl. Res.* **2022**, *15*, 927.
[365] E. J. Emanuel, D. Wendler, C. Grady, *JAMA, J. Am. Med. Assoc.* **2000**, *283*, 2701.
[366] M. Aboy, C. Crespo, A. Stern, *npj Digital Med.* **2024**, *7*, 29.
[367] S. M. Ben-Menahem, R. Nistor-Gallo, G. Macia, G. von Krogh, J. Goldhahn, *Nat. Biomed. Eng.* **2020**, *4*, 585.
[368] F. A. Manno, *Nature* **2024**, *625*, 30.
[369] A. Wexler, E. Largent, *Nat. Commun.* **2023**, *14*, 2325.
[370] H. J. Marcus, A. Bennett, A. Chari, D. Toni, H. Allison, H.-H. Archie, K. Angelos, R. M. Kwasnicki, J. P. Martin, R. Maroeska, S. E. Squire, P. McCulloch, *Ann. Surg.* **2022**, *275*, 73.
[371] J. R. Walter, S. Xu, J. A. Rogers, *Nat. Commun.* **2024**, *15*, 123.
[372] L. Drew, *Nat. Med.* **2020**, *26*, 1154.
[373] A. Barfeie, J. Wilson, J. Rees, *Br. Dent. J.* **2015**, *218*, E9.
[374] M. Luo, A. W. Martinez, C. Song, F. Herrault, M. G. Allen, *J. Microelectromech. Syst.* **2013**, *23*, 4.



Hadi Mirzajani is a Marie Skłodowska-Curie postdoctoral fellow at Koç University in Istanbul, Turkey, working on wearable and implantable bioelectronics for continuous health monitoring. Before his current role, he was a researcher at the University of Tennessee, Knoxville, developing technologies in capacitive ACEK-based biosensors and drug delivery systems. He has authored and co-authored over 40 papers in peer-reviewed journals and conference proceedings. His research interests include wearable biosensors, biodegradable electronics, and microneedles for ISF sampling and sensing.

© 2024 The Author(s). Advanced Functional Materials published by Wiley-VCH GmbH

16163028, 2025, 3, Downloaded from https://advanced.onlinelibrary.wiley.com/doi/10.1002/adfm.202413324 by Koc University, Wiley Online Library on [22/05/2025]. See the Terms and Conditions (https://onlinelibrary.wiley.com/terms-and-conditions) on Wiley Online Library for rules of use; OA articles are governed by the applicable Creative Commons License



Parviz Zolfaghari earned his B.Sc. and M.Sc. degrees in Electrical Engineering with a focus on Electronics from the University of Tabriz and Sahand University of Technology in Iran, respectively, in 2010 and 2013. In 2018, he joined the Electro-Optic Devices Laboratory at Istanbul Technical University as a graduate researcher, where he specialized in Optical-mess sensors. Following completing his Ph.D. in 2023, he joined the Optical Microsystems Laboratory at Koç University as a postdoctoral scholar. His research focuses on sensor development, optics, and MEMS technology.



Sattar Akbari Nakhjavani earned his Doctor of Veterinary Medicine from Azad University of Tabriz. Then, he started his Ph.D. in Molecular Medicine at Tehran University of Medical Sciences, where his research focused on developing biosensors for detecting breast cancer biomarkers. His work has been published in Biosensors and Bioelectronics, *Trends in Biotechnology, and Trends in Analytical Chemistry Journal*. He also worked as a visiting scientist at EPFL, developing electrochemical sensors for drug detection. He is currently a postdoctoral fellow at Koç University in Istanbul, Turkey, where he is developing innovative biosensors for the early and accurate detection of diseases.



Beril Yagmur Koca earned her B.Sc. in Biomedical Engineering from Yeditepe University, Istanbul, Turkey, in 2023. During her undergraduate studies, she worked as a research assistant at the Yeditepe University Biotechnology Laboratory, where she led her own project from 2021 to 2023. She is currently pursuing her M.Sc. at Koç University, Istanbul, Turkey. Her research interests focus on developing wearable, implantable, and biodegradable biosensors and bioelectronics.



Mehrdad Khodapanahandeh received his B.Sc. degree in Electrical and Electronics Engineering from Urmia University of Technology, Urmia, Iran 2015. He then joined the Microelectromechanical Systems (MEMS) research group at Sahand University of Technology, where he completed his M.Sc. in Electronic Engineering focusing on Radio Frequency (RF) MEMS in 2018. He is pursuing his Ph.D. at Koç University, where his research is centered on Biomedical and Microsystems. His research interests include optical microdevices and biosensors.

© 2024 The Author(s). Advanced Functional Materials published by Wiley-VCH GmbH

16163028, 2025, 3, Downloaded from https://advanced.onlinelibrary.wiley.com/doi/10.1002/adfm.202413324 by Koc University, Wiley Online Library on [22/05/2025]. See the Terms and Conditions (https://onlinelibrary.wiley.com/terms-and-conditions) on Wiley Online Library for rules of use; OA articles are governed by the applicable Creative Commons License



Hakan Urey earned his Ph.D. in Electrical and Computer Engineering from the Georgia Institute of Technology in 1997. He founded the Optical Microsystems Laboratory at Koç University, where his research focuses on biomedical systems, including diagnostic tests, neuroscience, and micromechanical systems. He has authored over 250 academic papers and delivered over 50 invited talks at international conferences. He holds over 60 patents, all licensed by industry, leading to the establishment of five spinoff companies from his lab. His work has been widely recognized and has received multiple prestigious awards, including four ERC grants in Europe.

© 2024 The Author(s). Advanced Functional Materials published by Wiley-VCH GmbH

16163028, 2025, 3, Downloaded from https://advanced.onlinelibrary.wiley.com/doi/10.1002/adfm.202413324 by Koc University, Wiley Online Library on [22/05/2025]. See the Terms and Conditions (https://onlinelibrary.wiley.com/terms-and-conditions) on Wiley Online Library for rules of use; OA articles are governed by the applicable Creative Commons License